Ref. Ares(2023)8820406 - 21/12/2023

D3.1. Thermal Management System Strategies, modelling and simulation

Reinventing High-performance pOwer converters for heavy-Duty electric trAnSport

Grant Agreement Number 101056896

Deliverable name:	Thermal Managment System Strategies, modelling and simulation
Deliverable number:	3.1
Deliverable type:	R
Work Package:	WP3: Thermal Management System
Lead beneficiary:	AU
Contact persons:	Corneliu Barbu <coba@ece.au.dk> Arman Fathollahi <aman.f@ece.au.dk> Uffe Jakobsen <uja@ece.au.dk> Jørgen Houe Pedersen <jhp@ece.au.dk>
Dissemination Level:	PU
Due date for deliverable:	December 31st 2023

Funded by the European Union

Funded by the European Union. Views and opinions expressed are however those of the author(s) only and do not necessarily reflect those of the European Union or CINEA. Neither the European Union nor the granting authority can be held responsible for them.

DOCUMENT CONTROL PAGE

Author(s):	Uffe Jakobsen (AU), Arman Fathollahi (AU), David Lumbreras (UPC)
Contributor(s):	AU, UPC
Reviewer(s):	Jose Sáez (NION), Sebastian Dieterich (VALEO), Markus Rubi (VALEO), Carsten Siepker (VALEO), Stephan Hellmuth (VALEO)
Version number:	v.7
Contractual delivery date:	31-12-2023
Actual delivery date:	21-12-2023
Status:	Submitted

REVISION HISTORY

Version	Date	Author/Reviewer	Notes
v.0	20 – 11 – 2023	Arman Fathollahi (AU)	Creation, First Draft
v.1	20 – 11 – 2023	Arman Fathollahi (AU)	Minor Changes
v.2	05 – 12 – 2023	Jose Sáez (NION)	General Review
v.3	08 – 12 – 2023	Sebastian Dieterich (VAL), Markus Rubi (VAL), Carsten Siepker (VAL), Stephan Hellmuth (VAL)	General Review
v.4	11 – 12 – 2023	David Lumbreras (UPC)	Changes in T3.3 according to reviewers' comments
v.5	12 – 12 – 2023	Uffe Jakobsen (AU)	Changes in T3.1 according to reviewers' comments
v.6	12 – 12 – 2023	Arman Fathollahi (AU)	Revise the document according to reviewers' comments
v.7	20 – 12 - 2023	Corneliu Barbu	Final version submitted

ACKNOWLEDGEMENTS

The work described in this publication was subsidised by Horizon Europe (HORIZON) framework through the Grant Agreement Number 101056896.

DISCLAIMER

Funded by the European Union. Views and opinions expressed are however those of the author(s) only and do not necessarily reflect those of the European Union or CINEA. Neither the European Union nor the granting authority can be held responsible for them.

EXECUTIVE SUMMARY

The deliverable provides a comprehensive overview of thermal management system strategies, modeling, and simulation within the RHODaS project. Initially, it focuses on detailing the thermal interface between inverters and cooling systems, exploring estimated junction temperatures, and analyzing the potential impacts of design choices on equivalent thermal resistance. Subsequently, the document delves into advanced 3D thermal and power loss modeling, employing Finite Element Analysis, with COMSOL Multiphysics playing a crucial role in heatsink design. Fundamental simulations cover aspects like liquid-cooled heatsink design and sensitivity studies. Notable contributions include the introduction of the thermal equivalent circuit model, the RHODaS Thermal Management System Toolbox, and the strategic decision to design six heatsinks for a high-power converter. The document effectively communicates outcomes and methodologies, concluding by addressing advancements in temperature monitoring, proposing sensor networks, and outlining strategies for precise readings and a more effective thermal management approach.

Table of Content

INTRODUCTION 8
DESCRIPTION OF THE DOCUMENT AND PURSUE 8
WPS AND TASKS RELATED WITH THE DELIVERABLE 8
1. Thermal Cooling Management Strategies 9
1.1. Thermal interface 9
1.1.1. Key performance indicators and requirements for the thermal parts 9
1.1.2. Assumptions for estimations 11
1.1.3. Estimated temperatures based on assumptions 12
1.1.4. Design choices that increase thermal resistance of the interface 13
1.1.5. Proposed interface design 14
1.1.6. Partial conclusion for the thermal interface 14
1.2. Proposed thermal architecture 15
1.2.1. Hardware platform for the cooling system 15
1.2.2. Software for the cooling platform and the TMS 16
1.2.3. Detailed hydraulic architecture 17
1.2.4. Inverter thermal management system (TMS) 19
1.2.4.1. The relation from output power to the motor current 19
1.2.5. Partial conclusion of thermal architecture 19
2. THERMAL MODELLING AND SIMULATIONS 20
2.1. 3D Thermal Modelling of Heatsink 20
2.1.1. COMSOL Multiphysics and its advantages in design of the heatsink 20
2.1.2. Fundamental simulations in the COMSOL Multiphysics software 21

2.1.2.1. COMSOL Simulation with Solid Mechanics Physics: 21
2.1.2.2. COMSOL Simulation with Heat Transfer in Solids Physics: 22
2.1.2.3. COMSOL Simulation with Heat Transfer in Solids and Fluids Physics 27
2.1.2.4. Symmetry Tools and Heat Transfer Analysis 29
2.1.2.5. Parameter Sweeping Analysis 34
2.1.2.6. Reynolds Number Analysis 36
2.1.3. High-power, Liquid-Cooled Heatsink Design 37
3. RHODaS Thermal Management System Toolbox 40
4. Thermal equivalent circuit of high-power converter with GaN and SiC 42
5. Sensitivity analysis of the GaN switches junction temperature 48
6. New Sensors Networks for Advanced Temperature Control and Monitoring 56
6.1.1. Exploration of Advanced Temperature Sensor Networks 56
6.1.2. Key Functions of the Sensors Network 59
6.1.3. Integration of Intelligent Soft Sensors 61
7. Conclusion 63
8. Bibliography 64
Appendix A – Low power design mail 65
Appendix B – High power design mail 66
Appendix C – Pump curves for Grundfos Magna3 25-60 68
Appendix D – Fischer Elektronik Silicone foil 68
Appendix E – Ideal load calculations 69
Appendix F -Key impact pathways from the Grant Agreement 71
Appendix G – Low/high-power Inverter Specifications 73
Appendix H – SiC-CAB450M12XM3 from Wolfspeed Cree 76

Appendix I – GaN-GS66516T from GAN systems 85

Appendix J – Thermal interface material..... 94

LIST OF ACRONYMS

Acronyms	Definition
RHODAS	Reinventing High-performance pOwer converters for heavy-Duty electric trAnSport
WP	Work Pakage
DC	Direct Current
SiC	Silicon Carbide
GaN	Gallium Nitride
AIT	Austrian Institute of Technology
UPC	Universitat Politecnica de Catalunya
VS	Valeo Powertrain Electrified Mobility
AU	Aarhus University
VAL	Valeo Powertrain Systems Driveline
KPI	Key Performance Indicators
TO	Technical Objectives
KIP	Key Impacts Pathways
GA	Grant Agreement
TMS	Thermal Management System
IMD	Integrated Motor Drives
TCU	Thermal Control Unit
PMSM	Permanent Magnet Synchronous Motor
IOT	Internet Of Things
FEA	Finite Element Analysis
CFD	Computational Fluid Dynamics
PCB	Printed Circuit Board
NTC	Negative Temperature Coefficient

INTRODUCTION

DESCRIPTION OF THE DOCUMENT AND PURSUE

This report describes the RHODaS project's multifaceted endeavours in thermal management, meticulously documenting key aspects to provide a comprehensive understanding of its progress and innovations. The exploration begins with a detailed exposition on the thermal interface between the inverter and cooling system, elucidating the intricacies of the thermal cooling system architecture. The subsequent sections delve into the interplay between inverters and cooling systems, revisiting, and applying the Key Performance Indicators (KPI) and Requirements inherent to Work Package 3 (WP3). Additionally, the document provides insights into estimated junction temperatures, offering a crucial perspective on the implications of specific design choices for the equivalent thermal resistance—a pivotal factor informing the proposed interface design. As the narrative evolves, the report seamlessly transitions to highlight the achievements of Task 3.2 in WP3, concentrating on the 3D thermal and power loss modelling aspect. Advanced methodologies such as Finite Element Analysis and Computational Fluid Dynamics take centre stage, emphasizing the instrumental role of COMSOL Multiphysics in optimizing heatsink design. The document meticulously presents fundamental simulations within COMSOL Multiphysics, utilizing a solid mechanic's case study—an elongation problem—to exemplify the application of these methodologies. Further exploration encompasses analyses of air-cooled heatsink design, sensitivity studies, and the investigation of pin-based structures, complemented by illustrative figures for clarity. Beyond these technical aspects, the report extends its purview to encompass broader contributions to the RHODaS project. It sheds light on the introduction of the thermal equivalent circuit model for the T-type power converter, the development of the RHODaS Thermal Management System Toolbox, and the strategic decision to design six heatsinks for a high-power converter. These elements collectively contribute to the project's overarching objective of achieving robust and efficient thermal management solutions. In addition to the technical discourse, the report widens its lens to encompass the imperative of enhancing temperature monitoring within the project. It explores advanced temperature sensor networks, providing insights into the selection criteria for sensors in the low-power converter and addressing intricacies in sensor selection for the high-power converter. Proposals for leveraging temperature sensor data to estimate die temperature, adjust converter operation, and detect faults contribute to a forward-looking perspective, paving the way for a more effective and adaptive thermal management strategy within the dynamic landscape of the RHODaS project.

WPS AND TASKS RELATED WITH THE DELIVERABLE

This deliverable refers to Task 3.1, Task 3.2 and Task 3.3 included in WP3: Thermal Management System.

1. Thermal Cooling Management Strategies

This section first describes the thermal interface between the inverter and cooling system and, secondly, the thermal cooling system architecture.

1.1. Thermal interface

This chapter describes aspects of the thermal interface between the inverters and the cooling systems for RHODaS. First, the KPI and Requirements relevant to WP3 are reiterated. Based on certain assumptions, the document describes the estimated junction temperatures. Then there is a short description of how certain design choices may increase the equivalent thermal resistance, which is then used to guide the proposed interface design.

1.1.1. Key performance indicators and requirements for the thermal parts

Technical Objectives (TO) and KPI from the Grant Agreement (GA), and Key Impacts Pathways (KIP) can be found in the following Tables.

Table1.1. TO and KPI of the RHODaS project from Grant Agreement

From GA and WP1	
TO1.4	Develop a more effective hybrid thermal management system (TMS) of the IMD combining liquid-cooling and air-cooling to mitigate negative effects of high current on health and ageing of the materials and components.
TO2.2	Develop and fabricate highly integrated base modules for modular power electronics using 3D design and simulation.
TO3.1	Design effective sensor networks able to detect changes in relevant parameters at material, component, and system level to develop more accurate models for characterisation and control.
KPI 1:	40% reduction of thermal losses[1], temperature operation up to 175ºC, truck driving range +10%[2].
KPI 2:	50% reduction of size[3], 30% reduction of weight, 15 dB reduction of EMI noise[4].
	In addition to the use of novel semiconductor materials and the integration of optimised thermal management systems within the Integrated Motor Drives (IMD) with advanced control strategies based on AI will contribute to achieve a 20% cost reduction of powertrains, increasing the affordability and promoting a full-market penetration of heavy-duty EVs

1 "Heat loss is the intentional or unintentional movement of heat from one material to another (https://www.watlow.com/blog/posts/heat-loss-factors). So, less movement of heat from what to what and relative to what?
2 UPC will provide an appropriate benchmark.
3 UPC will provide an appropriate benchmark.
4 UPC will provide an appropriate benchmark.

From GA and WP1	
	Exploiting the wide frequency range of the WBG materials integrated in the powertrains, RHODaS will develop novel control approaches improving the reliability while reducing the losses by 40%, apart from reducing noise and interferences, based on adaptive switching frequency control depending on the driving mode. The capabilities hybrid SiC/GaN switches reduce the complexity of the control, allowing new adaptive switching frequency strategies, and increase the temperature of operation up to 175ºC. In addition, RHODaS will implement a more effective hybrid thermal management system combining micro liquid- cooling and air-cooling systems to mitigate negative effects of high current on health and ageing of the materials and components. This will significantly improve the thermal performance of the powertrains, which allows to extend the truck driving range in a 10%.
	Significant advancements in efficiency (reduction of losses by 25%) (of the power electronics) and thermal performance (increased maximum operational temperature), both parameters versus the state of the art of the targeted application. This allows further driving range extension, faster charging, and easier thermal management of the whole powertrain, as well as possible improvement in cabin-heating and defrosting in winter.

Table1.2. Requirements for the thermal parts of the RHODaS project from WP1

Parameter	Value
Ambient temperature range	From -20 ºC to 50 ºC
Altitude	Up to 2000 m
Maximum relative humidity	90%
Power to be dissipated	Depends on the losses from the power converter and depends on achieved efficiency and power needed.
Cooling system	Glycol + water for cooling the inverter
Surface area needed for 150kW with no overload capacity at 97.5% efficiency	Minimum needed cooling area 263cm2. With a converter height of 57 mm this gives approximately, 100kW/liter (assumes no spacing between power modules). The final implementation geometry should accommodate the cooling needs.

Table1.3. Requirements for the electrical parts of the RHODaS project from WP1

Parameter	
Length	400 mm
Width	380 mm
Height	30 mm
Power density[5]	100 kW/L
Maximum efficiency	> 97.5 %
DC bus voltage	Up to 1000 V (Overshoots limited to 1.2x)
Rated power	150 kW (Continuous <150 kW @ 650 VDC, subject to change with DC voltage)

1.1.2. Assumptions for estimations

The calculations use a simple lumped-parameter equivalent circuit steady-state model of the thermal circuits. Based on the thermal resistance and ambient temperature, the average junction temperature can be estimated with a lumped-parameter steady-state model. Peak temperature may be higher in transients.

$$\underbrace{\Delta T}_{\text{Change of temperature across barrier}} \approx \underbrace{P_{loss}}_{\text{Power loss}} \cdot \underbrace{R_{rt}}_{\text{Thermal resistance}}$$

For the simplified case where we assume a constant case temperature, the junction temperature may be estimated as:

$$T_{junction} \approx T_{case} + \underbrace{P_{loss} \cdot R_{th}}_{\Delta T}$$

Maximum losses allowed may also be calculated based on the reverse calculation:

$$\frac{T_{\text{junction_max}} - T_{case}}{R_{th}} = P_{\text{loss_max}}$$ (See Appendix E – Ideal load calculations for more details.)

The design target for the cooling system is to have a $\Delta T < 20K$ relative to the cooling liquid.

With the following assumptions, an estimated equivalent thermal resistance can be made:

- Flow of glycol: $Q_{glykol} = 0.158\, L/s$ with a 38% glycol water mixture. This can be operated with the pump shown in Appendix C – Pump curves for Grundfos Magna3 25-60.
- Heatsink fins of 5mm height

[5] Converter power density excluding cold plate and auxiliary connections.

- Fin cylinders in 20% of the area with a fin efficiency of 50%
- $60\mu m$ thick thermalpaste DowCorning 340.5F[6]
- One heatsink Meccal PBS500 132 at 500mm length with a forced airflow of $1600\,m^3/h$.

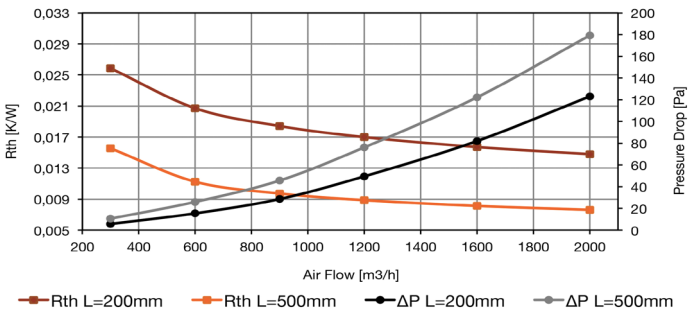

Figure 1.1. Thermal resistance for Meccal PBS500 132 at 500mm length with a forced airflow

- The resulting estimated thermal resistance for the thermal paste + heatsink + glycol + cooling to ambient is estimated to be: $R_{th,combined} \approx 40\,mK/W = 0.040\,K/W$ that is approximately 1/3 of the thermal resistance of the powermodule.
- The ambient temperature is assumed to be constant 50.

1.1.3. Estimated temperatures based on assumptions

Table1.4. Junction temperature estimation based on different switching frequency

f_{switch}/kHz	P_{loss}/W	avg. Junction Temp./C
70	5200	**183**
50	3800	152
35	2700	129
20	1700	107

So, for 70kHz, it is based on the assumptions impossible, but 50 kHz may be possible under good conditions. Design choices that increase the thermal resistance may make even 50 kHz difficult to achieve.

[6] The thermal interface material dimensions and performance are highly dependent on the mechanical and electrical design of the converters. If isolated power modules with screw mounting are chosen, graphite thermal interface material may be used. If non-isolated modules are chosen, isolated thermal pads may be needed instead. The mounting force allowed by the PCB design determines the pressure that can be used and, thus, the de facto thickness of the thermal interface.

1.1.4. Design choices that increase thermal resistance of the interface

From Appendix A – Low power design mail on page, some design choices may increase the thermal resistance:

- *The thermally and mechanically simplest interface to handle is if the power transistors have a uniform well defined height relative to their thermal interface. If the distance is not clearly defined, this means that additional non-conductive flexible material (pads) between the heatsink and power module needs to be added → increased thermal resistance*[7]. Furthermore, uneven height heatsink may increase surface roughness since it is more difficult to machine and verify a good surface smoothness on an uneven surface.
- *If the heatsink mounting force applied is not well defined, this may require additional non-conductive flexible material between heatsink and power module needs to be added → increased thermal resistance. If the inverter is glued to the thermal interface, it will also require multiple spare inverters + multiple heatsinks since they will be difficult/impossible to disassemble once mounted on the cooling circuit.*
- *The non-conductive flexible material (pads) must have sufficient dielectric strength (more than 2 times the DC-link voltage) → thicker pads → increased thermal resistance. This extra material is only needed if the power module does not have its own internal electrical insulation.*

A bigger thermal resistance also means that the amount of material needed to cool the inverter increases→ higher cost. Increased losses also mean the amount of material needed to cool the inverter increases→ higher cost.

7 See https://multimedia.3m.com/mws/media/122268O/characteristics-of-thermal-interface-materials.pdf.

1.1.5. Proposed interface design

- For the low-power inverter: The thermal interface material has to be non-conductive7F[8] and compressible8F[9] → Silicone/non silicone materials.
- For the low-power inverter: Mounting with epoxy glue and potting glue9F[10] and using a vice to force the materials in contact. Method needs testing.
- For the low power inverter: The thermal transfer in copper tracks on the PCB and through VIAs need to be simulated du the high losses.
- For the high-power inverter: The thermal interface material can be conductive10F[11] and compressible11F[12]. → Silicone/non silicone materials or graphite12F[13]
- Copper may be needed for the heatsink for the high-power design and the lower-power design may be sufficiently cooled with an aluminium heatsink.
- For both high and lower power inverters the heatsink will be made up of multiple parts→ increased volume
- Since both high and low power inverters do not have a uniform height, thermal resistance will probably be increased due to lower surface smoothness.
- The cooling system will either use a manifold design for the glycol/water circuit or separate glycol circuits.

1.1.6. Partial conclusion for the thermal interface

Design choices are always trade-offs, and certain design choices in the low and high-power inverters may lead to increased thermal resistance and thus lowered cooling. Methods to adjust for the design choices have been presented, as well as their possible consequences. The design should be able to dissipate 3kW of heat with a differential temperature less than 20C from the heatsink surface to the ambient. A solution is to consider different operating regions where we may have different thermal envelopes, e.g., higher power if ambient temperatures are low compared to the worst case with high ambient temperature. The next section describes the proposed thermal architecture used for the project.

8 Since the transistors are not isolated
9 To compensate for the ildefined mounting force and distances.
10 https://www.intertronics.co.uk/product/wacker-thermally-conductive-silicone-adhesives-potting-compounds/ seen 15/6 2023.
11 It assumed the chosen power modules have sufficient isolation.
12 To compensate for the ildefined distances.
13 https://www.fischerelektronik.de/web_fischer/en_GB/heatsinks/E01.01.002/High%20thermoconducting%20graphite%20foils/search.xhtml seen 15/6 2023. But mounting force will need to be high to deform the graphite sheets.

1.2. Proposed thermal architecture

1.2.1. Hardware platform for the cooling system

The hydraulic hardware is shown below and consists of a Thermal Control Unit (TCU), a cold plate, a pump, and a radiator with a fan. The cold plate absorbs the heat from the inverter and transfers the heat to the cooling liquid. The pump ensures the cooling liquid is passing through the radiator with sufficient flow. As the liquid is passed through the radiator, a fan ensures sufficient air is blown through the radiator too cool the liquid to the desired temperature. The TCU controls the pump for the cooling liquid and the fan for the radiator to ensure that sufficient flow is present, but unneeded excessive flow is not produced.

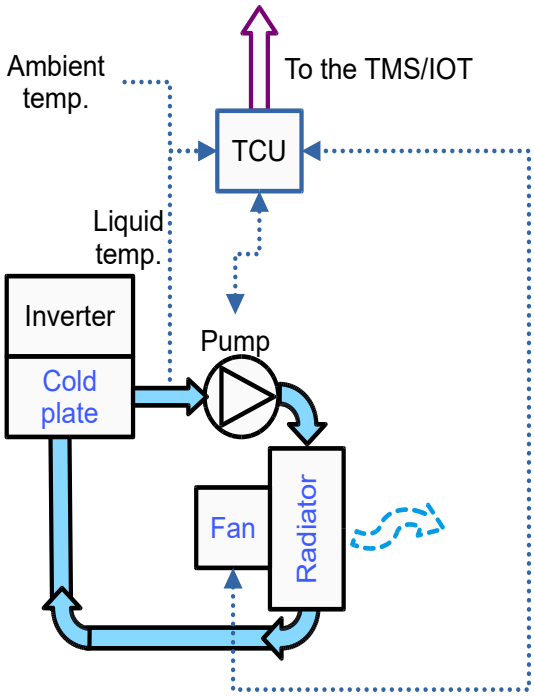

Figure 1.2. Designed Hydraulic system

The cold plate size is determined by the design of the inverter. The components chosen here are the preliminary components chosen, since they also may be impacted by the inverter design. The two temperature sensors are PT1000 sensors connected to the TCU, as shown in the figure.
The TCU consists of an Olimexino Stm32F3 microcontroller with CAN communication chosen elsewhere. If long distances are needed, optical cables may be needed, such as IF-E10.
The TCU controls the pumps and fans to keep the glycol-water coolant mixture at a relative constant temperature of approximately 80 °C. The TCU then sends the estimated flow/estimated differential pressure experienced by the pump to the IOT platform. The chosen KSB Calio 32-120 pump has an internal rough estimate of both differential pressure and flow rate of the pump. The preliminary radiator chosen is a standard low-cost car radiator (NISSENS 606514) and the preliminary fan is also a standard automotive fan (FEBI BILSTEIN 107256). The glycol chosen is shown in the table below:

Table1.5. Glycol selection

Manufacturer	Name	Concentration	Minimum operating point
GLYKOL & SOLE GmbH	GLYKOSOL N	34%	-20 C
GLYKOL & SOLE GmbH	GLYKOSOL N	44%	-30 C

Depending on the power module chosen, a thermal sensor/sensorless method needs to be chosen. This is the most critical sensor since it needs to be able to measure fast enough to detect thermal runaway in the power module. It would normally be included in most high-power integrated power modules. It still requires a thermal model of the system since the thermal resistance from the sensor to the power module junction may result in a significant difference between the measured temperature and the power module junction temperature.

1.2.2. Software for the cooling platform and the TMS

The thermal management system has two major tasks: ensuring sufficient cooling under normal conditions and reducing inverter output during abnormal conditions. The losses of the inverter are related to the current passing through the power module, and e.g., its equivalent on-state resistance may approximate the conduction losses in a MOSFET. Ignoring temperature dependency, the conduction losses increase with the current squared. So, half current means a quarter of the conduction losses. Since the current controller is orders of magnitude faster than the pumps, the current controller in case of abnormal situations, would normally handle the fastest temperature control. This may be done by limiting the current reference of the motor current controls. Under normal conditions, the pump and fan control performed by the TCU should be sufficient. A simple proportional integral controller should suffice for normal TCU operation.

1.2.3. Detailed hydraulic architecture

As described elsewhere, the inverter teams have decided to have separate heights and boards for SiC and GaN modules. There is also significant spacing between the different modules. Since the losses may also be significantly different from the SIC half bridges to the T-section GaN, two parallel manifold structures are proposed for the RHODaS cooling system shown in Figure 1.3.

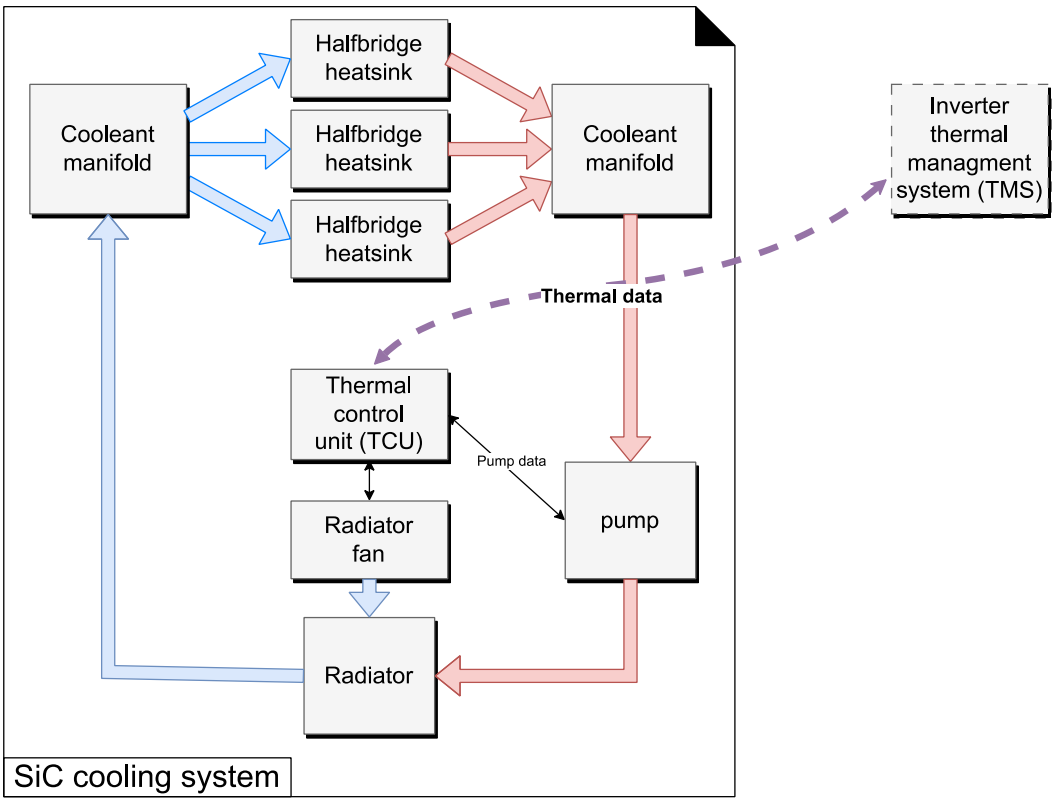

Figure 1.3. Two parallel manifold structures proposed for the RHODaS cooling system

The thermal system, excluding the inverter TMS, consists of:

- Cooleant manifold:
  - Since the heatsinks are separated even within the same type of semiconductor and to keep the pumps losses low, the manifold ensures that the differential pressure across the three parallel cooling branches is roughly equivalent.
  - Thermal interface material sits between the power modules and the heatsink. If the thermal interface also needs to ensure electrical isolation, the thermal resistance will likely also increase and exclude thermally good interface materials such as graphite due to graphite's conductivity.
  - The heatsinks are the interface between the thermal interface material and the cooling liquid. The basic task is to heat up the liquid as effectively13F [14] as possible

14 Efficiency for the heatsink is defined as low a thermal resistance as possible. Maximum thermal resistance for the heatsink surface to liquid is $\frac{20K}{3000W} = \frac{2}{300}\frac{K}{W}$ for all heatsinks combined in parallel.

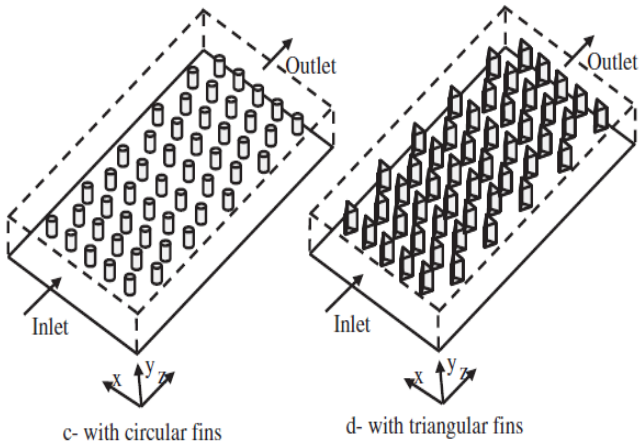

Figure 1.4. Proposed heatsink from [1], the paper focuses on comparing different cooling designs

The basic cooling principle is to have the coolant going into the inlet heated up and exiting through the outlet.

- The Thermal control unit (TCU) may directly control the coolant pumps and the radiator fan14F[15]. Based on the sensor input the pump flow and radiator fan speed may be reduced/increased to ensure sufficient cooling within the operational ambient envelope.
- To ensure sufficient coolant for the heatsink, the pump speed is controlled. The TCU
- The radiator will with radiation and convection, dissipate the heat from the coolant to ambient air.
- The radiator fan controls the forced convection.
- The inverter thermal management system (TMS) is described in a separate section.

15 The cooleant pump and radiator fan may also be controlled by failsafe logic such as NXP MFS2613AMDA2AD.

1.2.4. Inverter thermal management system (TMS)

The thermal management system (TMS) in the inverter is responsible for sending sensor data to the TCU and ensuring the motor current is limited, so the inverter stays within the thermal envelope.

1.2.4.1. The relation from output power to the motor current

The truck output power (P_{out} is crudely approximated by:

$$P_{out} \approx \frac{d}{dt}W \approx F_{load} \cdot v\text{-}_{truck}, \quad (1)$$

where W is the work done by the truck, F_{load} is the resulting force on the truck, and $v\text{-}_{truck}$ is the truck velocity. The shaft power ($P\text{-}_{shaft}$) is similarly proportional to:

$$P\text{-}_{shaft} \approx \tau_{motor} \cdot \omega \approx \frac{P_{out}}{\eta_{gear}} \approx \frac{F_{load} \cdot v\text{-}_{truck}}{\eta_{gear}}, \quad (2)$$

where τ_{motor} is the shaft torque, ω_{motor} is the motor radial speed, η_{gear} is the gear efficiency. Since the RHODaS motor is a permanent magnet synchronous motor (PMSM, the motor torque is proportional to the motor currents id & i_q in Clarke/Park transformed set of motor equations. Assuming sinusoidal back electro-motoric force/flux linkage and no stator & rotor saturation, we get:

$$\tau_{motor} = \frac{3}{2} \cdot p_{pair} \cdot \left(\underbrace{\lambda_{pm} \cdot i_q}_{\text{magnet torque}} - \underbrace{(L_q - L_d) \cdot i_d \cdot i_q}_{\text{reluctance torque}} \right) \quad (3)$$

where $p\text{-}_{pair}$ is the number of rotor magnet pole pairs, λ_{pm} is the permanent magnet flux linkage, $L\text{-}_q$ is the quadrature axis inductance, $L\text{-}_d$ is the direct axis inductance, $i\text{-}_d$ is the direct axis current. From equations (1)-(3), it is clear that the motor power will be at least linearly proportional to the quadrature motor current (i_q). If we assume the power losses are proportional to the motor power, then the power losses will be proportional to the motor current (i_q). So, the fastest way to limit the losses is to limit the motor current to stay within the thermal envelope of the motor and the inverter. This limit may be needed if/when unforeseen events happen, e.g., the ambient temperature is hotter than expected, losses are higher than expected, power module thermal interface material is not mounted properly, etcetera. But this also means that the TMS needs to be considered when designing the current control, since the current limits will be calculated based on ideally integrated power module temperature sensors or external sensors. The sensor can then be used to estimate the junction temperature of the semiconductors. An alternative would be a synchronized direct measurement of the on-state voltage drops over semiconductors or an estimation of the on-state voltage drop.

So, the inverter TMS needs to be able to set a current limit to enable the inverter to stay within safe operational limits.

1.2.5. Partial conclusion of thermal architecture

A proposed thermal architecture was presented, and some details regarding the components of the thermal architecture were also presented.

2. THERMAL MODELLING AND SIMULATIONS

This section provides a comprehensive overview of the key developments and crucial undertakings within T3.2 on Thermal Modelling and Simulations, within WP3 of the ROHDaS project. The primary goal of this task is to conduct 3D thermal and power loss modelling, encompassing both transient and steady-state time scales. These simulations are accomplished through the application of advanced methodologies, including Finite Element Analysis (FEA) and Computational Fluid Dynamics (CFD). The scope of this endeavour encompasses a wide range of passive and active components, such as WBG-based switching devices, inductors, capacitors, and the integrated cooling system. Advanced simulation software tools like ANSYS and COMSOL are employed. Furthermore, a simulation toolbox is developed by AU, which integrates suitable thermal prediction models to facilitate the estimation of power losses, efficiency, and thermal performance under varying simulation parameters and operating conditions. This document encapsulates the actions taken and the outcomes achieved in the T3.2 of WP3.

2.1. 3D Thermal Modelling of Heatsink

In this chapter, the thermal management system architecture, developed by the AU team in T3.1, serves as the basis for designing a 3D model for the heatsink. This architecture comprises a thermal control unit (TCU), a cold plate, a pump, and a radiator with a fan. The design process is guided by the specified operating conditions detailed in WP, which include parameters such as ambient air temperature and various driving conditions. furthermore, COMSOL Multiphysics is the chosen tool for simulating a variety of scenarios during the heat sink design process.

2.1.1. COMSOL Multiphysics and its advantages in design of the heatsink

In this subsection, let's delve deeper into the application of COMSOL Multiphysics and highlight its advantageous role in heatsink design, particularly within the realm of Multiphysics simulation. This versatile software platform excels in simulating and analysing complex systems by considering the interactions and coupling of multiple physical phenomena. In the context of heatsink design, COMSOL Multiphysics offers invaluable capabilities, especially in modelling heat transfer within solids and fluids, which are critical aspects of optimizing thermal management.

The use of COMSOL Multiphysics allows for a comprehensive exploration of the intricate interplay between heat transfer in solid materials, like the heatsink itself, and heat dissipation through the surrounding fluid medium, including the convective cooling effects of the TMS component and the heat transfer within the coolant. Its Multiphysics capabilities enable the addressing of diverse thermal challenges encountered in real-world applications, providing a deeper understanding of the system's behaviour under varying conditions.

Leveraging COMSOL Multiphysics is essential for fine-tuning heatsink design to enhance its efficiency and overall performance, ensuring it meets the specific requirements outlined in the previous tasks and adapts to different operating conditions. The next section will detail the methodologies of utilizing COMSOL Multiphysics in the heatsink design process.

In the next section, we will provide an in-depth exploration of the methodologies employed to harness the full potential of COMSOL Multiphysics in the heatsink design process.

2.1.2. Fundamental simulations in the COMSOL Multiphysics software

In this subsection, a systematic approach to address the intricate challenges of Multiphysics simulations is employed. It is imperative to dissect these complex problems into comprehensible components, and this is achieved by dividing the section into three distinct parts, each focusing on specific aspects of the simulation:

2.1.2.1. COMSOL Simulation with Solid Mechanics Physics:

The initial segment of this subsection is dedicated to simulating the solid mechanics aspect within a Multiphysics context. This approach is grounded in the pursuit of a foundational understanding of the mechanical behaviour exhibited by systems. By specifically isolating the solid mechanics component, we can delve into the impact of forces, deformations, and stresses on a defined structure. This allows for a thorough validation of the accuracy of 3D simulations by comparing results obtained through COMSOL simulations with those derived from mathematical calculations. This systematic methodology is indispensable for attaining a comprehensive comprehension of the mechanical responses within the system. To exemplify this, we opt for an elongation problem as a case study, primarily chosen for its simplicity in mathematical calculations. The initial case study involves the analysis of the expansion in the length of a mild steel rod following the application of a 100 kips force or load. The dimensions of the rod, with a diameter and length of 0.5 inches and 36 inches, respectively, are considered. The mathematical calculations and the results obtained through simulations in the COMSOL Multiphysics software consistently align, providing a mutual validation of the accuracy within the realm of 3D simulations. This congruence between analytical calculations and simulated outcomes serves as a confirmation of the reliability and precision of the simulation methodology employed.

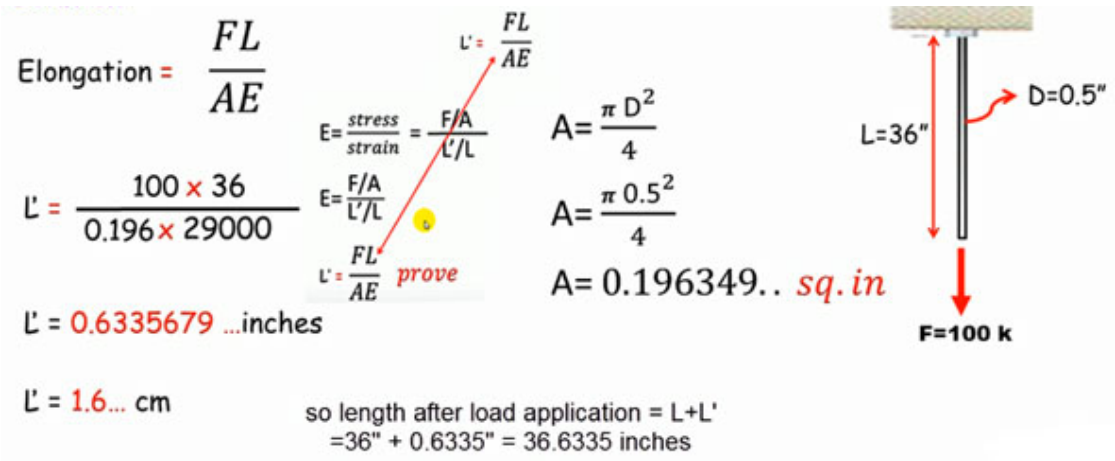

Figure 2.1. Rod elongation with its mathematical calculations

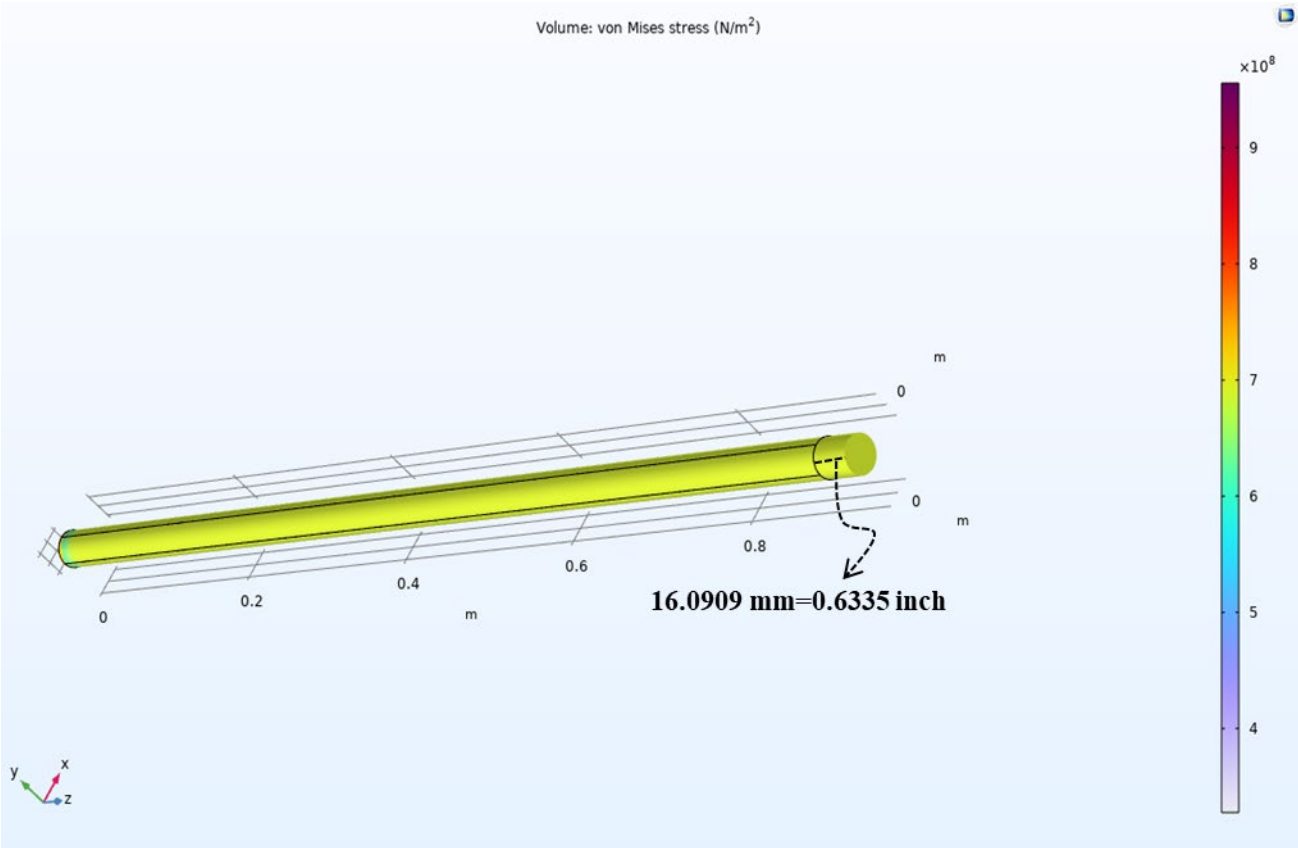

Figure 2.2. Rod elongation simulations in the COMSOL Multiphysics software

2.1.2.2. COMSOL Simulation with Heat Transfer in Solids Physics:

In the second part, our focus shifts to heat transfer within the solid components of the system. This step is pivotal in understanding how heat is conducted and distributed within the materials. Isolating heat transfer in solids helps us determine temperature gradients and thermal stresses, providing insights into the thermal performance of the system without the added complexity of fluid interactions. It is a necessary step to form a solid foundation for the subsequent stages of the simulation. In this stage we focused on the air cooled heatsink design and simulation in the small scale. This simulation helps us to understand the capability of the air cooled heatsinks and investigate if this type of cooling system can comply with the requirement of the project.

Following the design of the geometry and the establishment of a defined meshing strategy for the proposed structure, a thorough analysis is conducted on the designed air-cooled heatsink. The outcomes of this analysis are succinctly summarized in Figures 2.3-2.5. These figures encapsulate and present the key findings and performance characteristics of the air-cooled heatsink, providing a visual representation of the results obtained from the simulation. This comprehensive approach ensures a clear and concise presentation of the pertinent information derived from the analysis of the heatsink design.

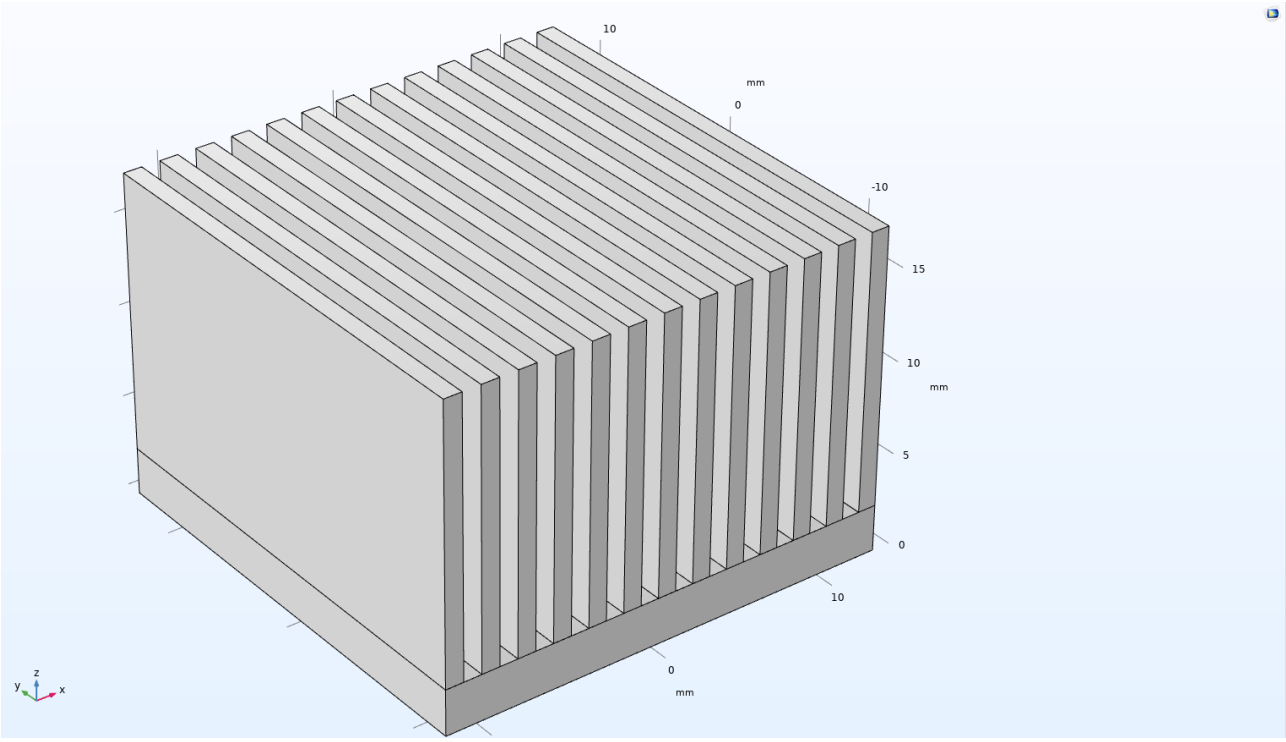

a) Air cooled heatsink geometry

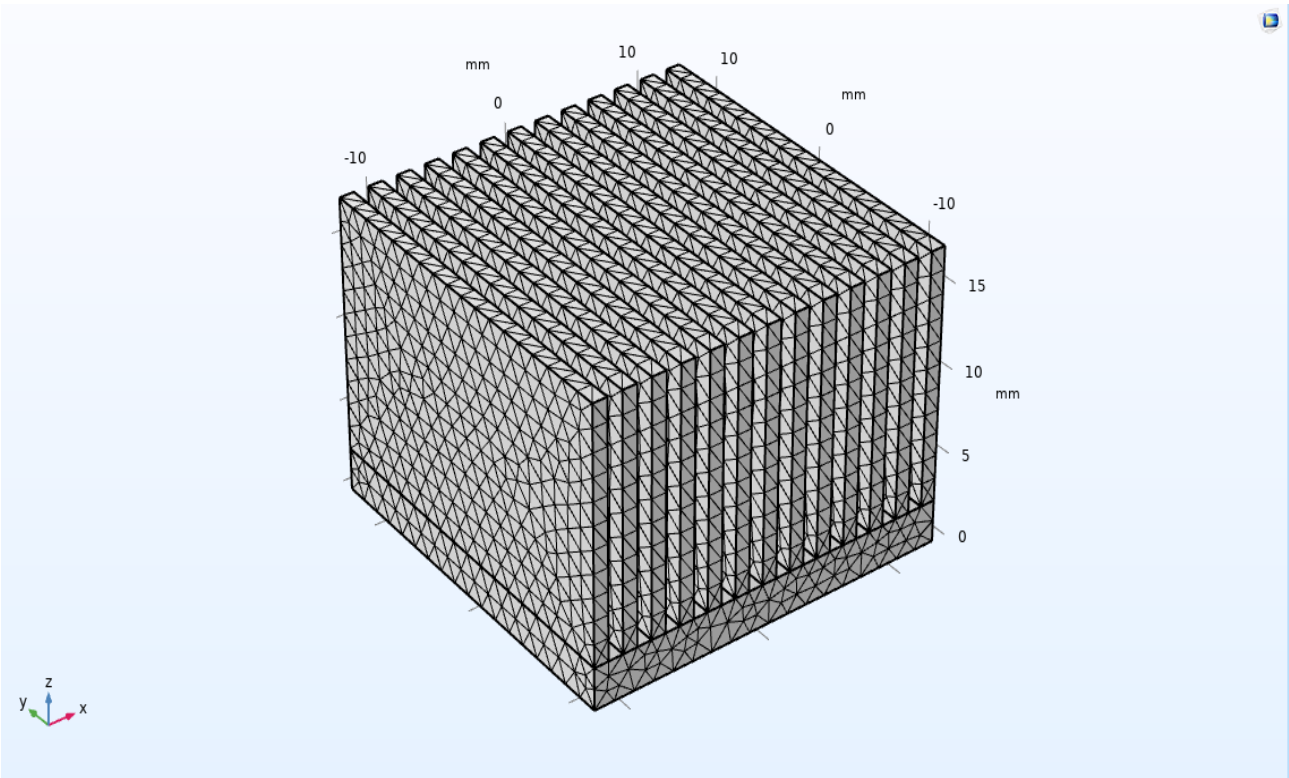

b) Air cooled heatsink meshing strategy

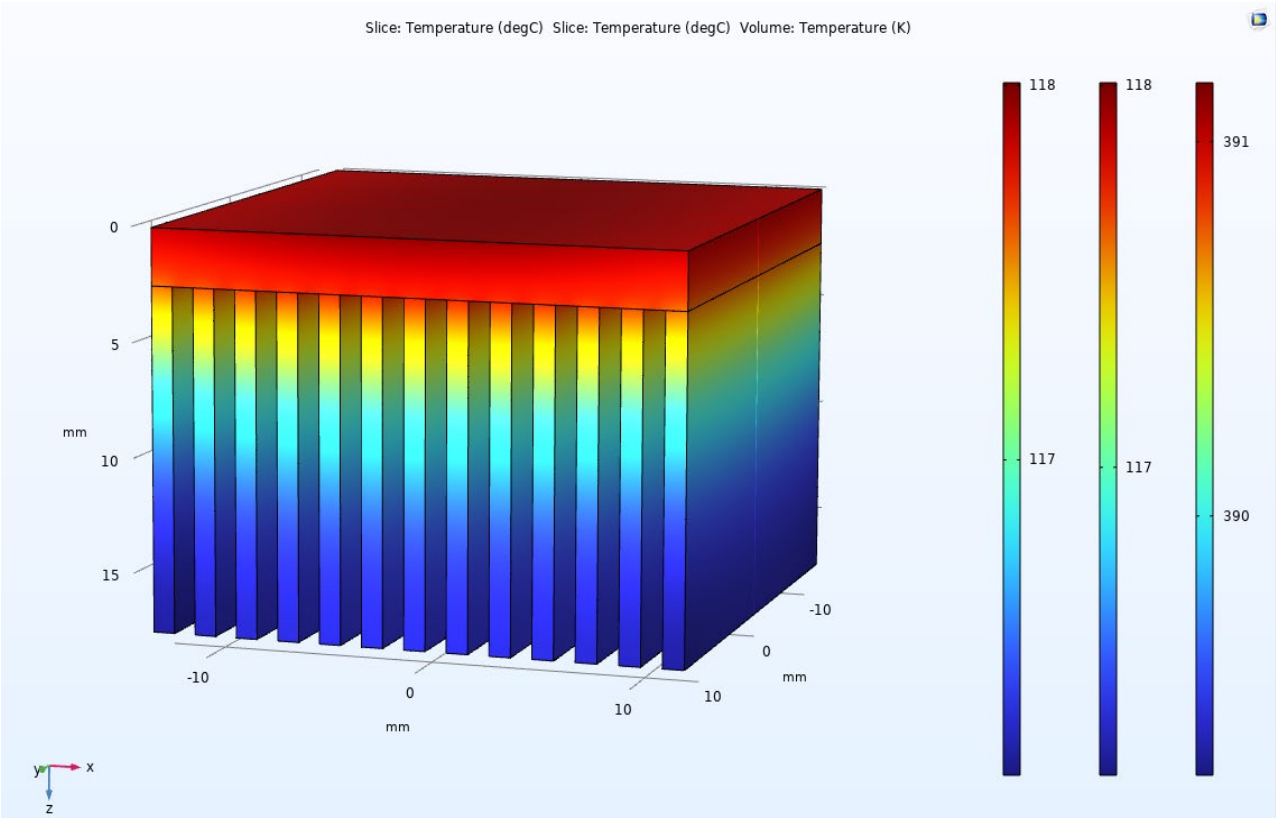

c) The results of temperature distribution in the designed air cooled heatsink

Figure 3. Air cooled heatsink design and simulation in the COMSOL Multiphysics software

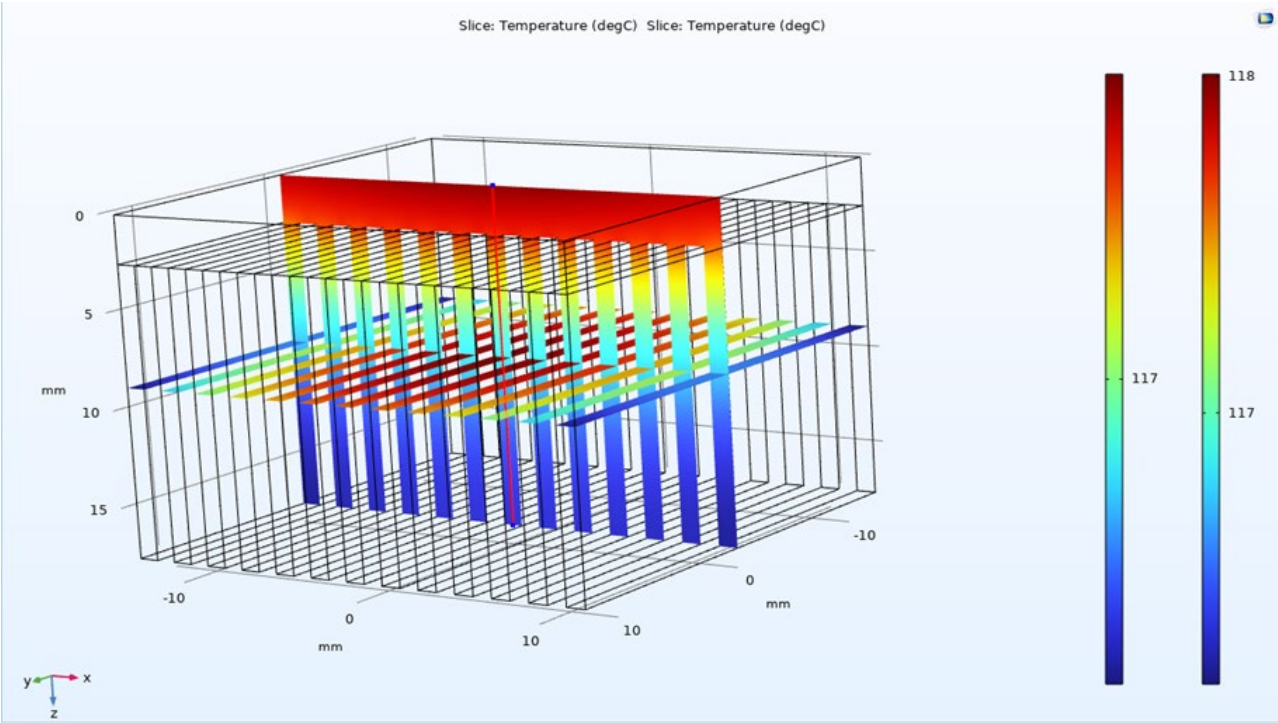

Figure 2.4. Results of temperature distribution inside two surfaces of the designed air-cooled heatsink

In Figure 2.3(a), elongated fins have been intricately crafted and positioned at the base of the heatsink to regulate the airflow. Figure 2.3(b) illustrates the meshing strategy employed in the design of the air-cooled heatsink. Moving on to Figure 2.3(c), it presents the temperature distribution results within the designed air-cooled heatsink subsequent to the application of a heat flux to the heatsink body. To gain a more in-depth understanding of the cooling behaviour of this heatsink, Figure 2.4 showcases the temperature distribution results within the two surfaces of the designed air-cooled heatsink. Furthermore, Figure 2.5 illustrates that the temperature increases progressively when moving from the corner to the centre of the heatsink.

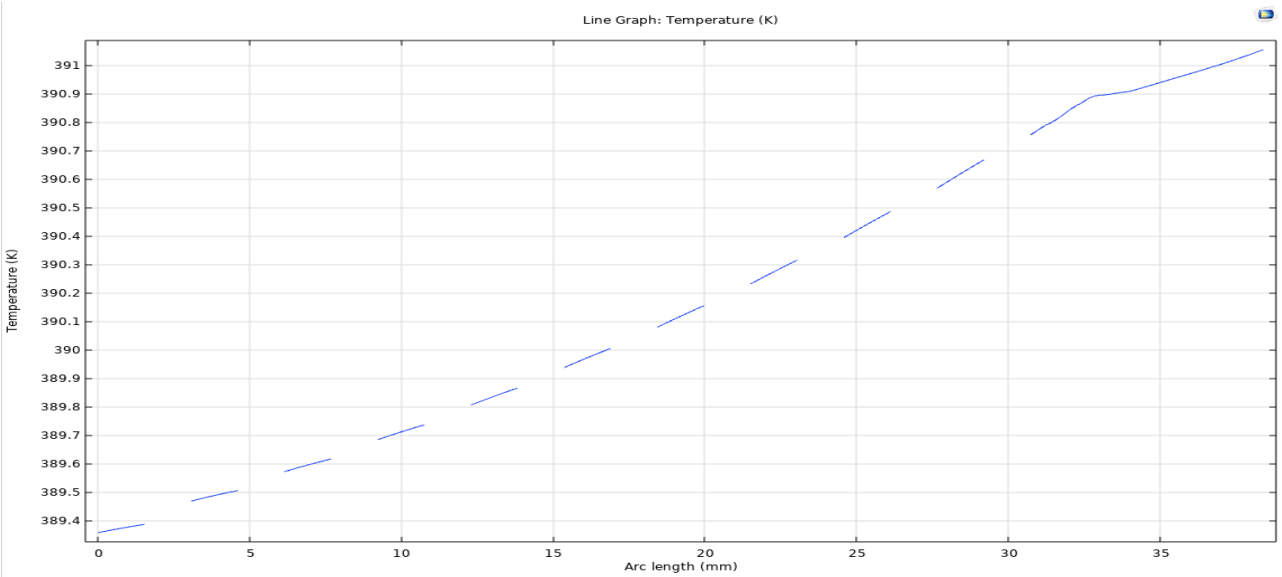

Figure 2.5. Results of temperature distribution over a line from a corner to the centre of the cold plate

In the realm of heatsink design, a critical consideration revolves around comprehending the ramifications of hot spots on power boards. These hot spots arise from the deliberate arrangement of switching elements in specific zones, necessitating a thorough investigation into their impact. To delve deeper into this phenomenon and gauge the viability of an alternative heatsink structure employing pins instead of conventional long fins, a simulation was undertaken.

The simulation protocol involved the strategic placement of a simulated hot spot at the top of the heatsink structure, mimicking a scenario where concentrated heat emanates from a specific source. To counterbalance and ameliorate potential temperature differentials, a series of pins were precisely simulated at the base of the hot spot region. This approach aimed to dissipate the accumulated heat efficiently and maintain optimal temperature distribution across the heatsink.

The outcomes of the simulation, illustrated in Figure 2.6, offer insights into the comparative effectiveness of pins versus long fins in the cooling process. The results confirm that the utilization of pins exhibits a marked enhancement in cooling efficiency compared to traditional long fins. This empirical validation underscores the potential advantages of incorporating a pin-based heatsink design for optimizing thermal management strategies.

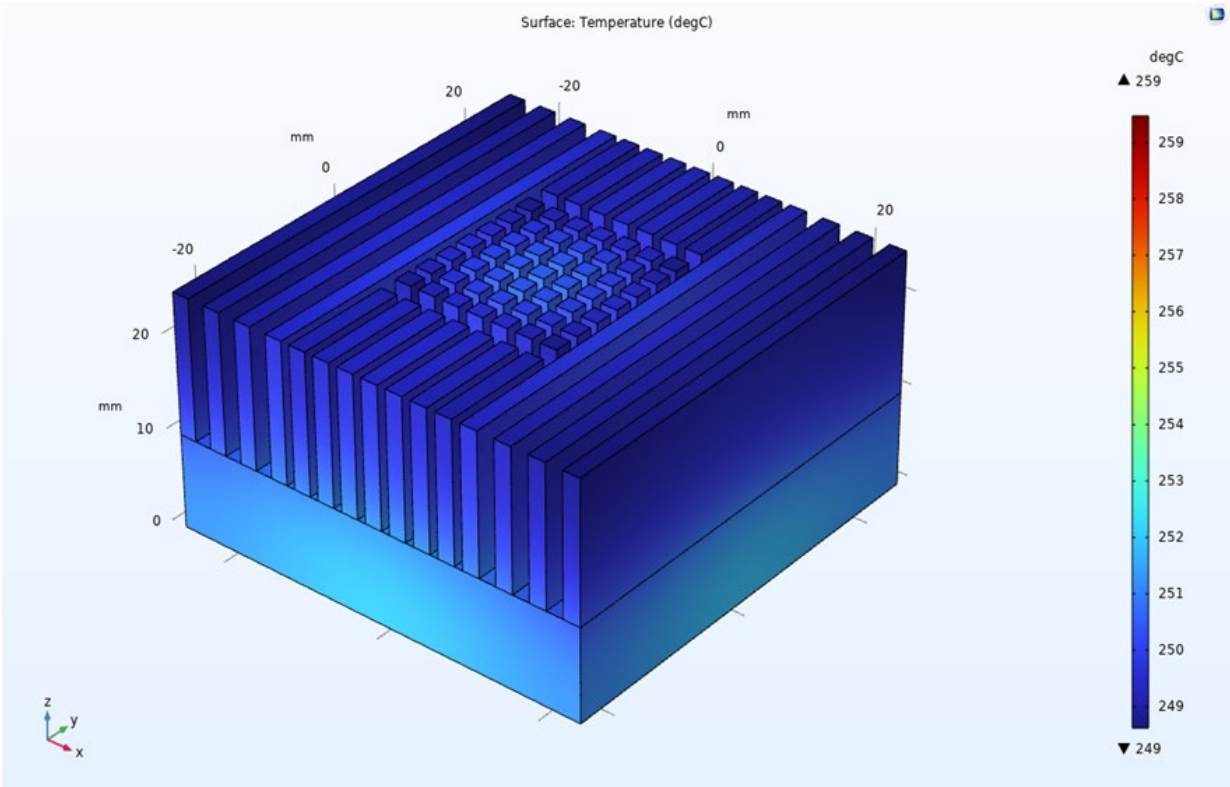

a) Air cooled heatsink geometry with various types of fins and Hot Spots

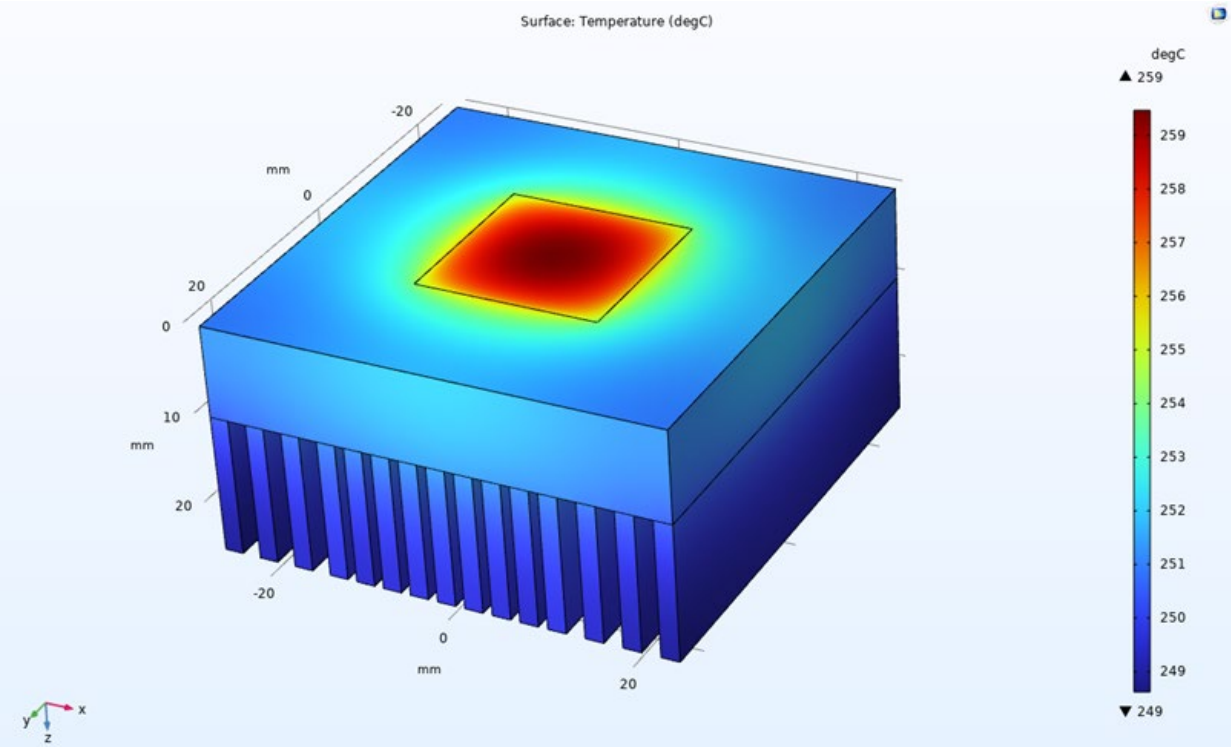

b) The results of temperature distribution in the designed heatsink with various types of fins and Hot Spots

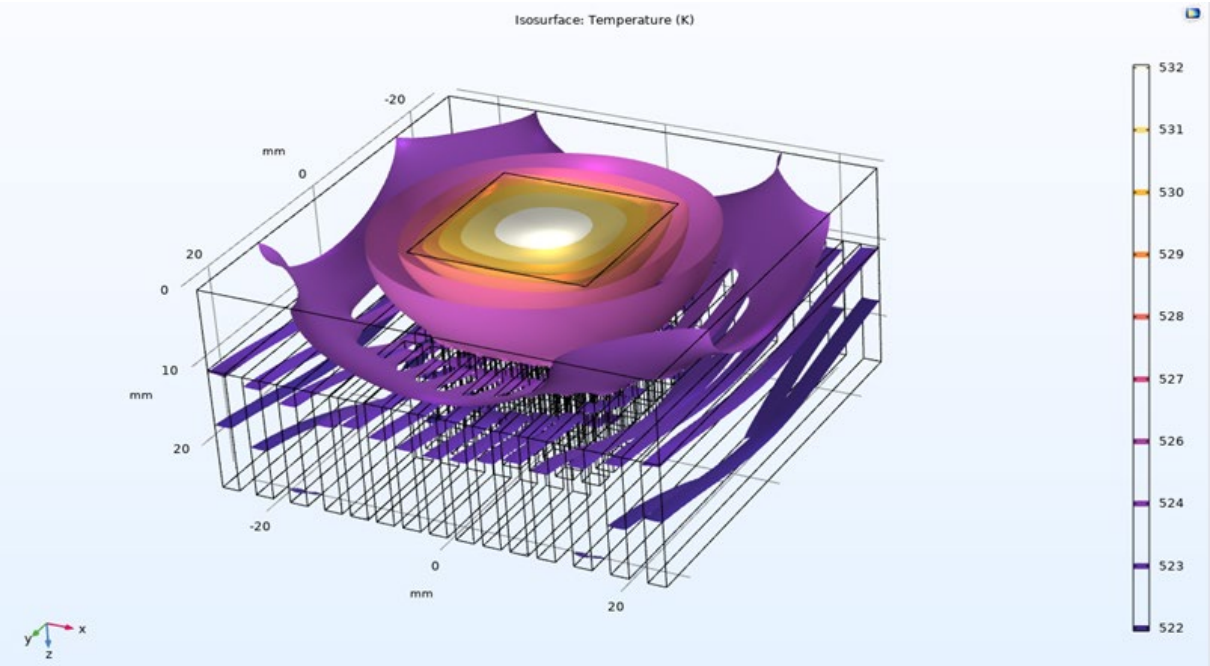

c) The results of temperature surface in the heatsink with various types of fins and Hot Spots

Figure 2.6. Air cooled heatsink design and simulation with various types of fins and Hot Spots

2.1.2.3. COMSOL Simulation with Heat Transfer in Solids and Fluids Physics

The final part of this subsection introduces the interaction between heat transfer in both solid components and fluids.

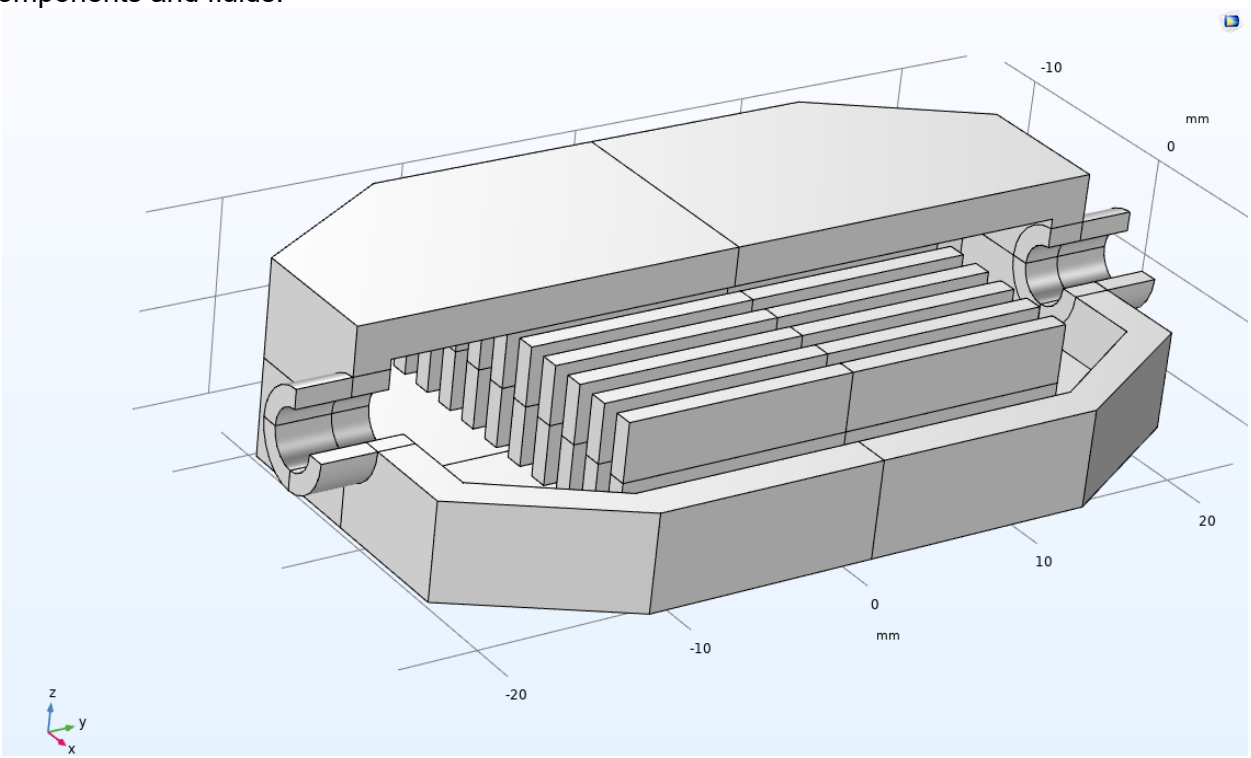

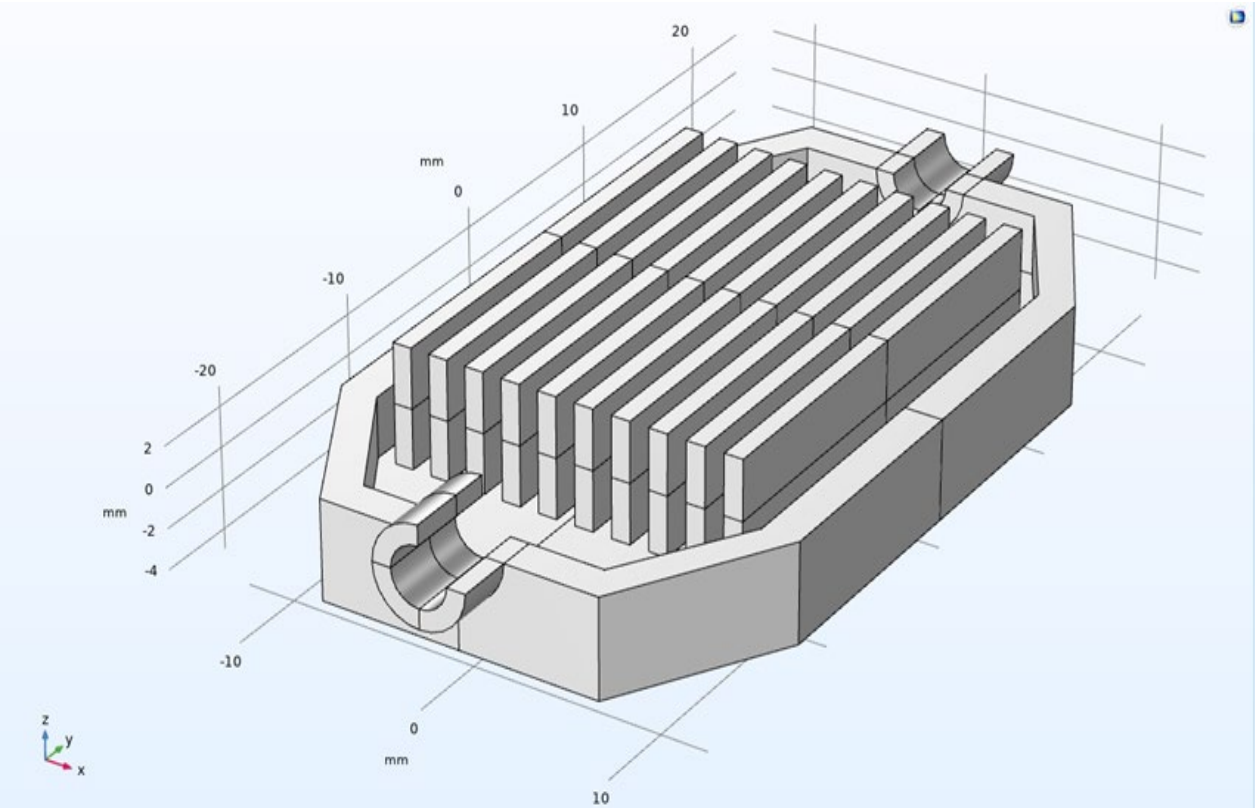

Figure 2.7. The primary configuration of the liquid-cooled heatsink simulated in COMSOL

This step is where the full complexity of the Multiphysics problem is addressed. By combining the insights gained from the previous two parts, we can now comprehensively model the system's behaviour. This includes the intricate interplay of heat conduction in solids and the convection of heat in the surrounding fluid medium. It is at this stage that we approach the problem in its entirety, accounting for all relevant physical phenomena. Subsequently, a foundational model in COMSOL Multiphysics is simulated by AU to facilitate finite element analysis of the liquid-cooled heatsink system under various topological and boundary conditions. The primary configuration of the designed liquid-cooled heatsink, characterized by a cylindrical inlet and outlet, a copper-based body, and multiple elongated fins, is shown in Figure 2.7. The assessment of meshing procedures and accuracy is of paramount importance in the realm of finite element analysis, particularly for liquid-cooled heatsinks. This rigorous examination ensures the reliability of simulation results, their proximity to real-world scenarios, and their applicability for decision-making and design optimization in thermal management applications. In light of this, a comprehensive analysis was conducted to investigate the influence of the meshing scheme on computational time and the precision of outcomes. This step was undertaken to strike a balance between modeling accuracy and computational efficiency, a critical consideration in heatsink model optimization. The result of applying the meshing scheme on described heatsink geometry is depicted in Figure 2.8.

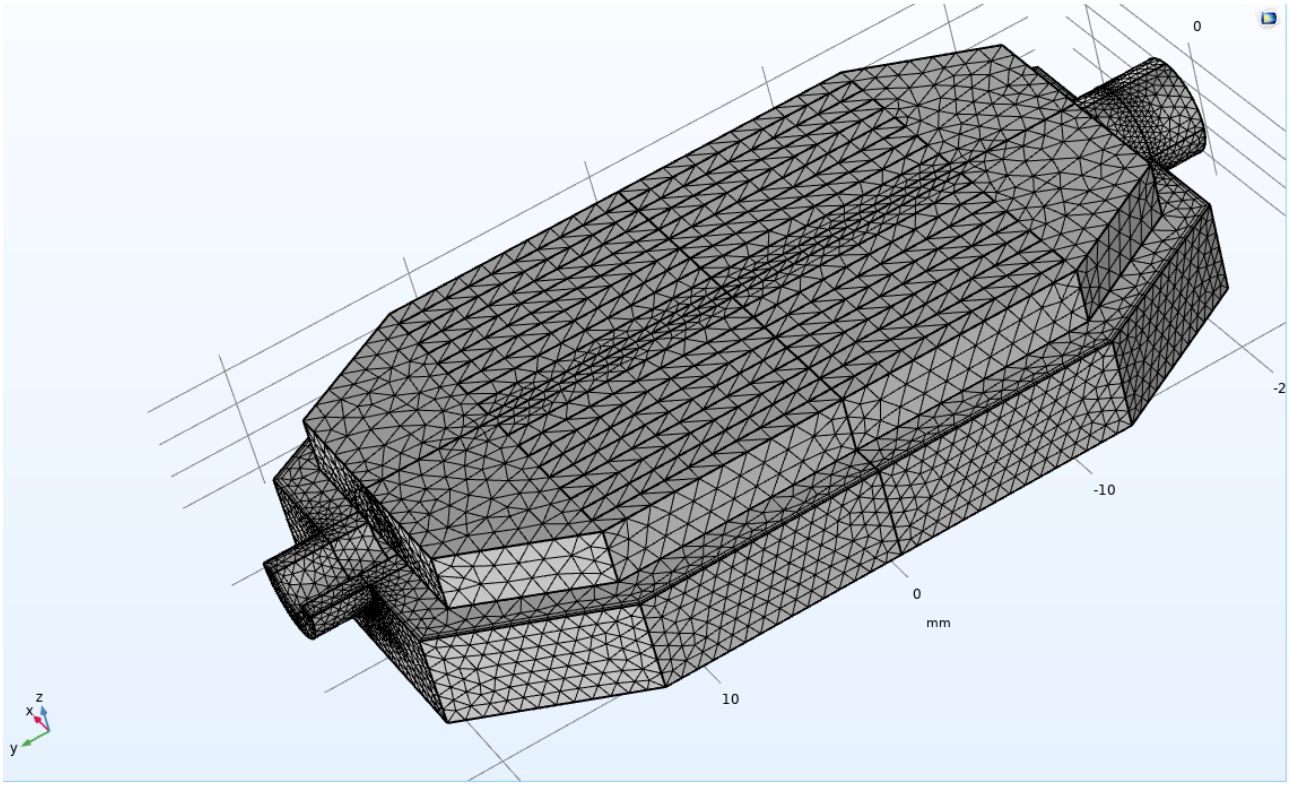

Figure 2.8. The result of applying the meshing scheme the liquid-cooled heatsink

2.1.2.4. Symmetry Tools and Heat Transfer Analysis

Our simulation strategically employed symmetry tools within the framework of finite element analysis. The integration of symmetry tools in software platforms like COMSOL or similar FEA applications is instrumental in curtailing computational time and resource utilization. The application of symmetry enables the modeling of a fraction of the authentic geometry, leading to more streamlined models, faster solution times, and expeditious parametric investigations. It streamlines the setup process, diminishes meshing complexities, and proves invaluable for design enhancement, all while affording essential insights into system behavior. The outcomes of heat transfer in both the solid and fluid components of the simulated liquid-cooled heatsink are presented in Figures 2.9-2.11.

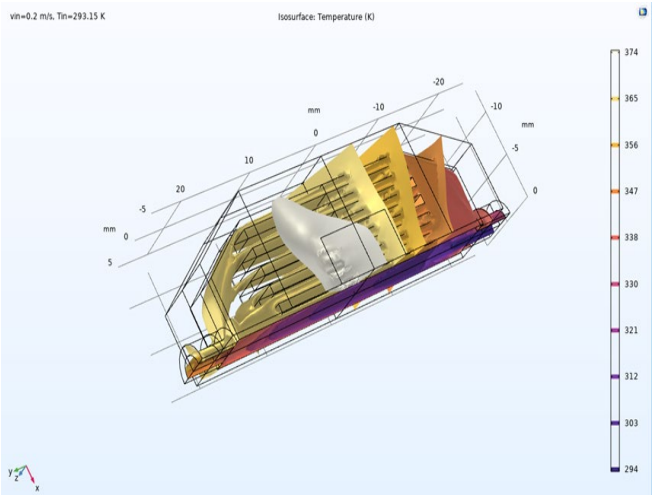
vin=0.2 m/s, Tin=293.15 K
Isosurface: Temperature (K)
374
365
356
347
338
330
321
312
303
294

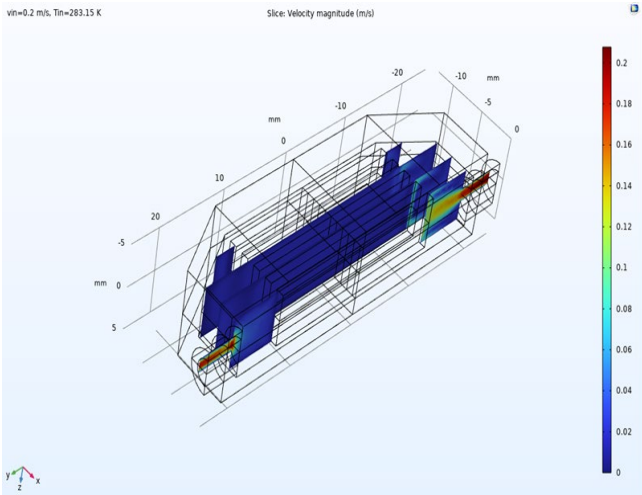
vin=0.2 m/s, Tin=283.15 K
Slice: Velocity magnitude (m/s)
0.2
0.18
0.16
0.14
0.12
0.1
0.08
0.06
0.04
0.02
0

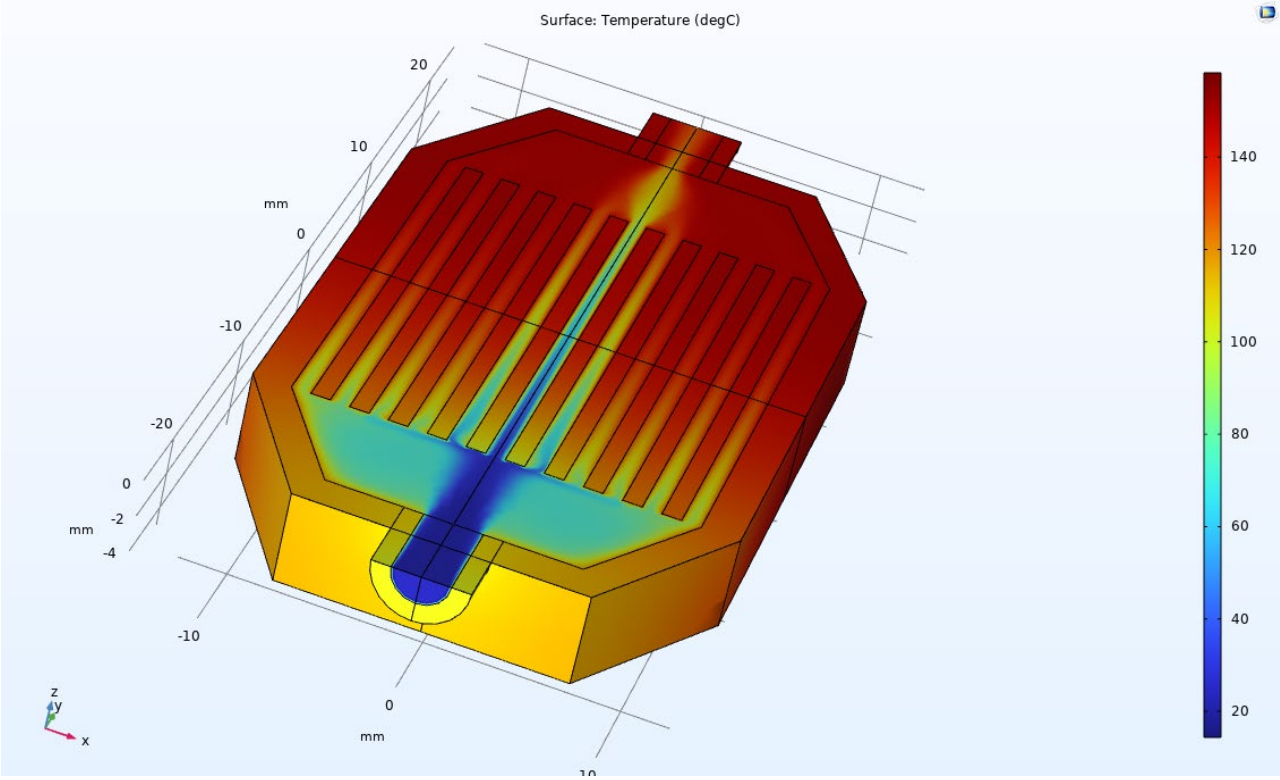
Surface: Temperature (degC)
140
120
100
80
60
40
20

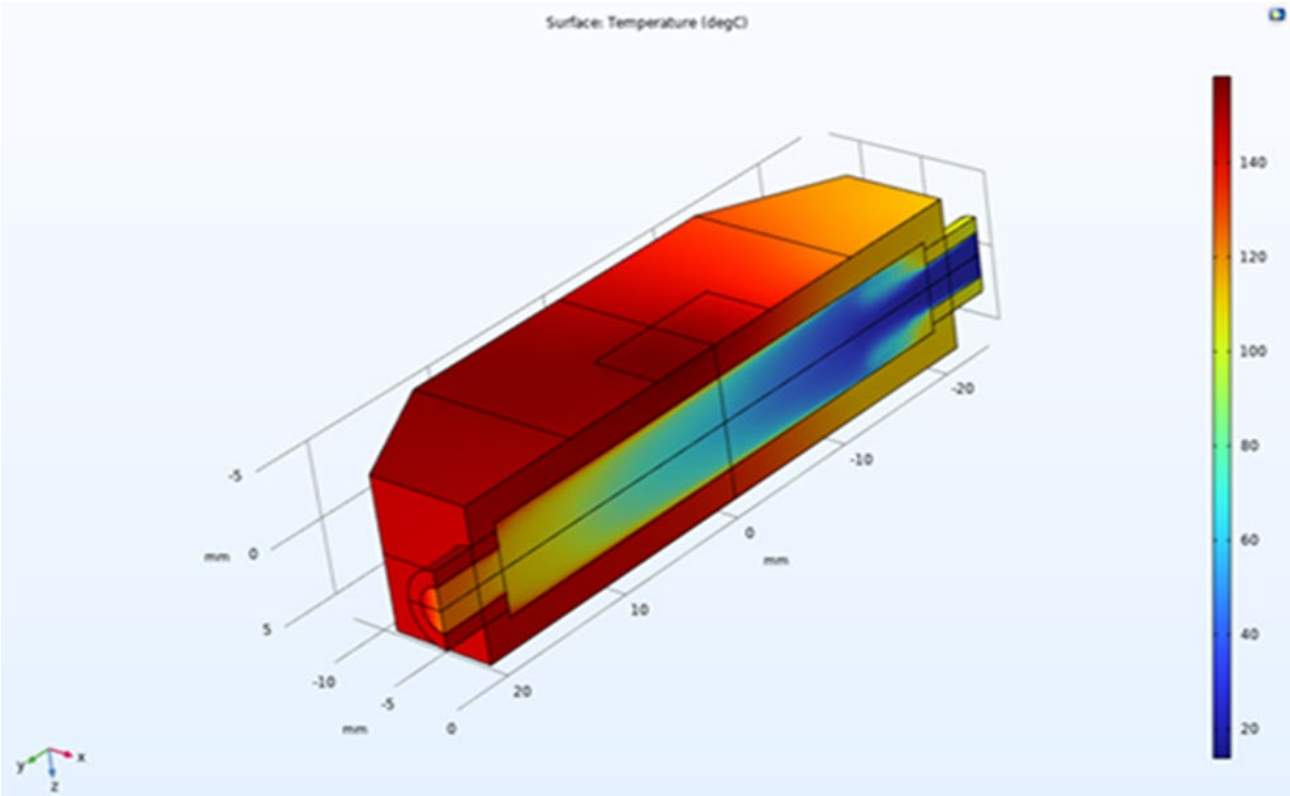

Figure 2.9. The result of temperature distribution in the liquid-cooled heatsink

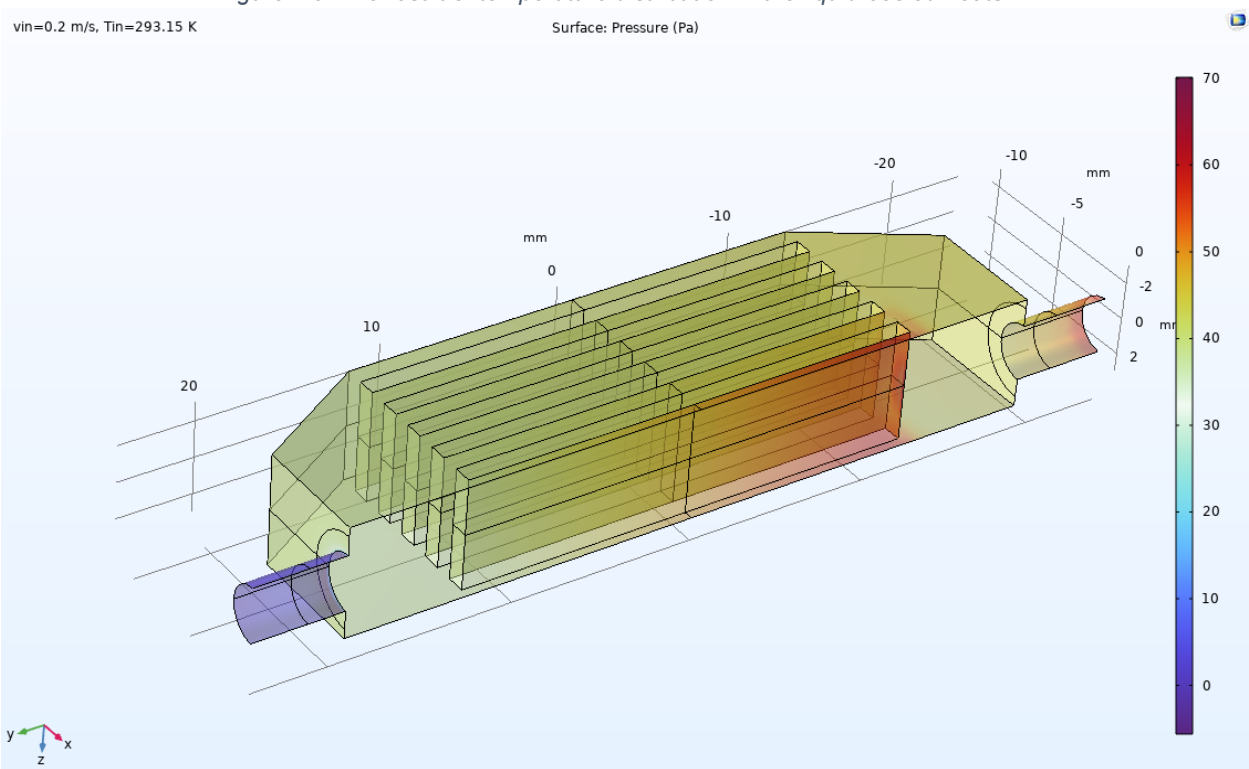

Figure 2.10. The result of flow pressure distribution in the liquid-cooled heatsink

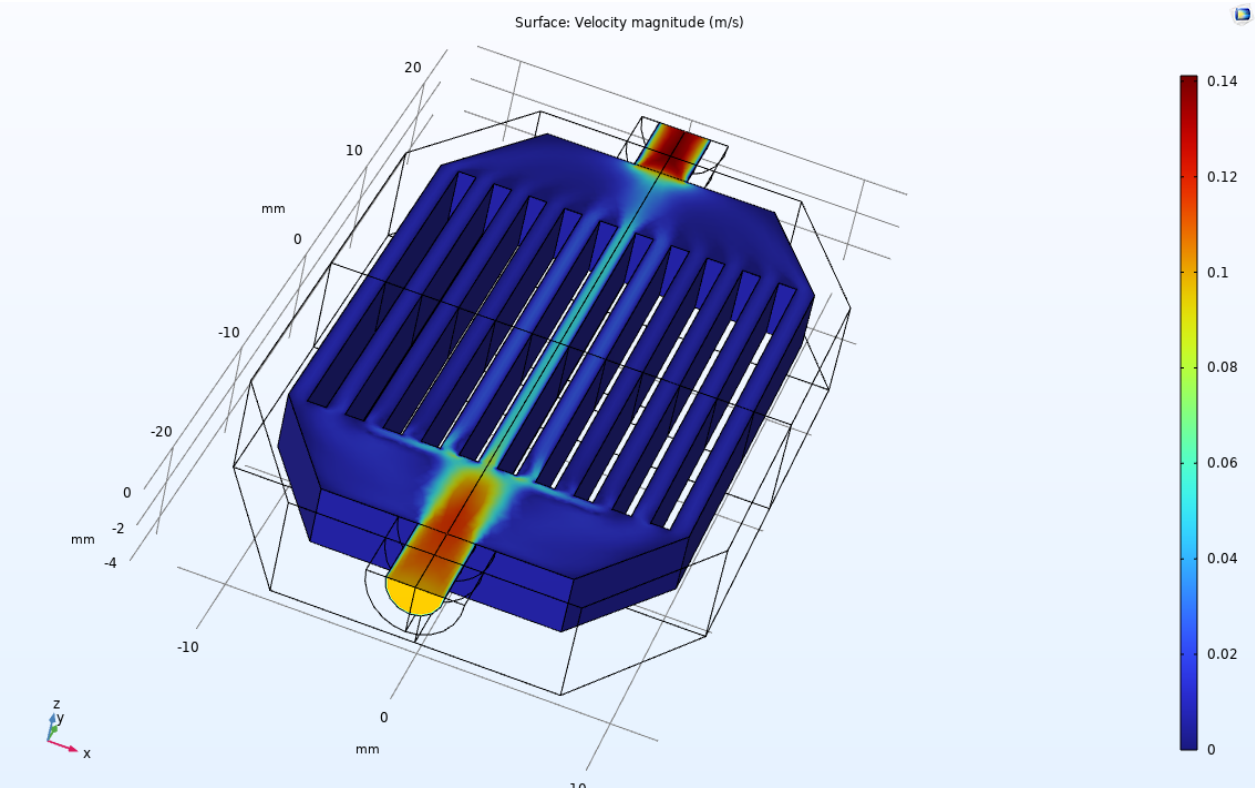

Figure 2.11. The result of flow velocity distribution in the liquid-cooled heatsink

To delve into the intricacies of heat transfer patterns and temperature distribution, an analysis of temperature distribution across the cold plate and the temperature difference from one corner to the center of the cold plate has been conducted. Figures 2.12-2.13 present a comprehensive overview of these findings.

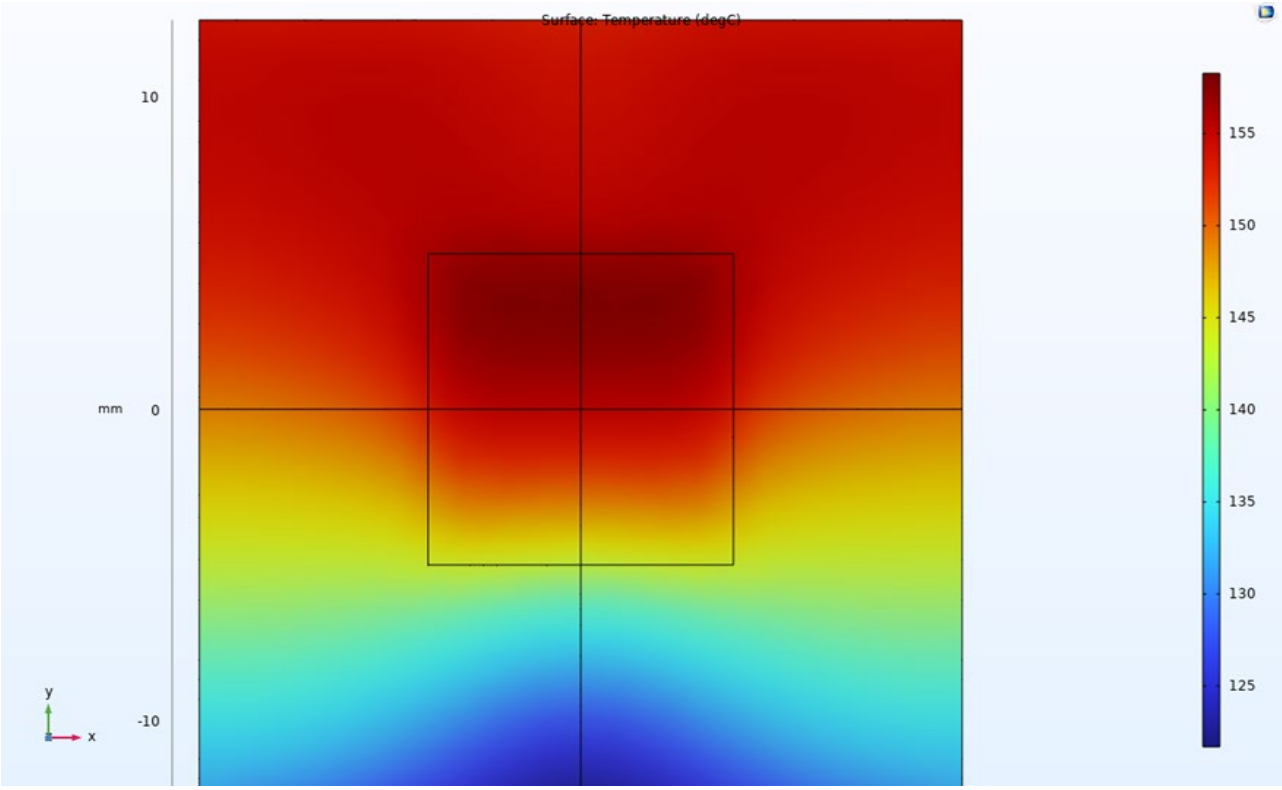

Figure 2.12. The result of temperature distribution in the cold plate of liquid-cooled heatsink

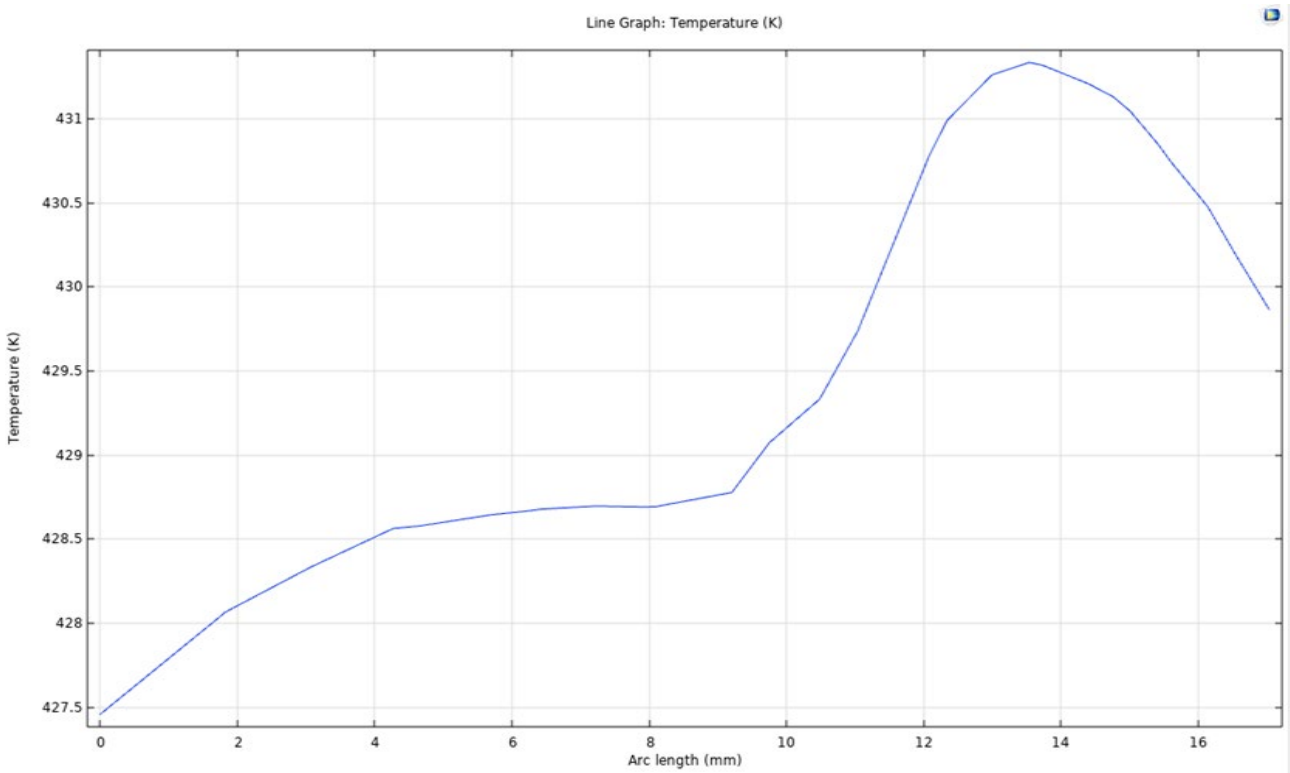

Figure 2.13. Results of temperature distribution over a line from a corner to the center of the cold plate of liquid-cooled heatsink

2.1.2.5. *Parameter Sweeping Analysis*

To delve into the ramifications of design parameters on thermal and fluid flow performance, the AU team conducted a sweeping analysis encompassing inlet velocity and temperature. This analysis serves to uncover optimal values, assess parameter sensitivities, predict heatsink performance across varying operating conditions, and attain a balance between design objectives. The results of the parameter sweeping analysis, focusing on inlet voltage and temperature, are succinctly illustrated in Figure 2.14. This figure illustrates the temperature variation along a line extending from the corner of the heatsink body to its bottom center.

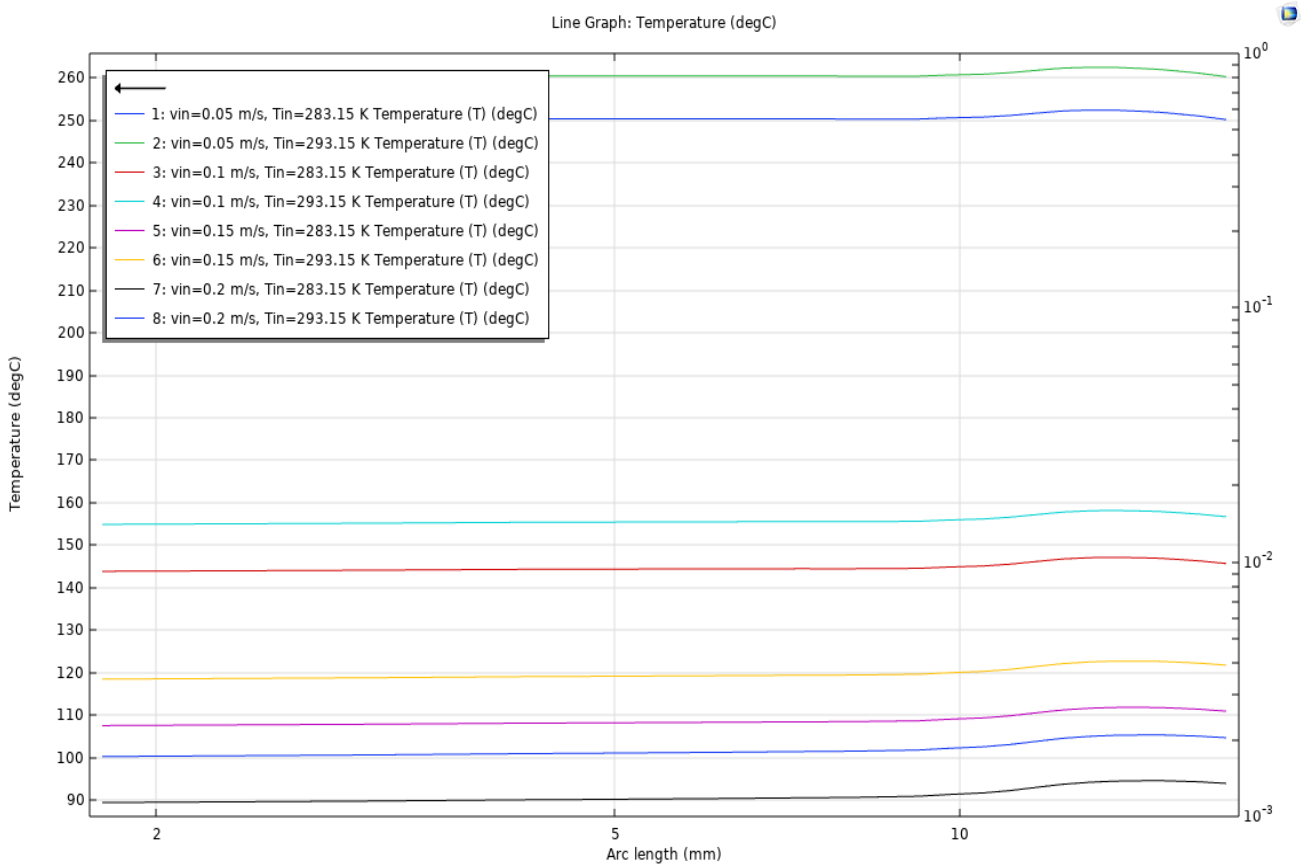

Figure 2.14. The result of inlet velocity and temperature sweeping analysis in the liquid-cooled heatsink

To further validate the thermal performance of the designed liquid-cooled heatsink, during the parameter sweeping analysis, the simulation results at an inlet velocity of 0.2 m/s and an inlet temperature of 293.15 K are illustrated in Figure 2.15.

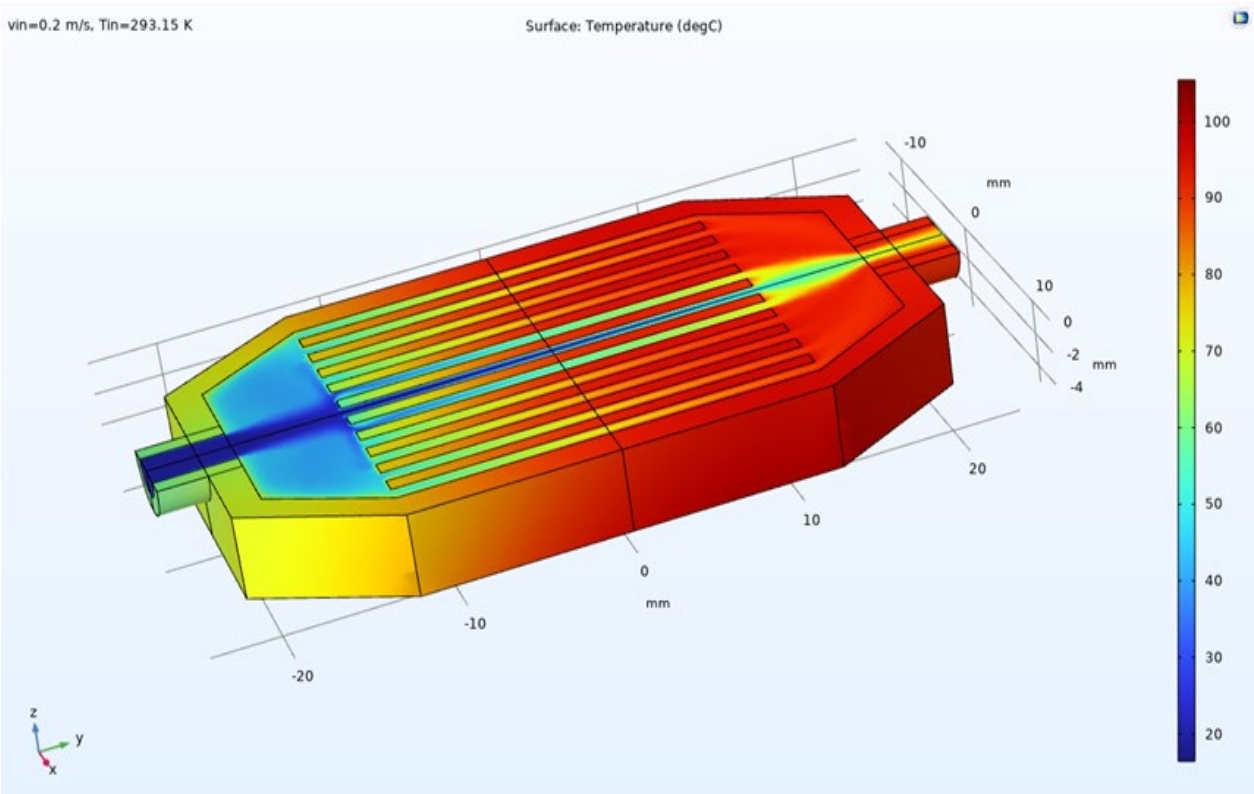

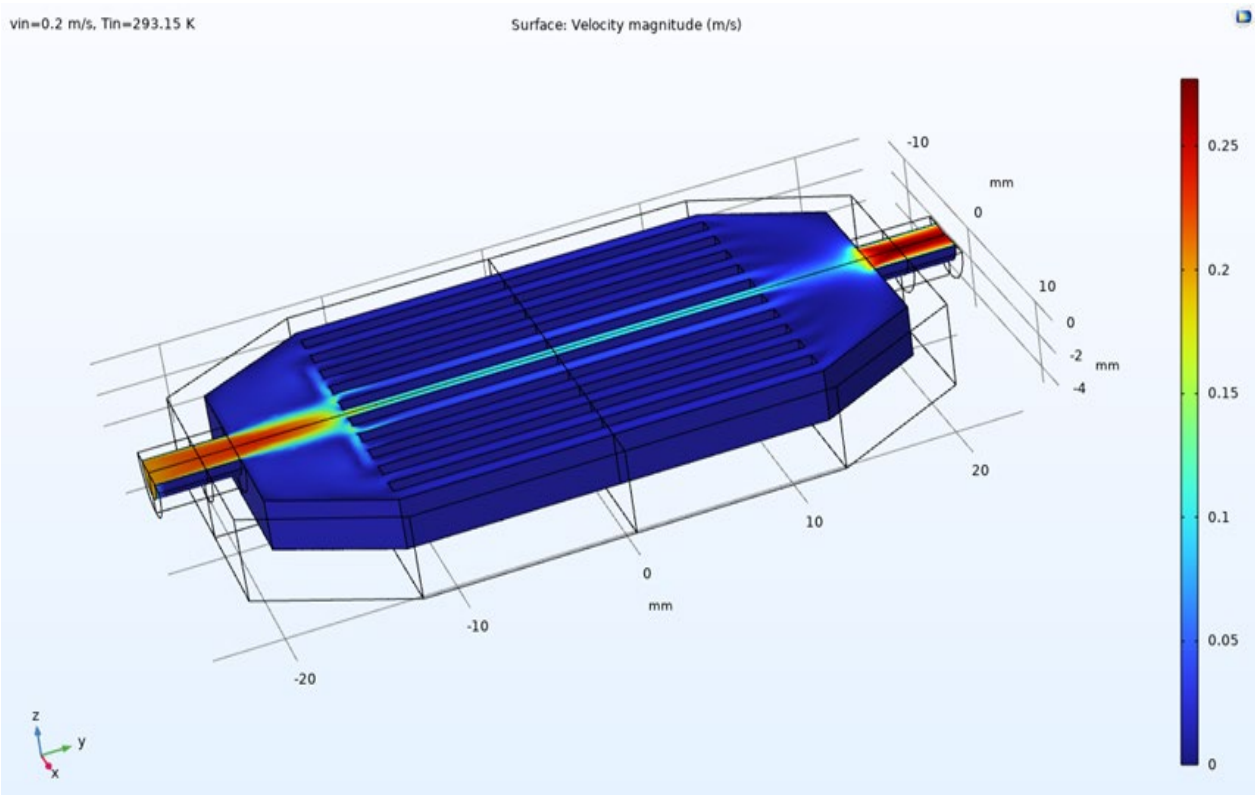

Figure 2.14. the results at an inlet velocity of 0.2 m/s and an inlet temperature of 293.15 K for the liquid-cooled heatsink

2.1.2.6. Reynolds Number Analysis

In alignment with the specified operating conditions as outlined in WP1, including parameters such as ambient air temperature, and driving conditions (see D1.1 and D1.2), and guided by the Thermal Architecture Design established in T3.1 of WP3, our team at AU executed a fundamental 3D thermal model of the liquid-cooled heatsink. This was accomplished using the computational capabilities of COMSOL Multiphysics software.

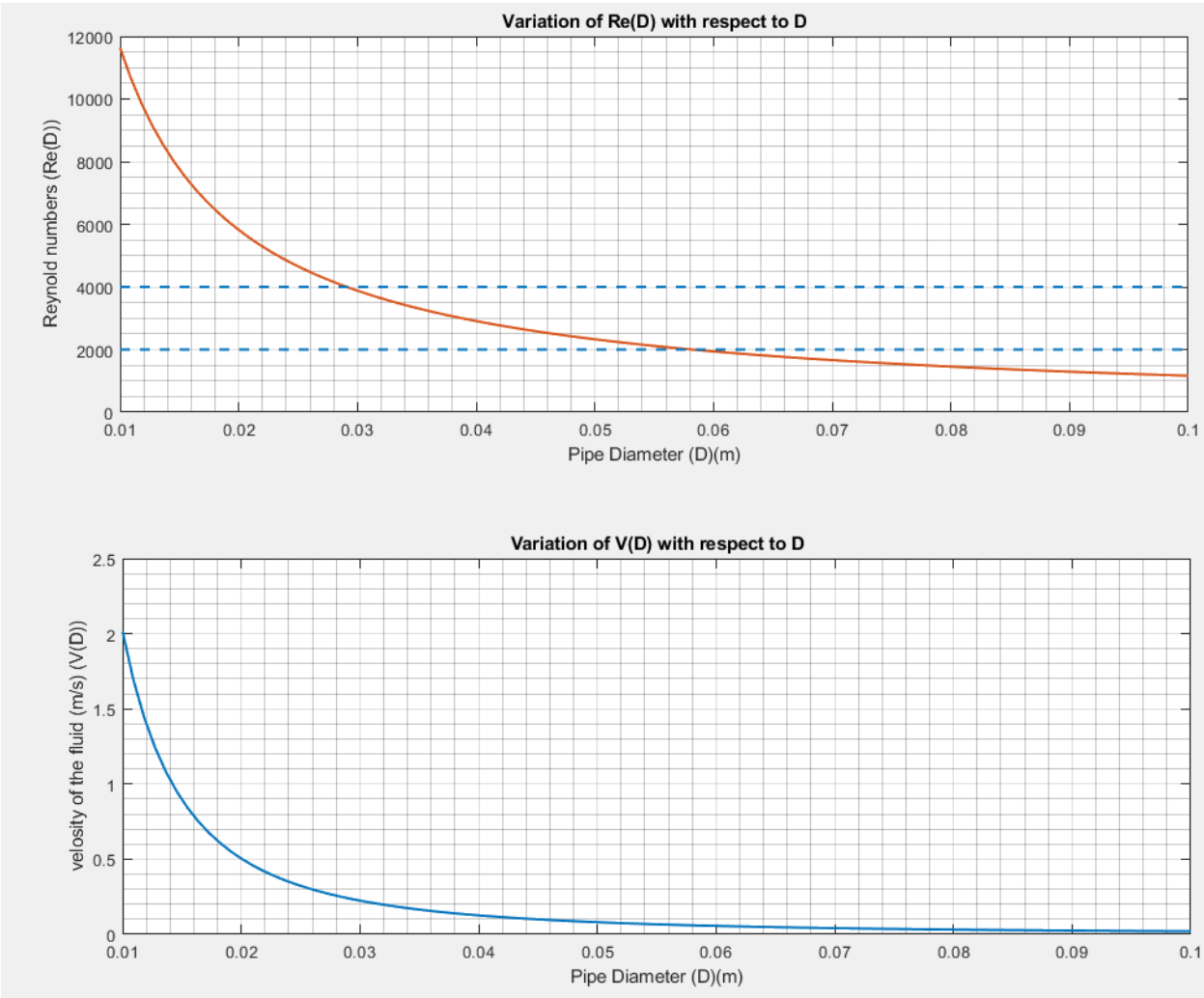

Figure 2.15. Analysis of Reynolds number and fluid velocity concerning variations in pipe diameter

Initially, based on the AU thermal calculations (see D1.2 and D1.4) and the required mass flow for the cooling system design (q=0.57/3600 m^3/s), we conducted an analysis of Reynolds number and fluid velocity concerning variations in pipe diameter. This analysis is crucial for understanding and predicting the behaviour of fluids, such as water or glycol, as they flow through surfaces or conduits. These calculations were based on a cylindrical pipe containing a mixture of 50% glycol (ethylene) and 50% water, with fluid properties represented by a density of 1010 kg/m^3 and a viscosity of 0.00175 kg/m·s. The outcomes of this study are presented in Figures 2.15, which delineate fluid regimes based on Reynolds number. Reynolds numbers below 2000 indicate a laminar flow regime,

while the range between 2000 to 4000 signifies a transitional flow regime, and values exceeding 4000 indicate turbulence regime. This figure illustrates that an increase in pipe size brings the fluid regimes closer to laminar flow, which correlates directly with fluid velocity, as depicted in Figure 2.15. This information is pivotal for making informed decisions regarding heatsink designs and component sizing.

2.1.3. High-power, Liquid-Cooled Heatsink Design

In this section, building upon the fundamental analysis conducted in preceding sections and leveraging the high-power inverter design executed by AIT for the RHODaS project, the AU team has designed the initial model for the high-power heatsink. During the design process, the key dimensions of the power boards were derived based on the detailed design by AIT, as illustrated in Figure 2.16.

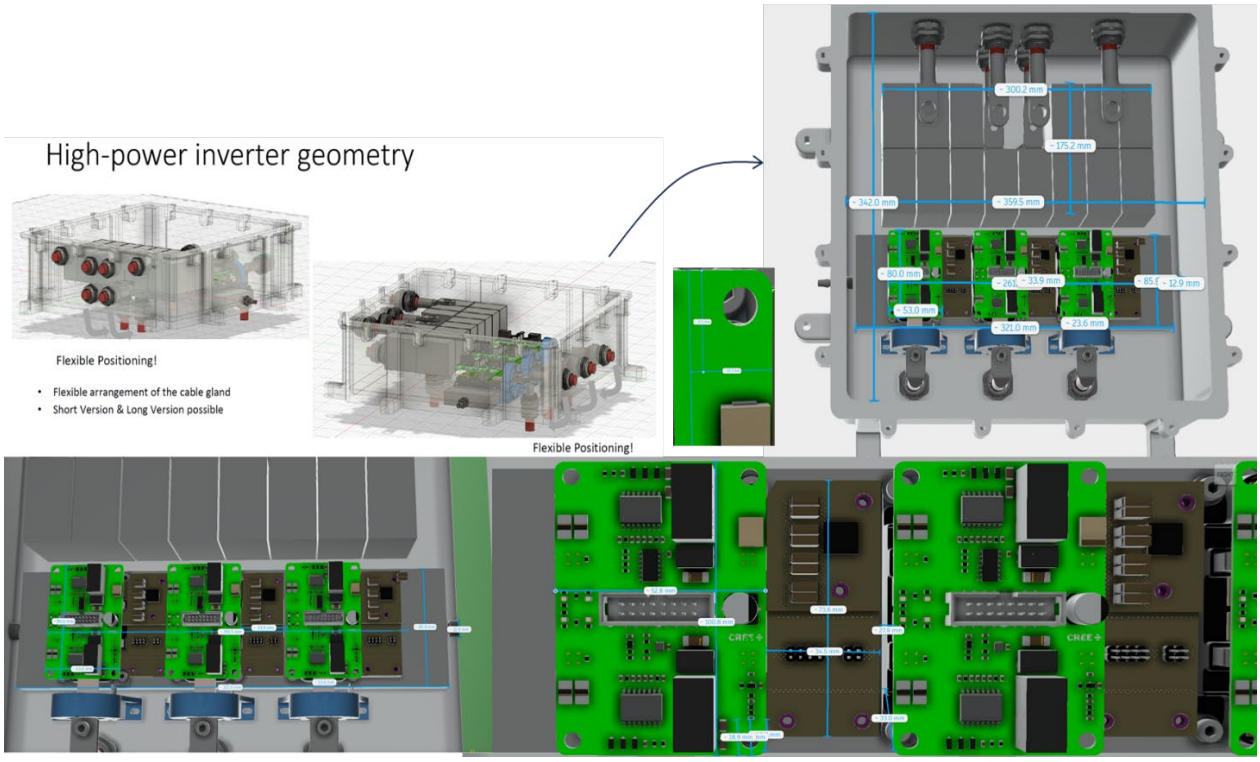

Figure 2.16. Dimensions of the high-power boards derived based on the detailed design by AIT

In the initial design, prompted by practical constraints and following calculations by the AU team, three separate heatsinks were devised to accommodate two power boards each, featuring SiC and GaN modules. The detailed specifications of the high-power inverter designed by AIT and low-power inverter designed by UPC are available in Appendix G. Figure 2.17 visually represents the quarter part of the heatsink geometry, strategically crafted to encompass both SiC and GaN power boards.

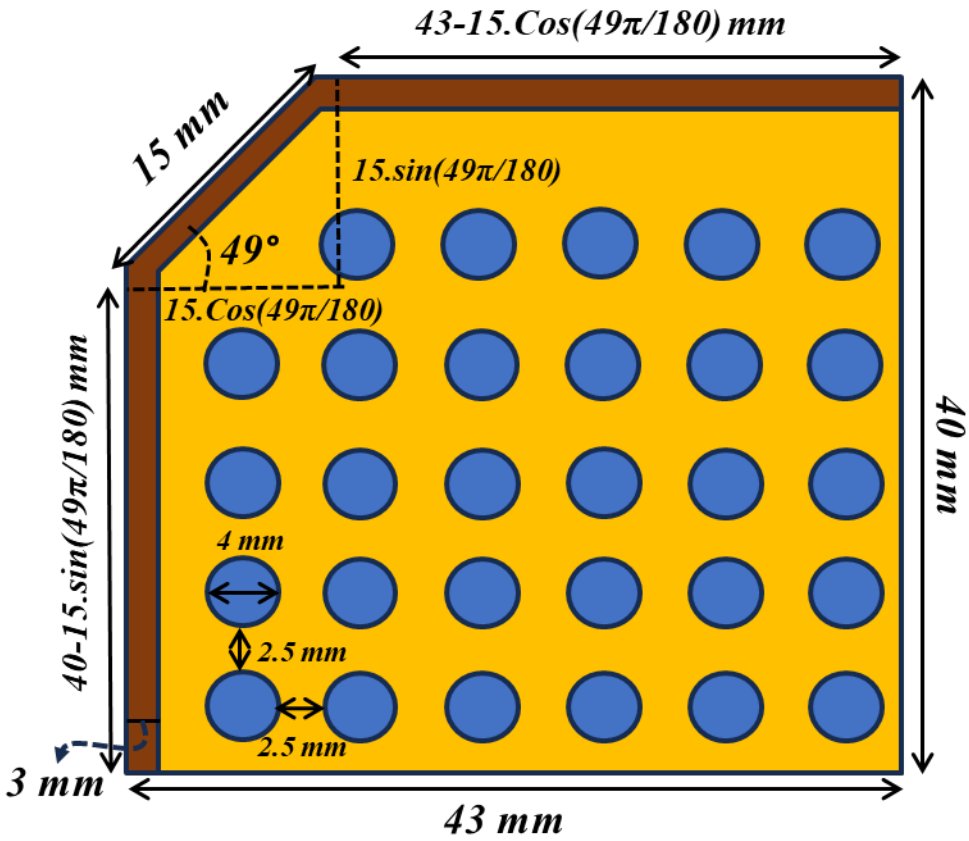

Figure 2.17. The quarter part of the high-power heatsink geometry designed by AU

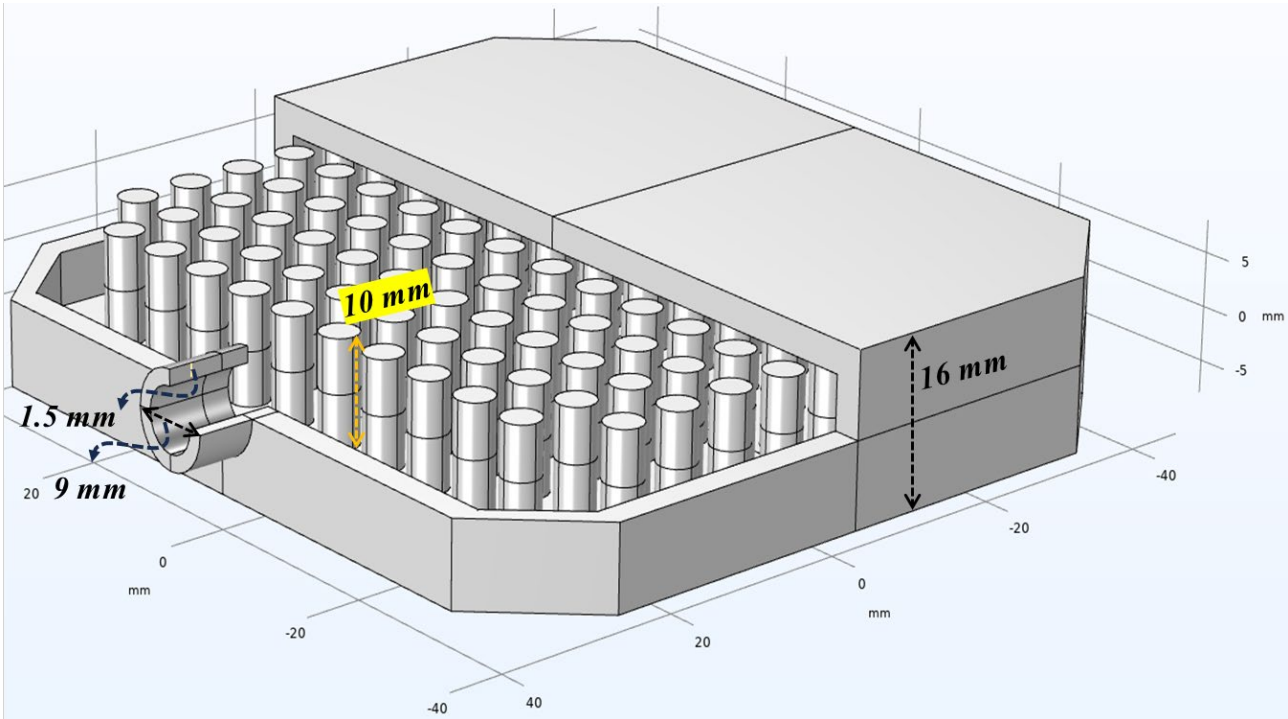

Figure 2.18. The simulation results of the high-power heatsink in the COMSOL Multiphysics software

The simulation results of the heatsink, conducted using COMSOL Multiphysics software, are presented in Figure 2.18. The configuration of the fins in this design is outlined in Figure 2.19, with plans by the AU team to explore an alternative arrangement, depicted in Figure 2.20, during the optimization procedures in the forthcoming Task 3.5.

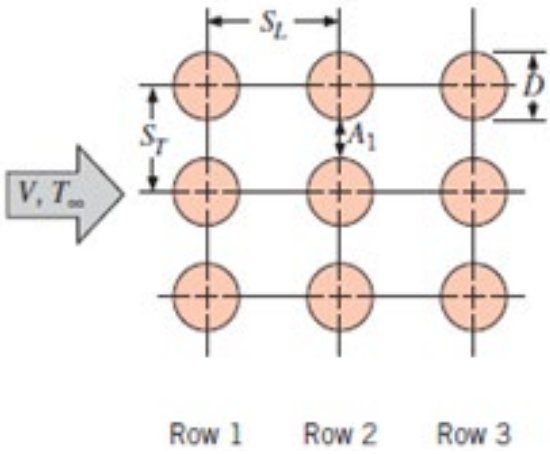

Figure 2.19. The configuration of the fins in the design of the high-power heatsink

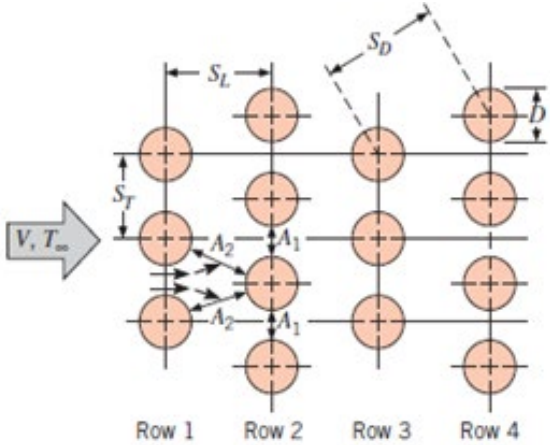

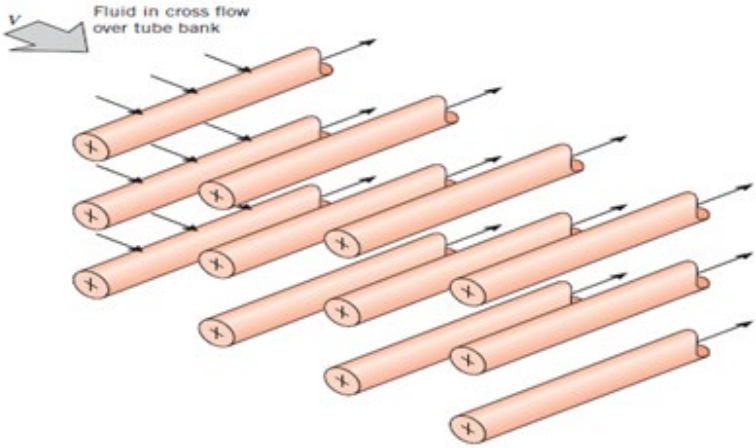

Figure 2.20. The possible configuration of the fins in the design of the high-power heatsink

3. RHODaS Thermal Management System Toolbox

In this section, AU has developed a simulation toolbox that incorporates suitable thermal prediction models to enable the estimation of thermal management systems under diverse simulation parameters and operating conditions.

To enhance the usability of this toolbox and enable its integration into other simulations, encompassing electrical, thermal, and control components, a MATLAB code has been written. This code prompts users to input initial parameters for the thermal management system and estimates its most critical features.

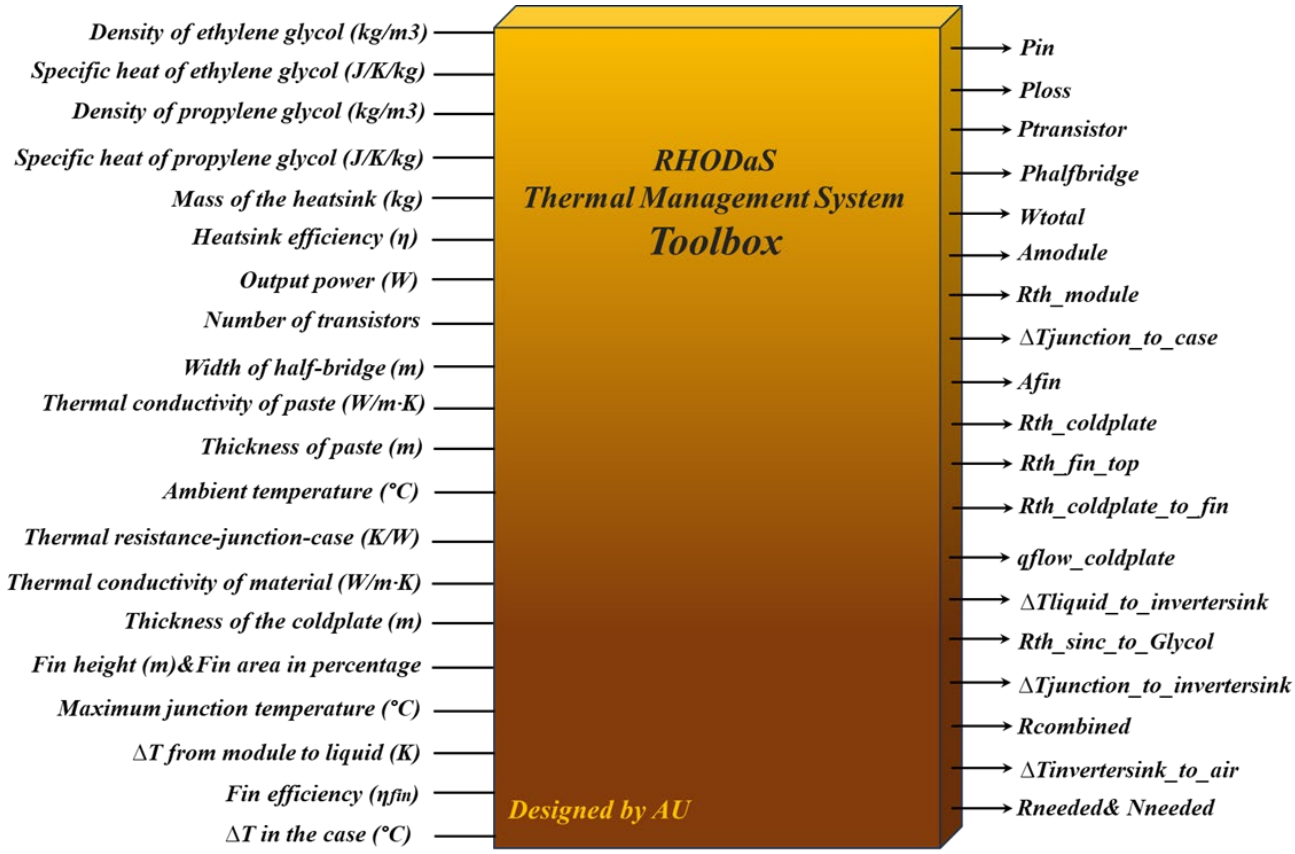

Figure 2.21. The block diagram of the RHODaS thermal management system toolbox

Figure 2.21 illustrates the block diagram of the RHODaS thermal management system toolbox crafted by the AU team. It is important to note that, throughout the design process of this toolbox, various analyses were conducted to establish relationships between different variables. Figure 2.22, for instance, demonstrates the impact of different fin efficiencies on the heatsink flow rate, offering insights into defining distinct fluid regimes that influence the heatsink's efficiency.

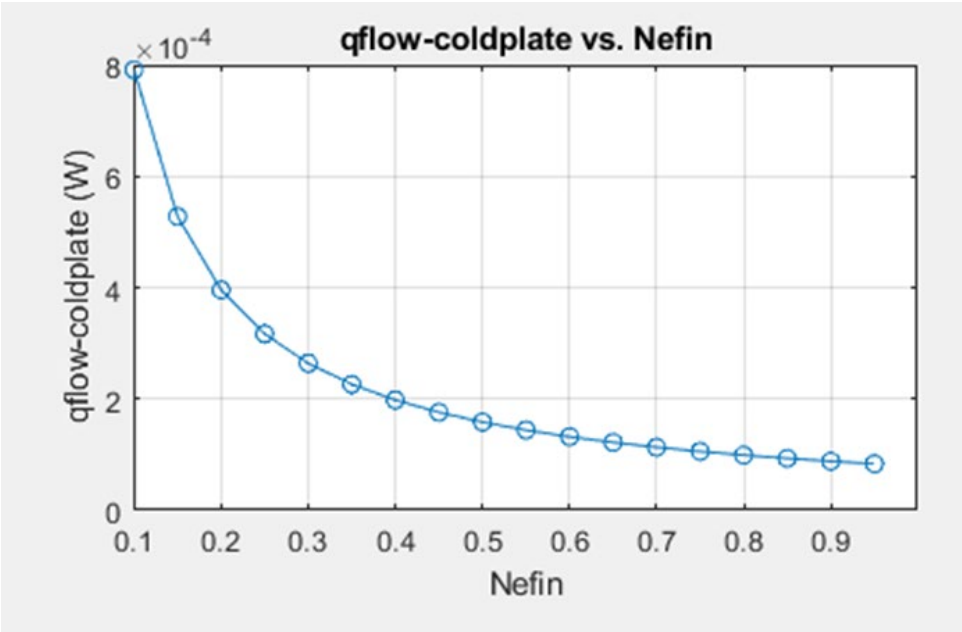

Figure 2.22. The impact of different fin efficiencies on the heatsink flow rate

4. Thermal equivalent circuit of high-power converter with GaN and SiC

The thermal equivalent circuit plays a critical role in the design and analysis of thermal management systems for power converters. It offers a simplified yet accurate representation of the thermal behaviour of power converters, allowing engineers to model and predict temperature variations in different components.

This systematic breakdown of the complex thermal system makes the analysis more efficient and manageable. The thermal equivalent circuit aids in optimizing cooling systems, evaluating the impact of different cooling methods on overall thermal performance, identifying critical hotspots, and enabling targeted cooling strategies. It facilitates parametric studies, assessing the influence of various parameters on thermal performance and contributing to the exploration of design trade-offs and optimization.

Integration with electrical circuit simulations provides a comprehensive understanding of coupled electrical and thermal behaviours, crucial for achieving a balanced and reliable power converter design. The thermal equivalent circuit proves to be a cost-effective tool, enabling engineers to evaluate different design options and cooling strategies through simulations, reducing the need for expensive and time-consuming physical prototypes. Additionally, it aids in early issue detection, allowing designers to address potential thermal challenges in the initial stages of the design process and minimizing the likelihood of costly redesigns later in the development cycle.

In this subsection, the thermal equivalent circuit model for the presented T-type power converter in the RHODaS project has been meticulously designed by the AU team. Following the design phase, simulations of this thermal equivalent circuit model were conducted in MATLAB Simulink, utilizing a thermal library to enhance compatibility with other project components. These simulations, incorporating the thermal mass considerations across different parts of the thermal system, not only capture the transient effects but also maintain efficient computation times.

The thermal equivalent circuit was derived for each component, encompassing device and device-to-heatsink interactions, as well as heatsink-to-ambient relationships. It is essential to note that the parameters for the thermal equivalent circuit model for the T-type high-power converter were calculated based on the characteristics of the thermal and electrical systems defined in WP1 and WP3, along with the real characteristics of SiC and GaN devices. The summarized results can be found in Figures 23-24, with additional information from the datasheets for SiC, GaN, and thermal interface materials provided in Appendices H, I, and J, respectively.

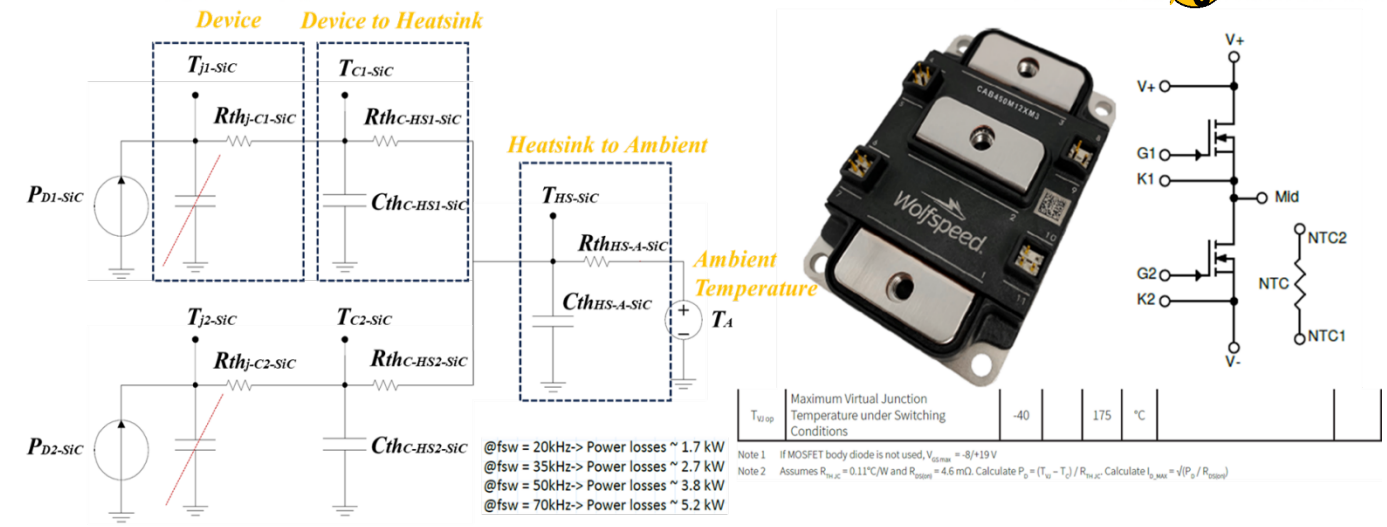

$T_{VJ\,op}$	Maximum Virtual Junction Temperature under Switching Conditions	-40		175	°C		

Note 1 If MOSFET body diode is not used, $V_{GS\,max}$ = -8/+19 V
Note 2 Assumes $R_{TH\,JC}$ = 0.11°C/W and $R_{DS(on)}$ = 4.6 mΩ. Calculate $P_D = (T_{VJ} - T_C) / R_{TH\,JC}$. Calculate $I_{D\,MAX} = \sqrt{(P_D / R_{DS(on)})}$

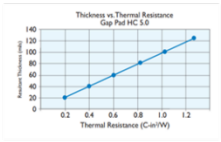

Parameter	value	Parameter	value	Parameter	value	Parameter	value
$P_{D1\text{-}SiC}$	$P_{LOSS}/6$= 634W	$P_{D2\text{-}SiC}$	$P_{LOSS}/6$= 634W	$Cth_{C\text{-}HS1\text{-}SiC}$	1.3 J/°C	$Cth_{C\text{-}HS2\text{-}SiC}$	1.3 J/°C
$Rth_{j\text{-}C1\text{-}SiC}$	0.11 °C/W	$Rth_{j\text{-}C2\text{-}SiC}$	0.11 °C/W	$Rth_{C\text{-}HS\text{-}SiC\,paste}$	0.021 C/W	T_A	50 °C
$T_{C1\text{-}SiC}$	25 °C	$T_{C2\text{-}SiC}$	25 °C	$Rth_{HS\text{-}A\text{-}SiC}$	0.04 °C/W	f_{SW}	50 kHz
$Rth_{C\text{-}HS\text{-}SiC\,PAD}$	7.44 °C/W	$Rth_{C\text{-}HS2\text{-}SiC}$	7.44 °C/W	$Cth_{HS\text{-}A\text{-}SiC}$	1.95 J/°C	P_{LOSS}	3800 W

Figure 2.23. Thermal equivalent circuit of SiC-CAB450M12XM3 from Wolfspeed Cree.

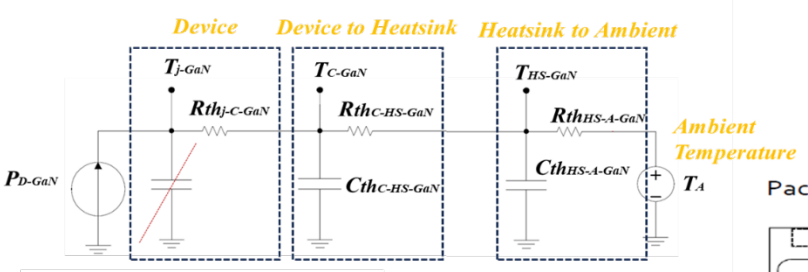

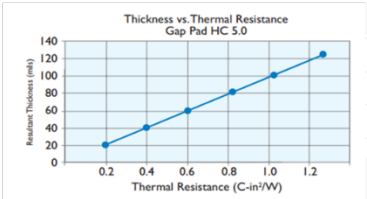

@fsw = 20kHz-> Power losses ~ 1.7 kW
@fsw = 35kHz-> Power losses ~ 2.7 kW
@fsw = 50kHz-> Power losses ~ 3.8 kW
@fsw = 70kHz-> Power losses ~ 5.2 kW

Package Outline

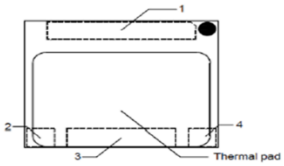

Circuit Symbol

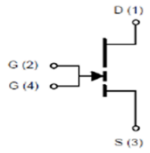

Thermal Resistance (junction-to-case) – top side	$R_{\theta JC}$	0.27	°C /W
Maximum Soldering Temperature (MSL3 rated)	T_{SOLD}	260	°C

Parameter	value	Parameter	value	Parameter	value
$P_{D\text{-}GaN}$	$P_{LOSS}/6$= 634W	$Cth_{C\text{-}HS\text{-}GaN}$	0.84 J/°C	T_A	50 °C
$Rth_{j\text{-}C\text{-}GaN}$	0.27 °C/W	$Rth_{C\text{-}HS\text{-}GaN}$	4.8 °C/W	f_{SW}	50 kHz
$T_{C\text{-}GaN}$	25 °C	$Rth_{HS\text{-}A\text{-}GaN}$	0.04 °C/W	P_{LOSS}	3800 W
$Rth_{C\text{-}HS\text{-}GaN\,PAD}$	4.8 °C/W	$Cth_{HS\text{-}A\text{-}GaN}$	1.25 J/°C	$Rth_{C\text{-}HS\text{-}GaN\,Paste}$	0.013 °C/W

RC breakdown of $R_{\theta JC}$

R_θ (°C/W)	C_θ (W·s/°C)
$R_{\theta 1}$ = 0.008	$C_{\theta 1}$ = 1.48E-04
$R_{\theta 2}$ = 0.124	$C_{\theta 2}$ = 1.37E-03
$R_{\theta 3}$ = 0.130	$C_{\theta 3}$ = 12.0E-03
$R_{\theta 4}$ = 0.008	$C_{\theta 4}$ = 3.7E-03

Figure 2.24. Thermal equivalent circuit of GaN-GS66516T from GAN systems.

After deriving the thermal equivalent circuit model for each component of the system, guided by the topology of the high-power inverter, the comprehensive thermal equivalent circuit model for the RHODaS high-power inverter, depicted in Figure 2.25, has been meticulously designed.

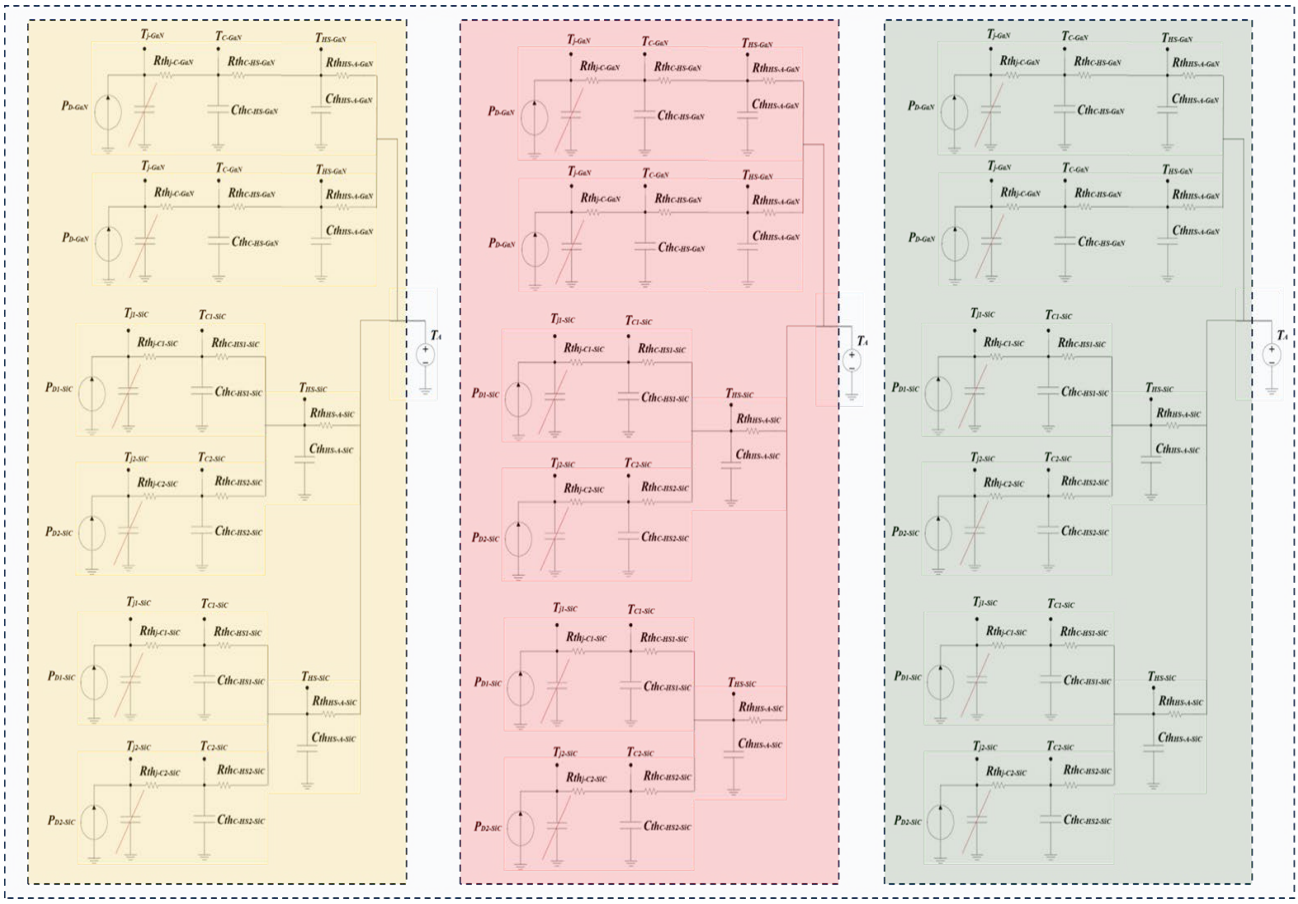

Figure 2.25. Thermal equivalent circuit of T-type power converter with GaN and SiC.

Prior to simulating the thermal equivalent circuit model for the designed inverter, our simulation procedure underwent verification by re-simulating a published paper. The selected paper for verification is presented in Figure 2.26. Furthermore, the comparison results between the paper's simulation outcomes and ours are depicted in Figure 2.27.

This comparison confirms the high accuracy of our simulation procedure. In the subsequent step, we simulated the thermal equivalent circuit of the T-type power converter with GaN and SiC, as illustrated in Figure 2.28. The simulation results are summarized in Figure 2.29.

Journal of Power Sources 194 (2009) 581–587

Contents lists available at ScienceDirect

Journal of Power Sources

journal homepage: www.elsevier.com/locate/jpowsour

Review

Thermal modeling and heat management of supercapacitor modules for vehicle applications

Monzer Al Sakka[a,b], Hamid Gualous[a,*], Joeri Van Mierlo[b], Hasan Culcu[b]

[a] Institut FEMTO-ST CNRS UMR 6174; Université de franche-Comté, FCLAB bat F, 90010 Belfort, France
[b] Vrije Universiteit Brussel, pleinlaan 2, B-1050 Brussels, Belgium

Table 2
Parameters values of 310 F and 1500 F supercapacitor cells.

Parameters	310 F	1500 F
T_a	22.5 (°C)	17.5 (°C)
$R_{convenction}$	11 (°C/W)	3.5 (°C/W)
R_{th}	6.5 (°C/W)	4.2 (°C/W)
C_{th}	44 (J/°C)	268 (J/°C)

Table 3
Characteristics of Maxwell 1500 F supercapacitor.

Parameters	Provided by Maxwell	Measured
Operating temperature range	−40 °C, +65 °C	–
Equivalent series resistance	ESR = 0.47 (mΩ)	ESR = 0.39 (mΩ)
Thermal resistance	R_{th} = 4.5 (°C/W)	R_{th} = 4.2 (°C/W)
Thermal capacitance	–	C_{th} = 268 (J/°C)

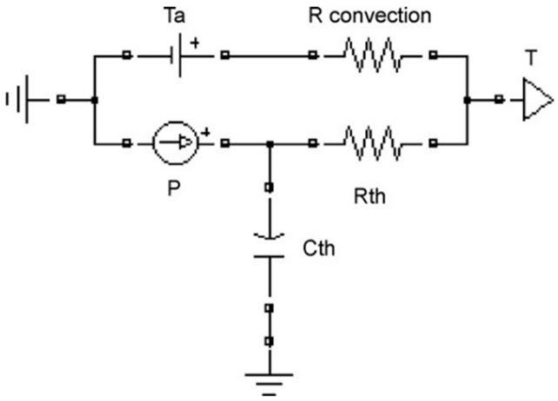

Fig. 5. Thermal-electric model of the supercapacitor.

Figure 26. Simulation procedure verification by re-simulating a published paper [2].

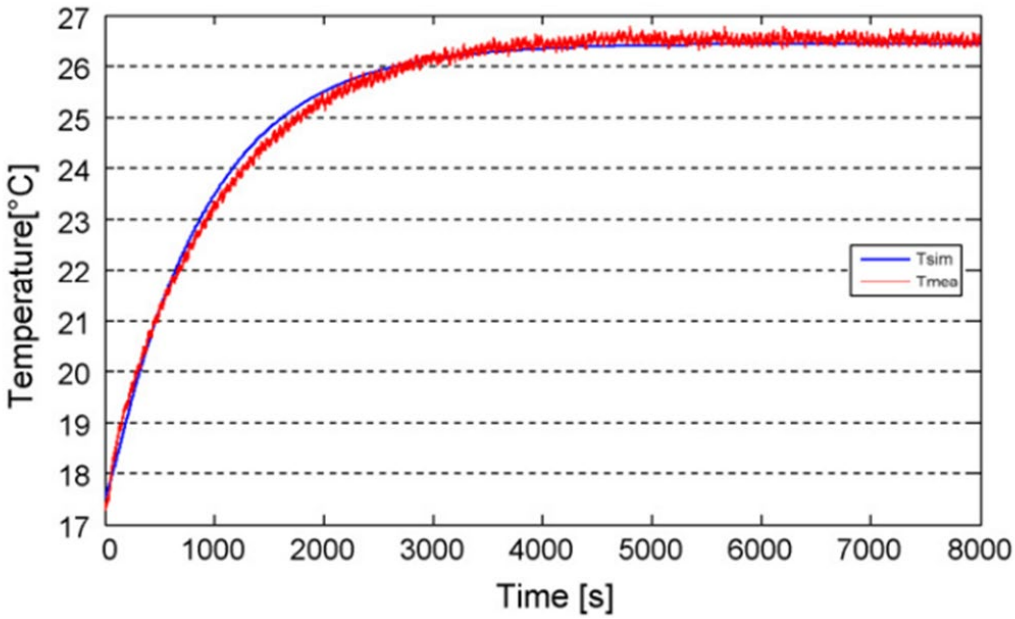

a) Simulation result of reference [2]

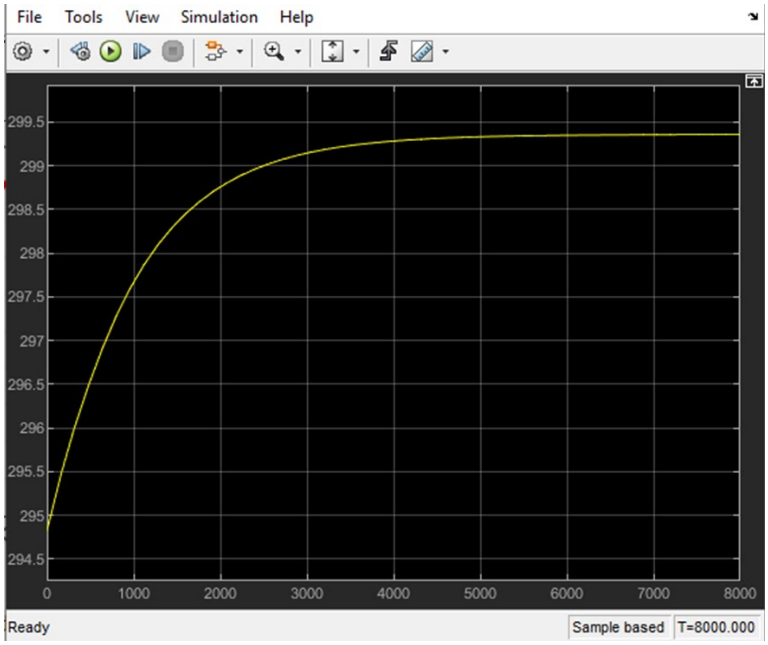

b) Simulation result of AU team simulations in MATLAB

Figure 2.27. Simulation result of re-simulating reference [2]

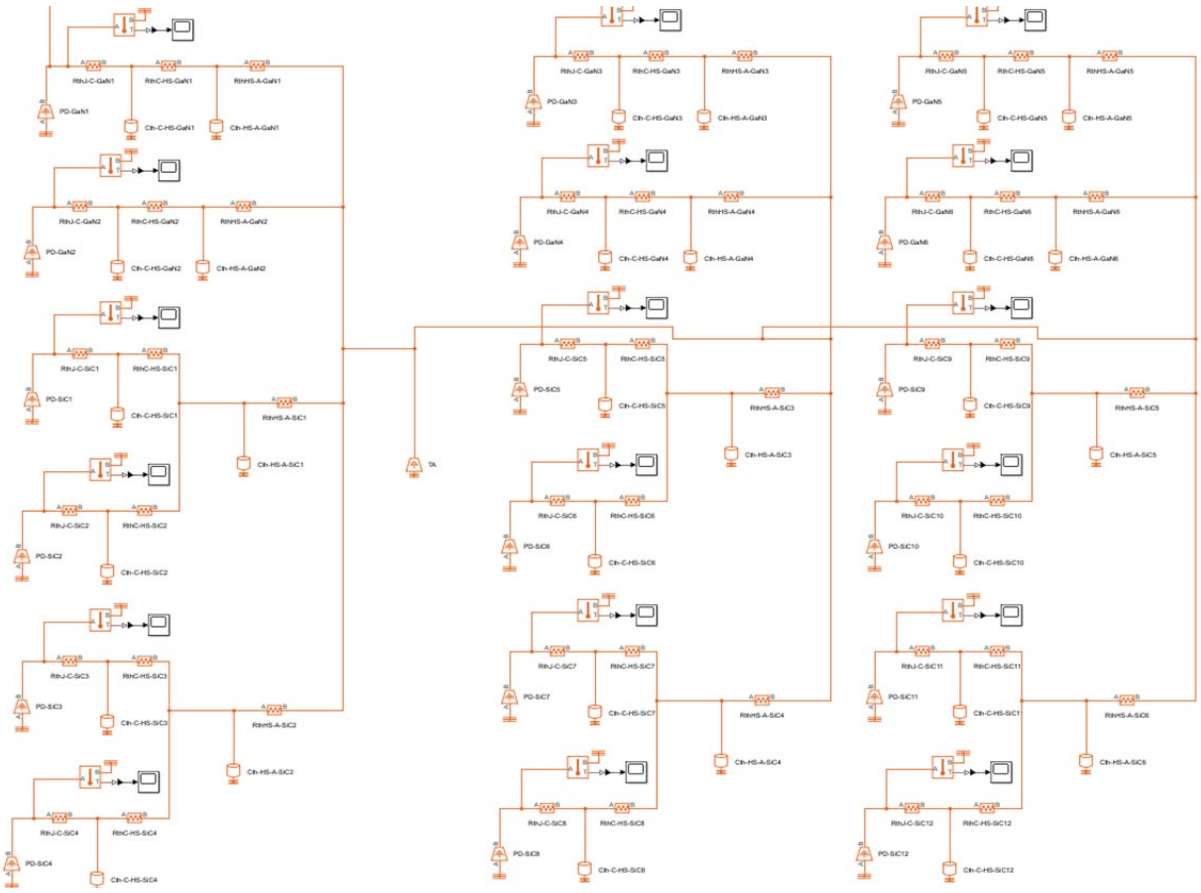

Figure 2.28. The simulated thermal equivalent circuit of the T-type power converter in MATLAB

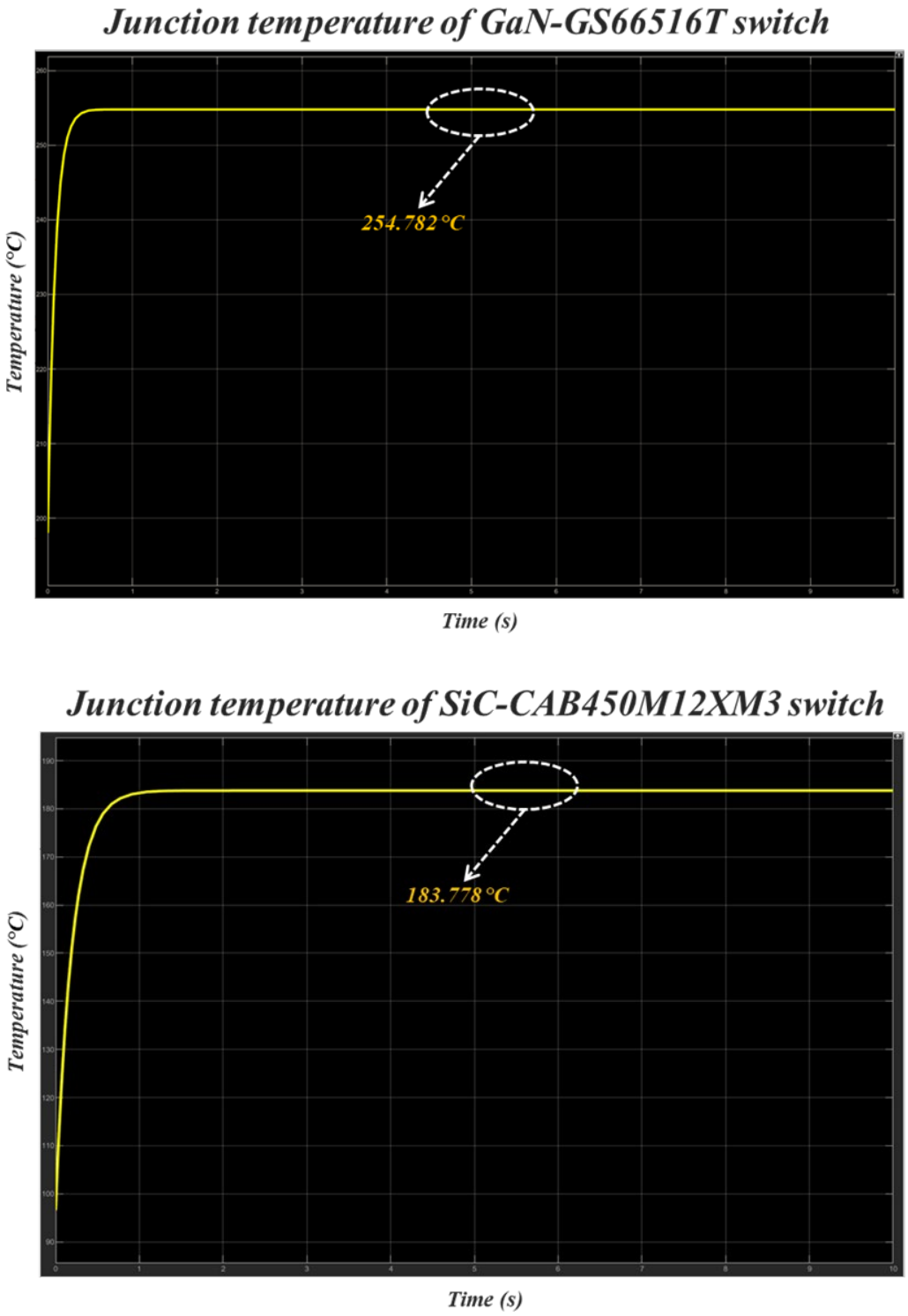

Figure 2.29. The simulation results of thermal equivalent circuit of the T-type power converter in MATLAB

5. Sensitivity analysis of the GaN switches junction temperature

Due to the limitations on the current level that GaN modules can handle, a comprehensive sensitivity analysis was conducted on the GaN switches' junction temperature. This analysis aimed to illustrate the thermal management system's boundaries and the influence of various thermal system parameters on the critical variable, i.e., the junction temperature of the transistors. The outcomes of the different sensitivity analyses are consolidated in Figures 2.30-2.33.

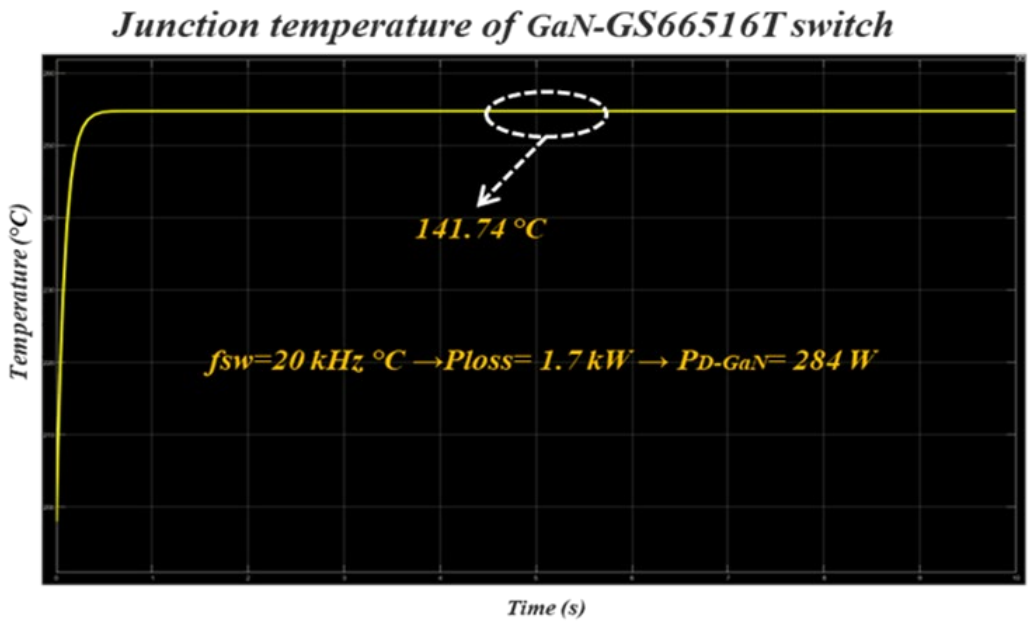

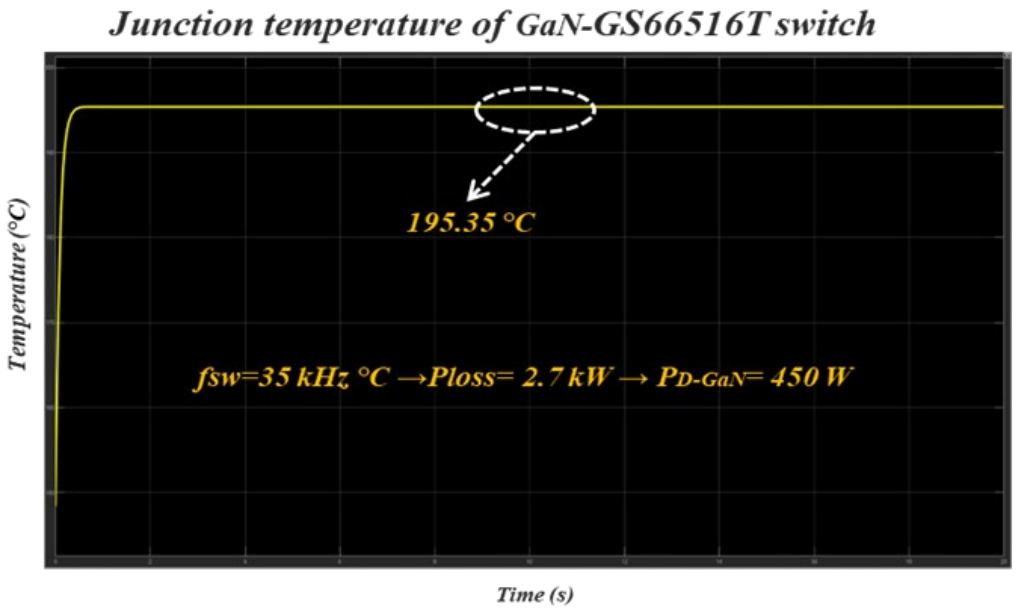

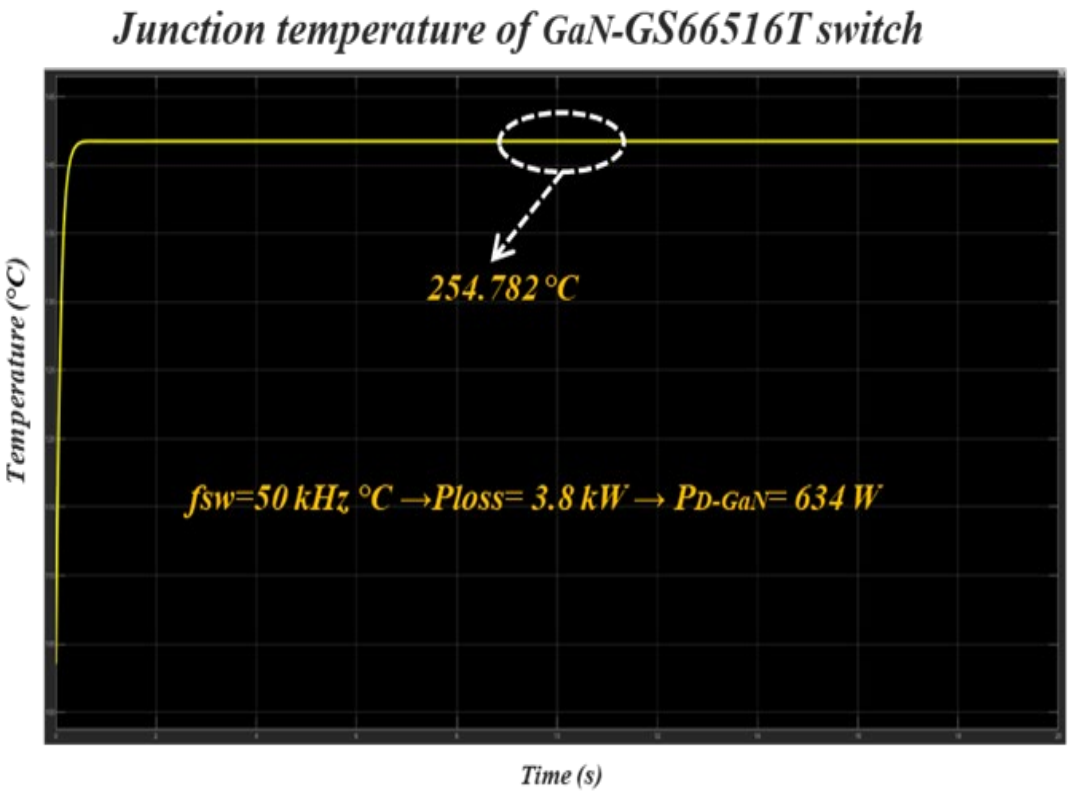
Junction temperature of GaN-GS66516T switch
254.782 °C
fsw=50 kHz °C →Ploss= 3.8 kW → PD-GaN= 634 W
Temperature (°C)
Time (s)

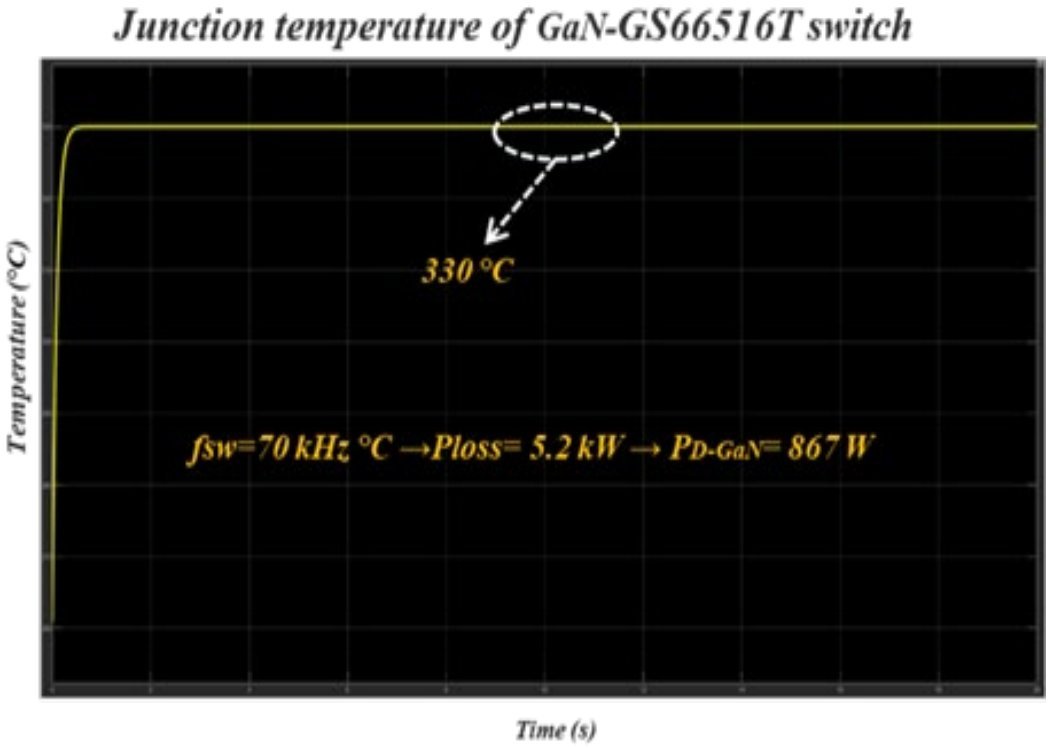
Junction temperature of GaN-GS66516T switch
330 °C
fsw=70 kHz °C →Ploss= 5.2 kW → PD-GaN= 867 W
Temperature (°C)
Time (s)

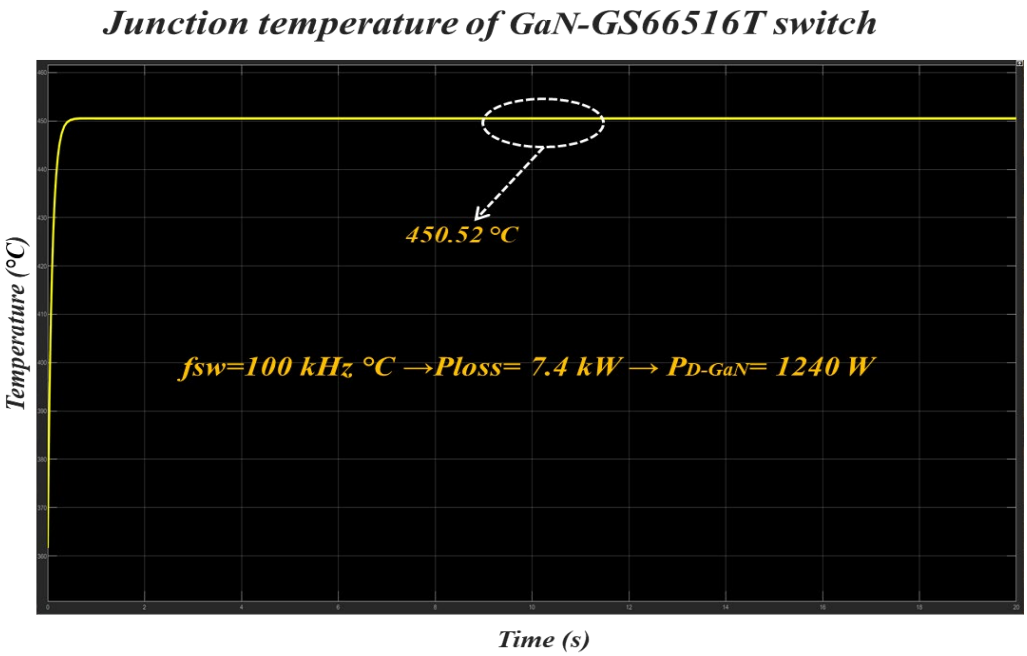

Figure 2.30. Sensitivity analysis of the GaN switches junction temperature- Variation in switching frequency

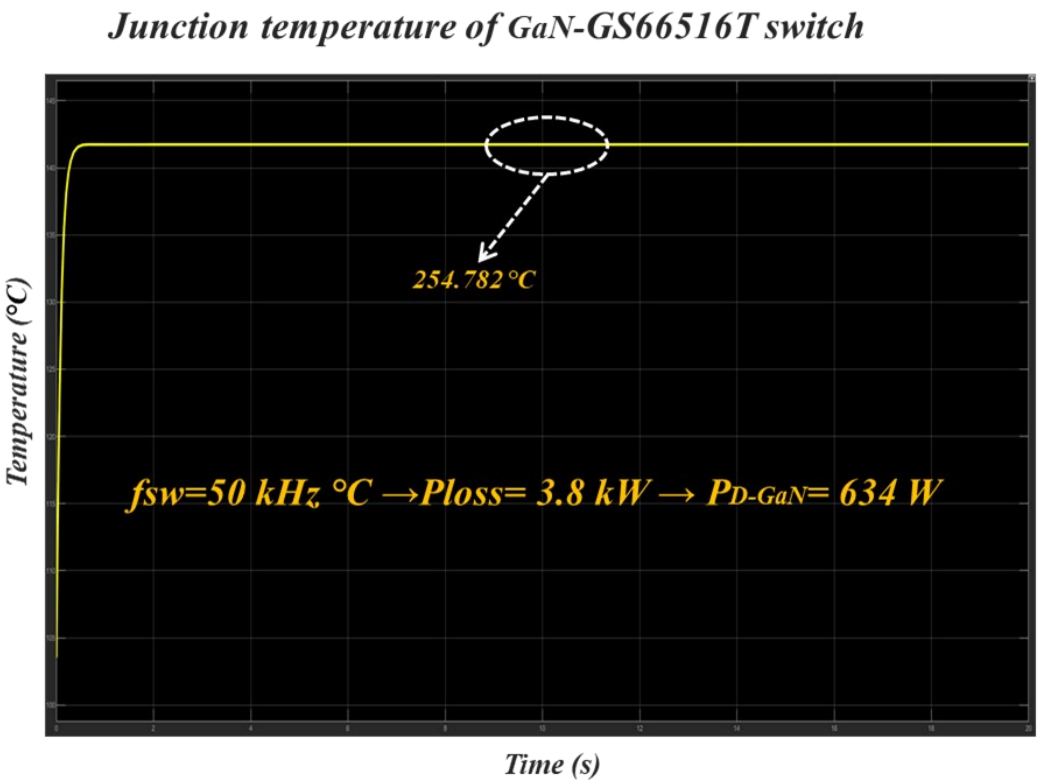

a) Utilizing 60 μm Thermal Paste (RthC-HS-GaN PAD=0.021 °C/W)

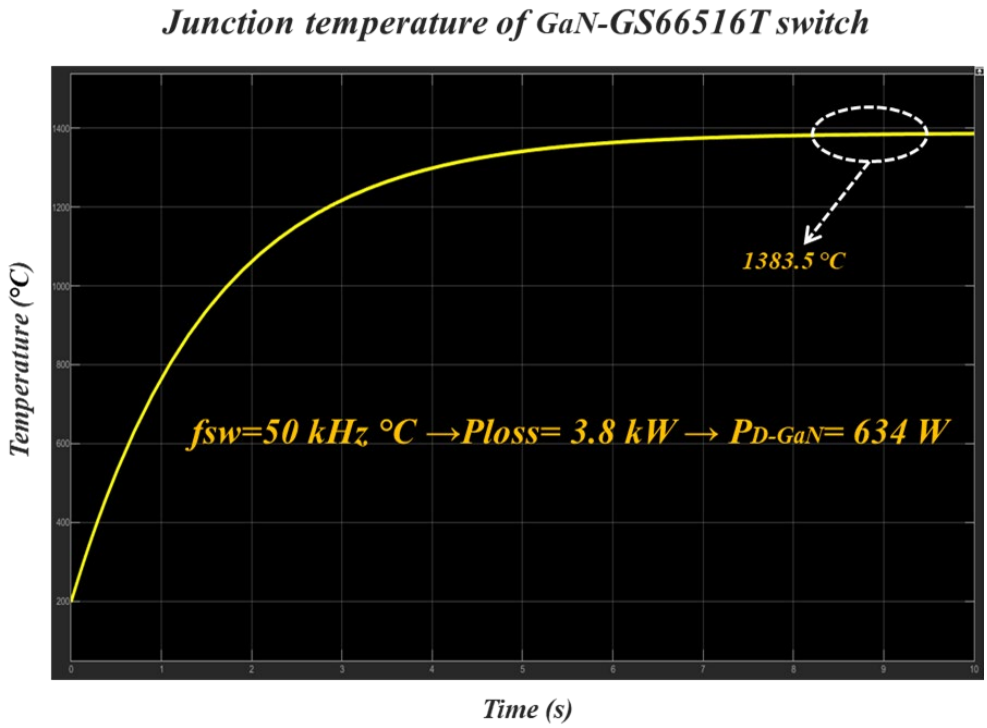

b) Utilizing Gap Pad (RthC-HS-GaN PAD=1.8 °C/W)

Figure 2.31. Sensitivity analysis of the GaN switches junction temperature- Utilizing various types of thermal interface materials

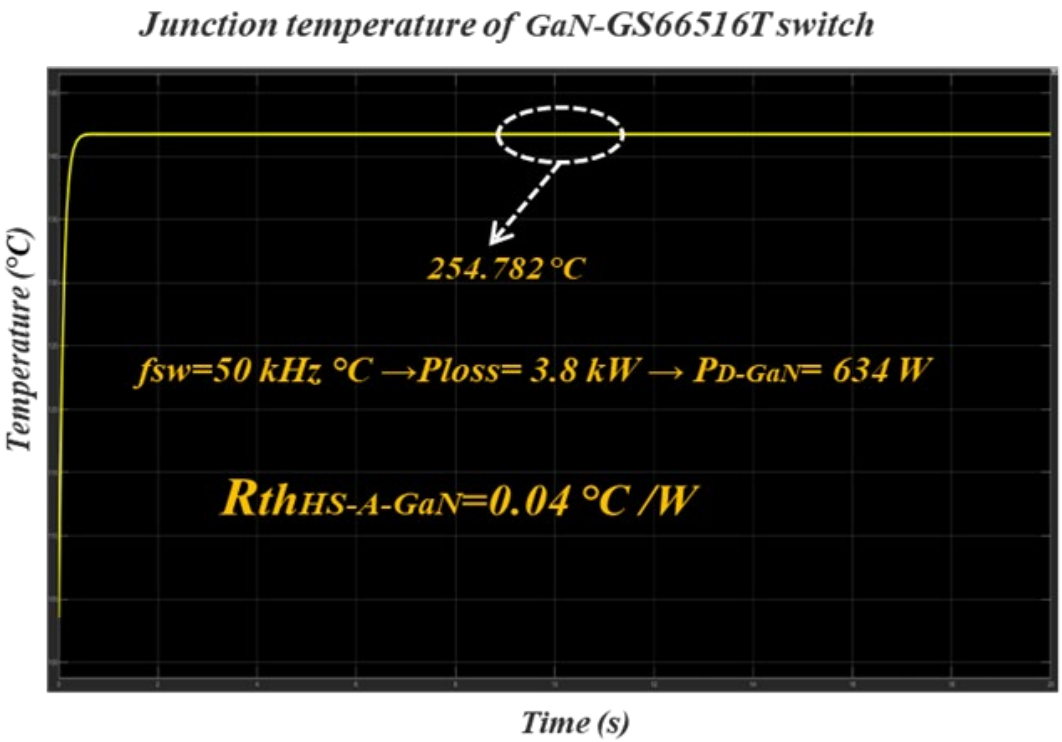

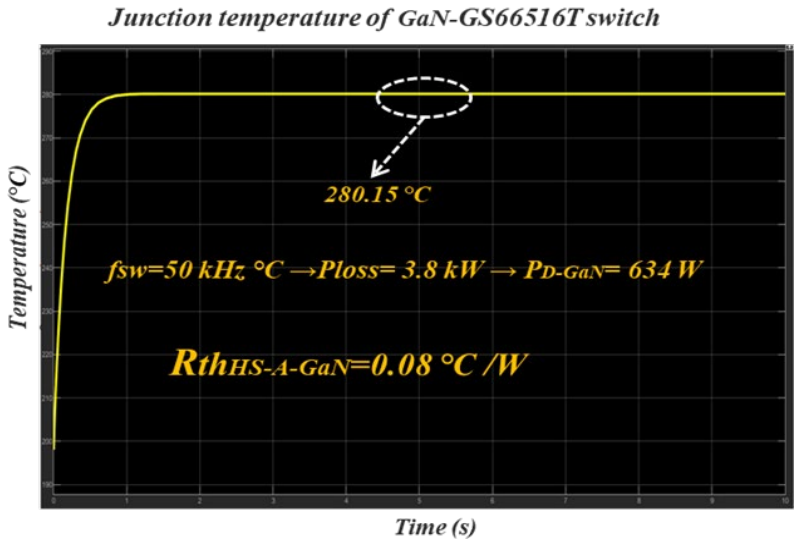
Junction temperature of GaN-GS66516T switch
Temperature (°C)
280.15 °C
fsw=50 kHz °C →Ploss= 3.8 kW → PD-GaN= 634 W
RthHS-A-GaN=0.08 °C /W
Time (s)

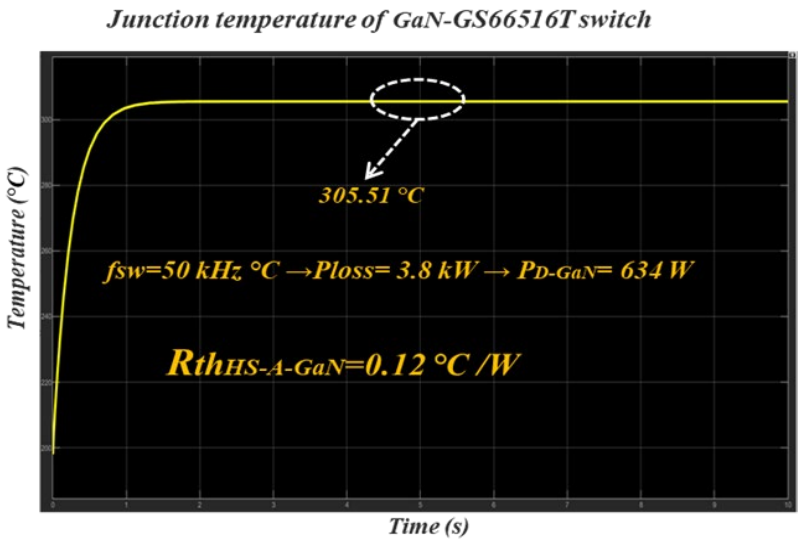
Junction temperature of GaN-GS66516T switch
Temperature (°C)
305.51 °C
fsw=50 kHz °C →Ploss= 3.8 kW → PD-GaN= 634 W
RthHS-A-GaN=0.12 °C /W
Time (s)

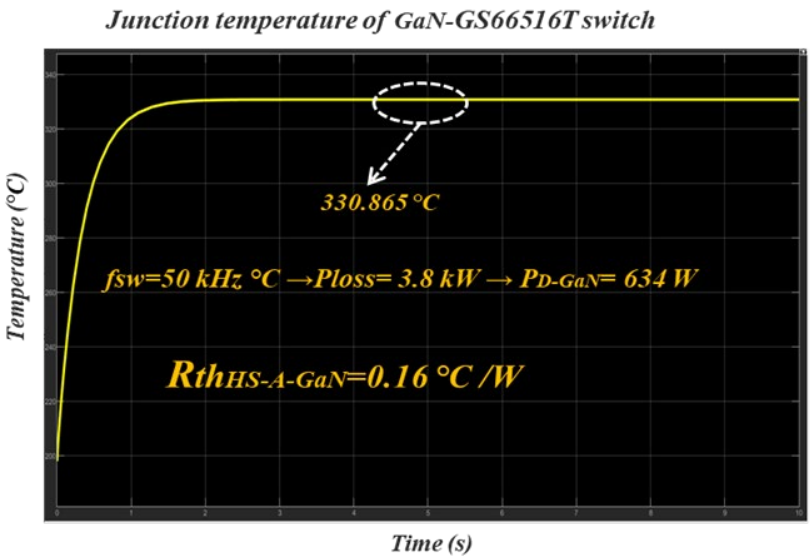
Junction temperature of GaN-GS66516T switch
Temperature (°C)
330.865 °C
fsw=50 kHz °C →Ploss= 3.8 kW → PD-GaN= 634 W
RthHS-A-GaN=0.16 °C /W
Time (s)

Figure 2.32. Sensitivity analysis of the GaN switches junction temperature- Variation in RthHS-A-GaN

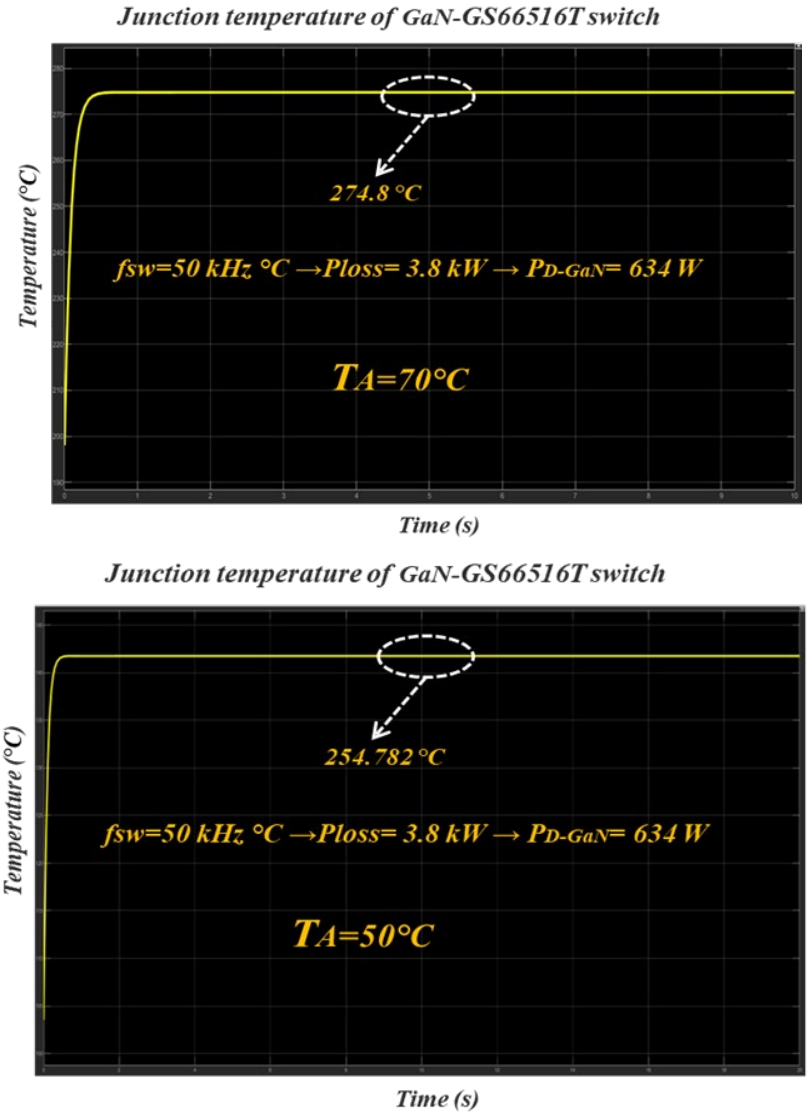

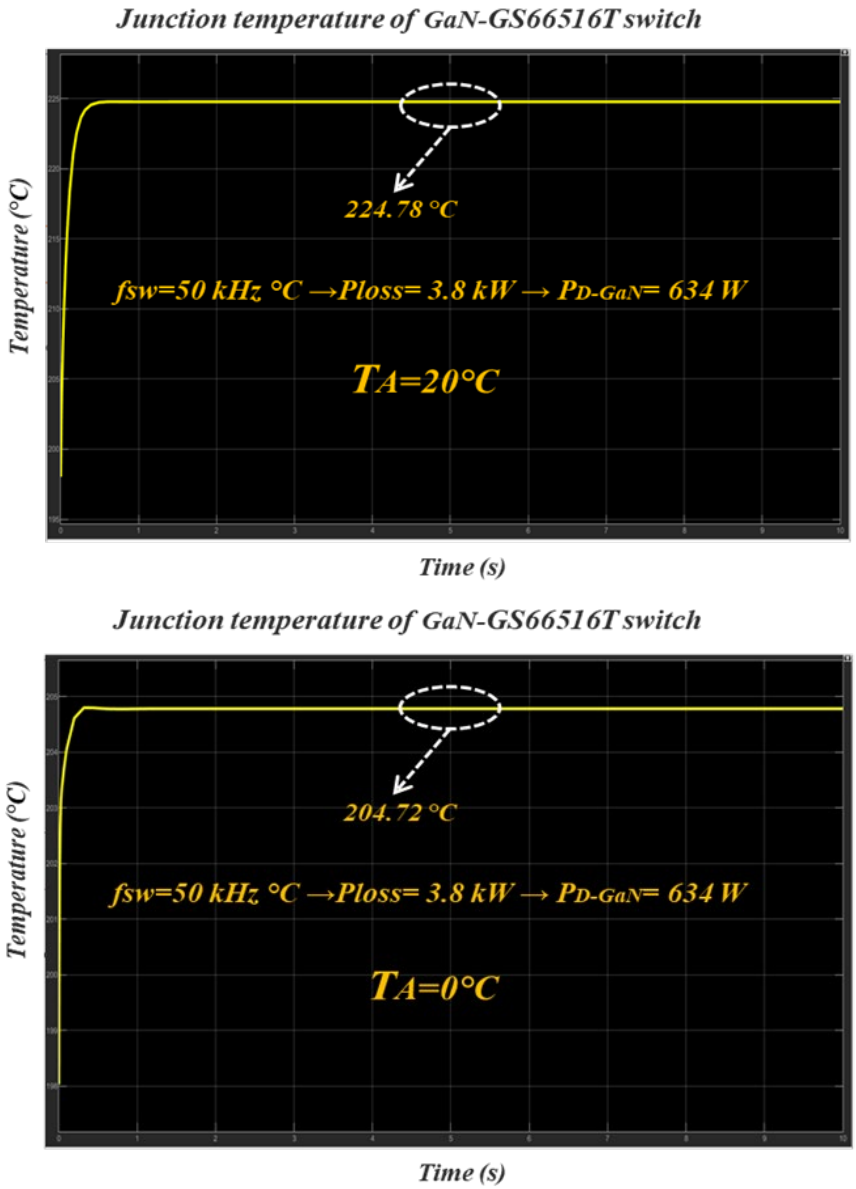

Figure 2.33. Sensitivity analysis of the GaN switches junction temperature- Variation in TA

In the final step, guided by the calculations and thermal sensitivity analysis results, the AU team has opted to design a set of six heatsinks for the presented high-power converter. As per the configuration outlined in Figure 2.34, this entails assigning a dedicated heatsink to each power board.

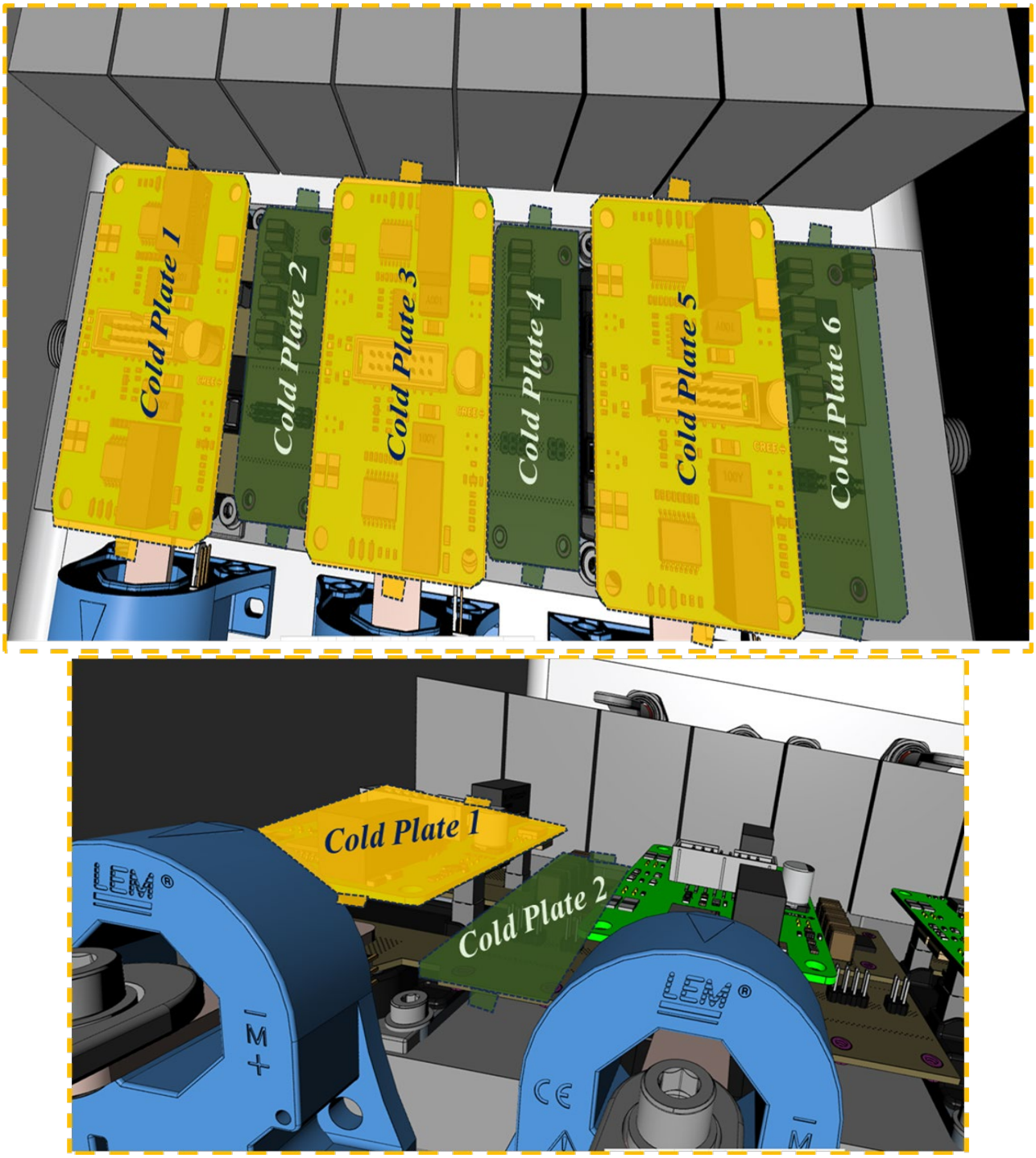

Figure 2.34. AU's Cooling System Design

6. New Sensors Networks for Advanced Temperature Control and Monitoring

This task aims to make significant strides in the application of advanced temperature sensor networks within its framework. The primary goal is to enhance the accuracy of temperature readings from components, particularly semiconductors, thereby directly contributing to the effectiveness of a more sophisticated thermal management system. The implementation of this sensor network not only seeks to obtain more precise measurements but also aims to enable the proactive detection of over-temperature situations. This proactive approach provides an essential layer of protection for transistors, ensuring a safe and sustainable operation of the power converter, the engine, and consequently, the powertrain.

Simultaneously, the task aspires to optimize the overall performance of the converter. The precise temperature information gathered by the sensor network will facilitate real-time adjustments, maximizing operational efficiency and enhancing the overall performance of the conversion system. This proactive approach to thermal management is expected not only to contribute to operational stability but also to have positive implications in terms of energy efficiency and component lifespan.

A distinctive aspect of this task involves incorporating intelligent soft-sensors, which extend beyond physical data collection. These soft sensors utilize both real-time data and models to make optimal estimations of core temperature and accurately predict thermal conditions in the die. This combination of physical and virtual technologies provides a comprehensive assessment of the system's thermal conditions. However, it's important to note that the development of algorithms and temperature estimations is still underway.

In terms of long-term management, the task also focuses on predicting the lifespan of components. Continuous monitoring of thermal conditions facilitates reliable estimates of the expected durability of materials, enabling more effective maintenance planning and contributing to the overall longevity of the system. Further details on this aspect will be provided in WP4.

In summary, the task addresses a series of interconnected objectives, ranging from improving the precision of temperature measurements to optimizing converter performance and predicting the lifespan of components. The following section provides a detailed status of the task and the progress achieved to date in attaining these objectives.

6.1.1. Exploration of Advanced Temperature Sensor Networks

The power converter will monitor the temperature of each transistor individually. This proposal enables us to observe the performance of each transistor and use this data to optimize the thermal control system, implement protective measures, or even enhance the digital twin for WP4.

In the low-power converter, there are 2 SiC transistors and 2 GaN transistors used per phase, meaning GaNs are not paralleled. Moreover, all components are discrete and lack integrated NTC probes. Therefore, it has been decided to incorporate 4 NTC thermistors (NTCLE413E2103F520L model) per module, one for each transistor. The specifications of these thermistors are outlined in the following table.

Table 3.1. Specifications of the NTC thermistors for the low-power converter

QUICK REFERENCE DATA		
PARAMETER	**VALUE**	**UNIT**
Resistance value at 25 °C	4.7K to 100K	Ω
Tolerance on R_{25}-value	± 1.0 to ± 5.0	%
$B_{25/85}$-value	3435 to 4190	K
Tolerance on $B_{25/85}$	± 0.5 to ± 1.5	%
Operating temperature range at zero dissipation	-40 to 105	°C
Maximum power dissipation at 55 °C	100	mW
Accuracy of temperature measurement (for 1 % types)	± 0.5 between 0 and 40 ± 1.0 between -40 and 80	°C
Dissipation factor δ (in still air)	≈ 3	mW/K
Response time (in oil)	≈ 2.5	s
Climatic category (LCT / UCT / days)	40 / 105 / 28	
Minimum dielectric withstanding voltage between leads and coated body	500	V_{RMS}
Weight (40 mm length)	0.2	g

In the high-power converter, the sensors employed have slight variations. On the one hand, this converter uses SiC modules that come equipped with their own NTC probes. On the other hand, multiple GaNs are used in parallel per phase to increase the maximum current at which the converter can operate when functioning as a 3-level system.

For the high-power inverter six IGI60F017A1L from Infineon will be used in parallel to achieve a total Rdson of 5.67 mΩ. Hence, each GaN branch connected to the midpoint consists of two transistors in antiparallel, and we use three branches, giving a total of six GaNs.

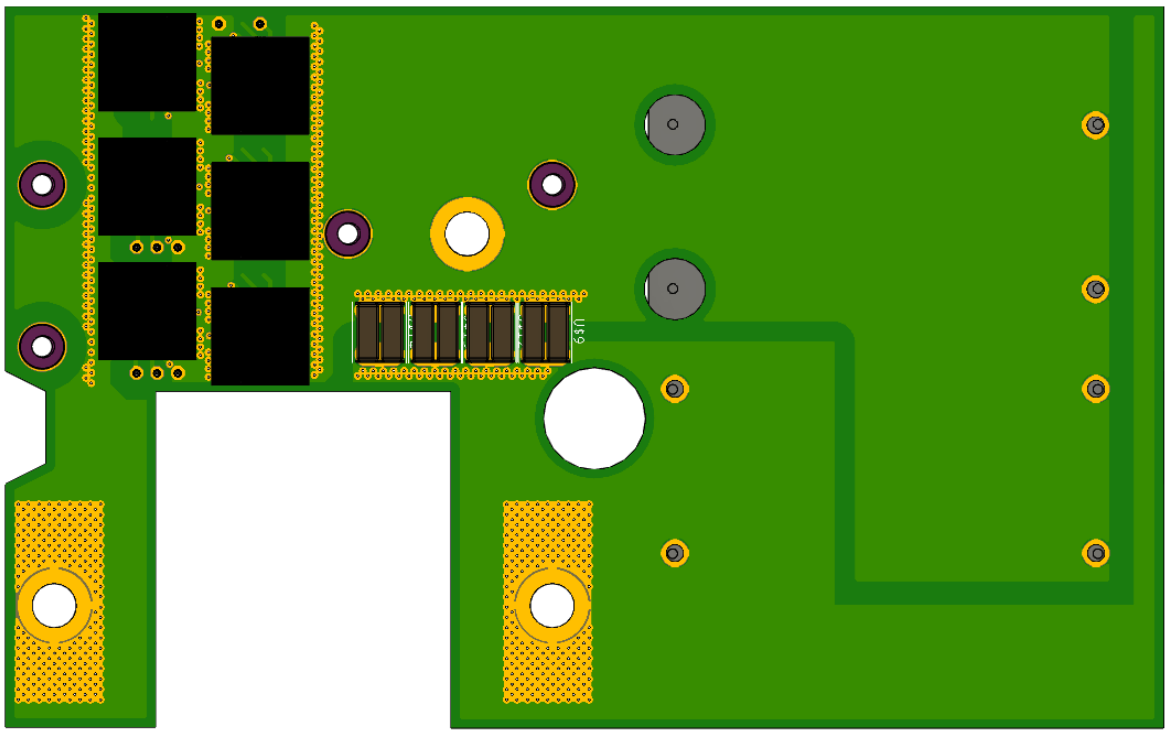

Figure 3.1. Common source configuration showing three GaNs in parallel.

The selected SiC transistors are CAB450M12XM3 from Wolfspeed Cree. Each module includes a 4.7k NTC temperature sensor. Figure 3.2 shows the temperature sensor parameters.

Temperature Sensor (NTC) Characteristics

Symbol	Parameter	Min.	Typ.	Max.	Unit	Test Conditions
R_{25}	Rated Resistance		4.7		kΩ	T_{NTC} = 25 °C
ΔR/R	Tolerance of R_{25}			±1	%	
P_{25}	Maximum Power Dissipation			50	mW	

Figure 3.2. SiC NTC parameters.

To measure the temperature of the discrete GaN semiconductors, multiple temperature sensors (10k NTCs) will be placed close to the GaNs. The exact type of these sensors has not yet been defined.

Moreover, Figure 3.3 shows the control PCB of the high-power inverter. Eight temperature sensor inputs are available. In addition to the semiconductor and module temperature sensors the heatsink and the motor temperature will also be measured.

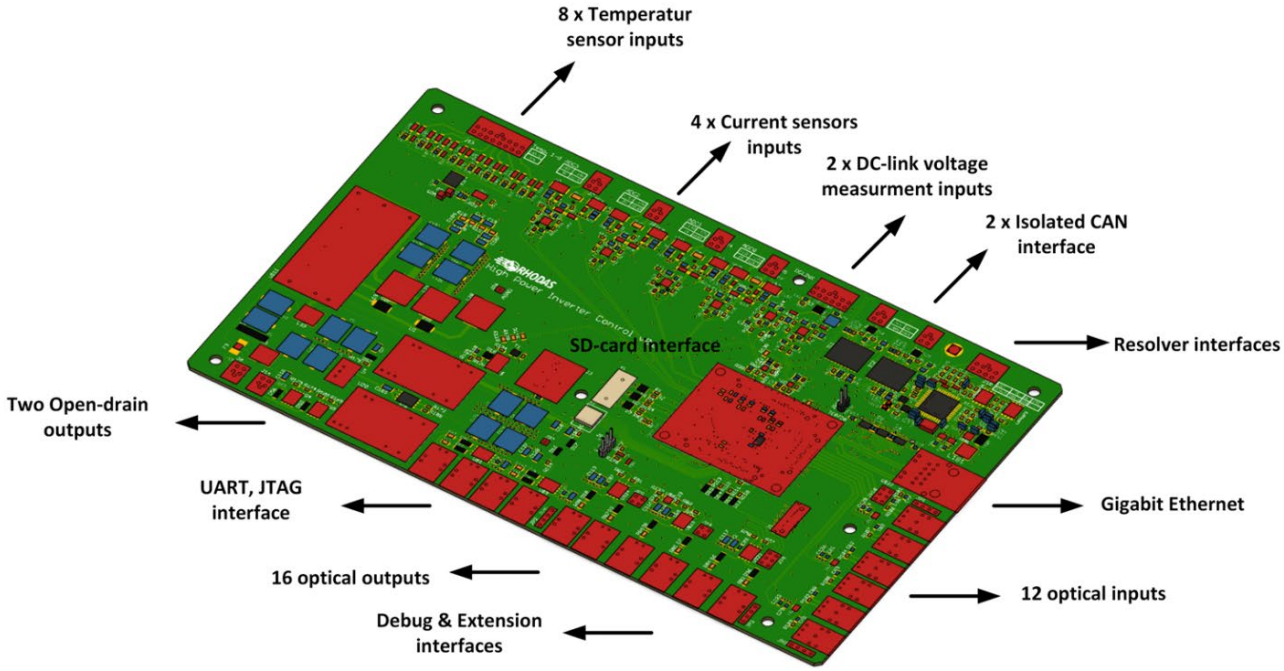

Figure 3.3 Rhodas high-power inverter control PCB.

6.1.2. Key Functions of the Sensors Network

The sensor network, within the context of power converters, is a multifaceted system with a diverse range of applications. It plays a pivotal role in enhancing performance, ensuring safety, and prolonging the lifespan of various components and materials. The utilization of temperature sensors, in particular, is instrumental in achieving these objectives, and their functions can be elucidated as follows:

a) **Transistor Fault Detection:** Temperature sensors are strategically positioned to monitor the thermal behaviour of individual transistors in real time. This granular oversight allows for the early detection of any abnormalities in temperature. For instance, if a transistor fails to heat up as expected, this could be indicative of a malfunction or complete failure. Conversely, if one transistor exhibits significantly higher temperatures compared to others, this anomaly may be attributed to suboptimal switching behaviour. The data provided by these sensors offers crucial insights into the health and performance of each transistor.

b) **Protection Mechanisms:** As discussed earlier, temperature sensors act as proactive sentinels, alerting the system to abnormal conditions in specific transistors. This early warning system is invaluable in enabling swift control interventions to rectify the situation. In the event of a fault in one of the GaN transistors, the converter can seamlessly transition to operate exclusively with SiC transistors, mitigating any potential loss in functionality. Similarly, if a fault is detected in a SiC transistor, the control system can take preventive measures such as halting the converter's operation or reducing its power output, thereby minimizing potential risks and damages.

c) **Over-Temperature Protection:** The network of temperature sensors serves as a guardian against overheating. Should the temperature of any component exceed safe limits, the sensors trigger protective measures. These measures can range from reducing the power output to activating cooling systems to maintain the converter's temperature within the safe operating range. By preventing overheating, the sensors contribute significantly to the longevity of the components and materials within the converter.

d) **Lifetime Prediction:** By continuously monitoring the temperature of various components, these sensors also play a role in predicting the remaining lifespan of the converter. Over time, temperature fluctuations can lead to wear and tear, and the data collected by the sensors can be used to estimate when components may require maintenance or replacement, thereby enhancing the converter's operational efficiency and minimizing unexpected downtime.

The interconnectedness of temperature sensors and their vital functions are visually represented in Figure 3.4, which depicts the operating modes and the strategic placement of these sensors in the low-power converter. This comprehensive system ensures the efficient operation, safety, and longevity of the power converter, making it an indispensable component in various industrial and technological applications.

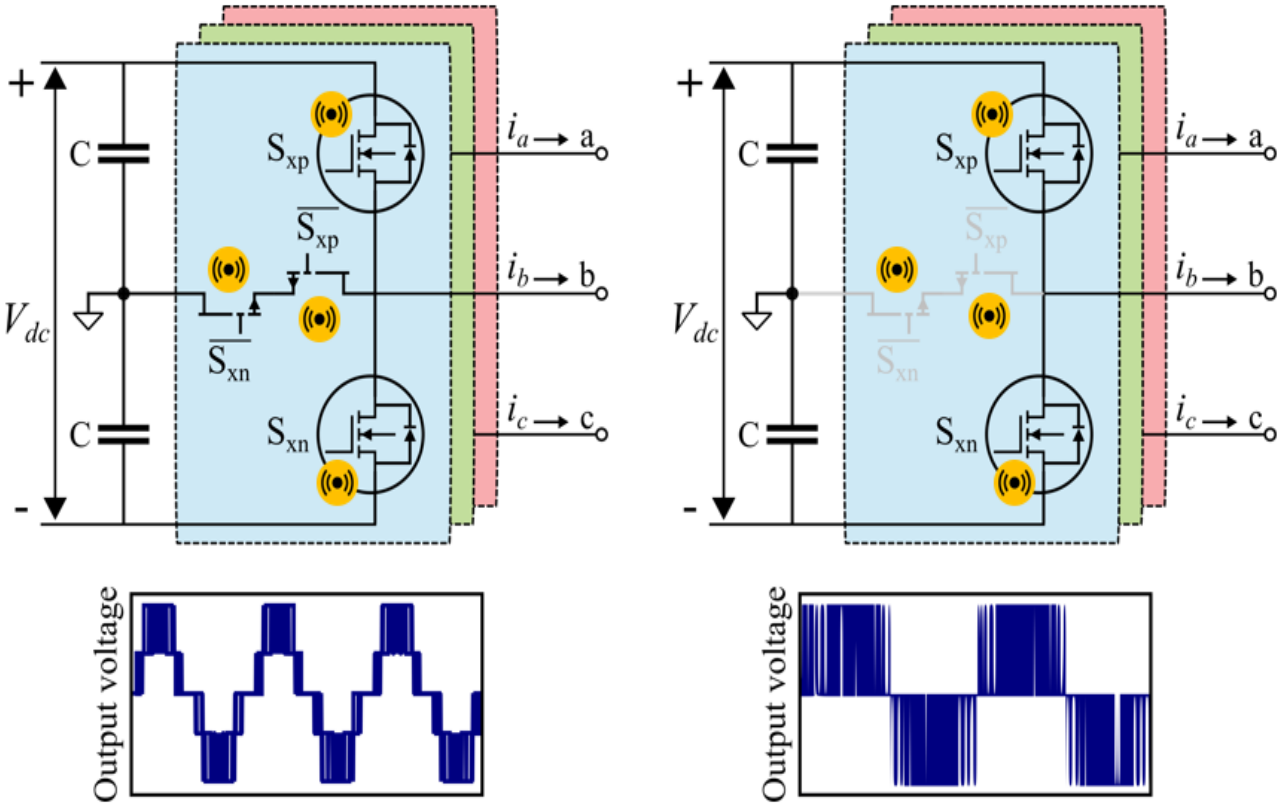

Figure 3.4. operating modes and temperature sensors in the low-power converter.

6.1.3. Integration of Intelligent Soft Sensors

The sensor network is complemented by a set of advanced intelligent soft-sensors, which utilize both data and models to achieve an optimal estimation of the core temperature and provide precise temperature estimations for the die.
These sensors will be implemented using software-driven solutions, which will leverage measurements obtained from the NTC sensors to accurately estimate the die temperature. The implementation involves the deployment of various sophisticated thermal models, ensuring robust and precise temperature calculations.

For sensors measuring the temperature of the transistor encapsulation, the primary consideration lies in the thermal resistance (R_{th}) of the transistors. This critical parameter allows for the estimation of the die temperature through the following equation:

$$T_{die} = T_c + P_d \cdot R_{th}$$

here, T_{die} represents the die temperature, T_c is the temperature of the transistor encapsulation, P_d signifies the power dissipation within the transistor, and R_{th} stands for the thermal resistance from die to encapsulation.

In cases where the temperature sensors are positioned on the opposite side of the PCB from the transistors, an additional factor must be accounted for – the thermal resistance of the PCB (R_{th_PCB}). This consideration is crucial for accurate die temperature estimation and can be described by the following equation:

$$T_{die} = T_{PCB} + P_d(R_{th} + R_{th_PCB})$$

in this equation, T_{PCB} signifies the measured temperature on the opposite side of the PCB.

It is important to note that these measurements will undergo rigorous validation through experimental testing, and if necessary, further verification may be conducted using destructive tests within a thermal chamber. These steps are essential to ensure the accuracy and reliability of the temperature estimations, which are of paramount importance for the safe and efficient operation of the system.

6.2. SPECIFICATIONS AND REQUIREMENTS

This task also involves addressing the specifications and requirements of the sensor networks, ensuring that they meet the necessary criteria for their intended functions.

Fortunately, temperature is a parameter that changes slowly, and the specifications regarding temperature sensors are not as critical as in the case of other sensors. The various specifications for the temperature sensors are detailed below:

- **Measurement Accuracy:** Measurement accuracy is a fundamental requirement to ensure reliable and precise temperature readings. In this case, an acceptable margin of error of ±5°C has been established, with a preference for a maximum of ±2°C. It is important to highlight that this precision is particularly critical for the most sensitive element of the system, which is the GaN transistors. Ensuring measurement accuracy within this range is essential for effective monitoring and protection of the system.

- **Temperature Range:** The specified temperature range for the power converter sensor network covers a minimum range from 0°C to 150°C. Given that transistors typically operate at temperatures around 90°C and are susceptible to damage at 125°C, this range provides a necessary safety margin to capture temperature variations and prevent critical situations. Notice that the electrical motor has different temperature ranges, from -40ºC to 180 ºC so their sensors should be capable of operating at this range.

- **Resolution:** While temperature resolution is not critical in this context, an acceptable resolution of 2°C has been defined. This means that sensors must be able to detect significant temperature changes in increments of 2ºC, which is sufficient for monitoring purposes.

- **Sampling Frequency:** Although real-time sampling is preferred, it is not a critical requirement since temperatures should not vary abruptly. A sampling frequency of every 10 to 20 seconds has been established, providing a balance between real-time temperature monitoring and system efficiency.

- **Calibration and Recalibration:** Sensor recalibration is not required, simplifying system operation and maintenance. This contributes to efficiency and resource savings.

- **Communication Interface:** In this case, no additional communication interface is needed as these are NTC probes designed primarily for temperature measurement.

- **Power Supply:** NTC sensors do not require an additional power source as they function passively and rely on resistance changes to measure temperature. This simplifies sensor installation and operation.

- **Robustness and Environment:** Sensors must be capable of withstanding the same environmental temperatures and conditions as the high-power converter. This robustness is essential to ensure that the sensors operate reliably in the specific environment in which they are deployed.

- **Regulatory Compliance:** Sensors must comply with applicable regulations in the European Union, with a special focus on ROHS (Restriction of Hazardous Substances) and WEEE (Waste Electrical and Electronic Equipment) regulations. Regulatory compliance ensures that sensors are safe and environmentally friendly, in accordance with current European regulations.

These requirements are fundamental to ensure the performance and reliability of the temperature sensor network in a specific environment and in compliance with European regulations.

7. Conclusion

The initial segments of this document detailed the thermal interface between the inverter and cooling system, coupled with an overview of the thermal cooling system architecture. This section further elucidates facets of the thermal interface between inverters and the cooling systems in the context of RHODaS. Firstly, it revisits the Key Performance Indicators (KPI) and Requirements pertinent to Work Package 3 (WP3), offering a foundation for subsequent discussions. With certain assumptions in mind, the document proceeds to delineate estimated junction temperatures, followed by a concise exploration of how specific design choices may impact the equivalent thermal resistance—a crucial factor informing the proposed interface design. Transitioning to the latter part of the document, it encapsulates the significant accomplishments of Task 3.2 within WP3 of the RHODaS project. The focus here is on 3D thermal and power loss modelling, employing advanced methodologies such as Finite Element Analysis and Computational Fluid Dynamics. Emphasis is placed on the pivotal role played by COMSOL Multiphysics in the design of heatsinks, particularly in the realm of Multiphysics simulations, affording a holistic comprehension of heat transfer across solids and fluids. The document then delves into fundamental simulations within COMSOL Multiphysics, employing an elongation problem as a solid mechanic's case study. Coherently presented are analyses of air-cooled heatsink design, sensitivity studies, and the exploration of pin-based structures, accompanied by illustrative figures. Noteworthy contributions include the introduction of the thermal equivalent circuit model for the T-type power converter, the development of the RHODaS Thermal Management System Toolbox, and the strategic decision to design six heatsinks for a high-power converter. The document adeptly communicates the outcomes, methodologies, and implications of the conducted simulations and designs, offering a comprehensive overview of the thermal modelling endeavours within the RHODaS project. Conclusively, the last section of this document canters on elevating temperature monitoring within the project. It investigates advanced temperature sensor networks to ensure precise material and component temperature readings, outlining the selection criteria for sensors in the low-power converter. Simultaneously, the document addresses the sensor selection process for the high-power converter. Proposals for leveraging temperature sensor data to estimate die temperature, adjust converter operation, and detect faults are presented, contributing to a more effective thermal management strategy.

8. Bibliography

1. Hasan, Mushtaq Ismael. Investigation of flow and heat transfer characteristics in micro pin fin heat sink with nanofluid. Applied Thermal Engineering. 2014, Vol. 63, Issue 2, pp. 598-607.

2. Al Sakka, Monzer, et al. "Thermal modeling and heat management of supercapacitor modules for vehicle applications." *Journal of Power Sources* 194.2 (2009): 581-587.

Appendix A – Low power design mail

Dear colleagues,

As we discussed in the last GA, the design of power converters is advancing. Hence, at the UPC, we have already considered the heat dissipation system of the converter, i.e. the location of the heatsinks. We want to share this information with you before our initial WP3 meeting so that you can start thinking about the final dissipation.

Attached are some pictures of the designed low-power converter. Fig_Top shows the top view of the converter, Fig_Bot shows the bottom view, and Fig_3D shows the isometric view. In this converter, the SiC is located in the top layer and the GaN in the bottom layer. The SiC will dissipate through the bottom side via thermal pathways, while each GaN dissipates through the top of its package. Therefore, it is necessary to put a heatsink on each bottom side of each converter, and it must accommodate for the difference in height between the GaN and the PCB. In addition, there must be electrical isolation between the heatsink, the components and various pads. We also prefer not to use screws to fix the heatsink as this would complicate the electrical design, so we prefer to use adhesive. In the pictures, you can see that there are some through-hole components. This should not be a problem as we will make sure that their legs do not touch the heatsink. Finally, this converter is modular, each phase of the converter will go on its own PCB and then these PCBs will be mounted on another PCB, a motherboard. Therefore, we will need a heatsink for each module or an equivalent system.

Regarding the high-power converter designed by AIT, 3D models are available on ownCloud server. In those models, you can see where they plan to place the heatsink.

I hope that the geometry of the low-power converter is clear from this explanation. Do not hesitate to contact me if you have any doubt.

Best regards,
--
Dr. David Lumbreras
Power Electronics Researcher
MCIA - Universitat Politècnica de Catalunya
email: david.lumbreras@upc.edu

MCIA Center Innovation Electronics
Rambla Sant Nebridi 22, GAIA Research Building - TR14
08222 Terrassa (Spain)

Appendix B – High power design mail

Dear Uffe,

please have a look at the following answers to your questions:

- What power modules have been chosen?

For the SiC half bridge we are using CAB450M12XM3 modules from Wolfspeed. For the T-type GaN branch GS66516T (25mΩ/ 650V) from GaN Systems or CoolGaN IGI60F017A1L (17mΩ/ 600V) will be used.

- What are the estimated losses?

Following assumptions have been made:
U_DC = 950V, Rth (junction to case) = 0.11K/W (in reality R_th of TIM and R_th of heat sink (Aluminium to water) need to be added and will therefore increase!), Water inlet temperature = 60°C, Inverter output power 150kW, Inverter in 2 level mode
@fsw = 20kHz-> Power losses ~ 1.7 kW
@fsw = 35kHz-> Power losses ~ 2.7 kW
@fsw = 50kHz-> Power losses ~ 3.8 kW
@fsw = 70kHz-> Power losses ~ 5.2 kW -> (only under 50°C Water inlet possible, since SiCs would overheat, even with ideal heat sink!)
Losses are nearly linear with switching frequency, because these losses will have biggest portion on total losses.

- Has it been considered how the power modules can be soldered after they have been mounted on the heatsink? (Mounting
procedure is critical to ensure good thermal contact with the heatsink.)

The SiC modules are mounted with four screws on the heatsink with TIM (not yet defined) in between. The GaNs are top cooled. Spacers define the distance between the GaN transistors and the heat sink (see picture below).

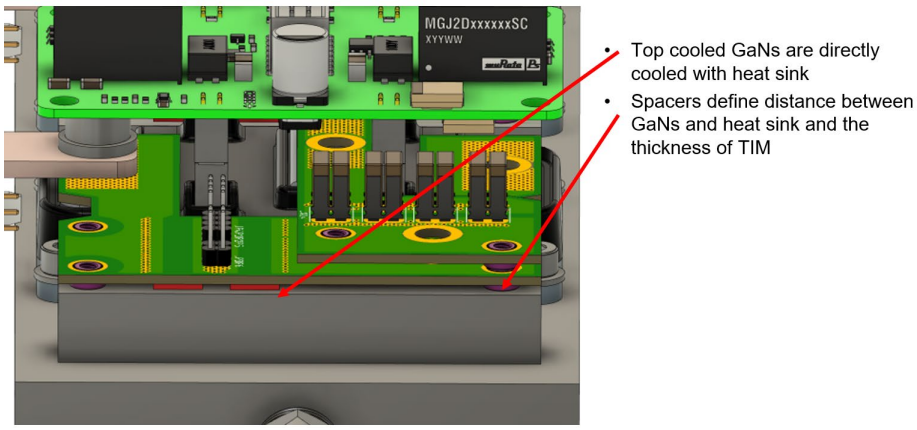

- What estimated capacitive current is going through the heatsink and should the heatsink be tied to inverter ground?

The heatsink should be connected to the inverter housing which is connected to PE or the chassis.

- What sensors are available regarding temperature and where are they placed?

The control platform has 8 NTC inputs. The location of each sensor is not defined yet, but we are planning to mount sensors on possible DC-link hot spots or close to the GaN transistors and on the heat sink. In addition, each SiC half bridge module includes a temperature sensor.

It's still an early stage in the development process (this week we received GaNs from Infineon with integrated driver which sound promising…but we still have to test them) but if you have any further questions I will try to answer them.

Best regards,
Markus

MARKUS KOLLER
Research Engineer
Electric Vehicle Technologies
Center for Low-Emission Transport

AIT Austrian Institute of Technology GmbH
Giefinggasse 2 | 1210 Vienna | Austria
T +43 50550-6617 | M +43 664 88256001
markus.koller@ait.ac.at | www.ait.ac.at

Appendix C – Pump curves for Grundfos Magna3 25-60

Grundfos Magna3 25-60 pump (has pressure sensor) with Modbus CIM module.

Appendix D – Fischer Elektronik Silicone foil

If the chosen transistor is non isolated, an isolated pad has to be chosen.

From Fischer Elektronik silicone foils:

Assumes 3kV isolation needed:

colour:	brown
foil type:	foil WB
for transistor:	3159
material:	silicone foil, GF reinforced
thermal resistance:	0.34 K/W
material thickness:	$0.15^{+0,020/-0,040}$ mm
hardness:	92 IRHD
thermal conductivity:	1.44 W/m·K
temperature range:	-40°C... +150°C
insulation resistance:	$1 \cdot 10^{13}$ Ω·m
elongation:	2 %
dielectric strength:	3 kV
class of inflammability:	UL 94 V-0

https://www.fischerelektronik.de/web_fischer/en_GB/heatsinks/E01.01/Silicone%20rubber%20insulating%20material%20for%20semiconductors/$catalogue/fischerData/PR/WB3159/search.xhtml seen 15/6-2023.

Appendix E – Ideal load calculations

$R_{th_junction_to_case} := 0.13 \ \frac{K}{W}$ $\qquad mK := 10^{-3} \cdot K$

@fsw = 20kHz-> Power losses ~ 1.7 kW
@fsw = 35kHz-> Power losses ~ 2.7 kW
@fsw = 50kHz-> Power losses ~ 3.8 kW
@fsw = 70kHz-> Power losses ~ 5.2 kW -> (only under 50°C Water inlet possible, since SiCs would overheat, even with ideal heat sink!)

$T_{ambient} := 50 \ °C$ $\qquad T_{junction_max} := 175 \ °C$

$\Delta T_{case} := 20 \ K$ $\qquad T_{case} := T_{ambient} + \Delta T_{case}$

$P_{transistor} := \frac{5.2 \ kW}{6} = 866.667 \ W$ 70kHz

$P_{transistor_max} := \frac{T_{junction_max} - T_{case}}{R_{th_junction_to_case}} = 807.692 \ W$

$\Delta_{junction_to_case} := P_{transistor} \cdot R_{th_junction_to_case} = 112.667 \ K$

$T_{junction} := \Delta_{junction_to_case} + T_{case} = 182.667 \ °C$

$R_{th_needed} := \frac{T_{junction_max} - T_{case}}{P_{transistor}} = 121.154 \ \frac{mK}{W}$ $\qquad R_{combined_cooling} := \frac{\Delta T_{case}}{P_{transistor}} = 0.023 \ \frac{K}{W}$

$P_{transistor} := \frac{3.8 \ kW}{6}$ 50kHz

$\Delta_{junction_to_case} := P_{transistor} \cdot R_{th_junction_to_case} = 82.333 \ K$
$T_{junction} := \Delta_{junction_to_case} + T_{case} = 152.333 \ °C$

$R_{th_needed} := \frac{T_{junction_max} - T_{case}}{P_{transistor}} = 165.789 \ \frac{mK}{W}$ $\qquad R_{combined_cooling} := \frac{\Delta T_{case}}{P_{transistor}} = 0.032 \ \frac{K}{W}$

$P_{transistor} := \frac{2.7 \ kW}{6} = 450 \ W$ 35kHz

$\Delta_{junction_to_case} := P_{transistor} \cdot R_{th_junction_to_case} = 58.5 \ K$
$T_{junction} := \Delta_{junction_to_case} + T_{case} = 128.5 \ °C$

$R_{th_needed} := \frac{T_{junction_max} - T_{case}}{P_{transistor}} = 233.333 \ \frac{mK}{W}$ $\qquad R_{combined_cooling} := \frac{\Delta T_{case}}{P_{transistor}} = 0.044 \ \frac{K}{W}$

$$P_{transistor} := \frac{1.7\ kW}{6}$$ 20kHz

$$\Delta_{junction_to_case} := P_{transistor} \cdot R_{th_junction_to_case} = 36.833\ K$$

$$T_{junction} := \Delta_{junction_to_case} + T_{case} = 106.833\ °C$$ +

$$R_{th_needed} := \frac{T_{junction_max} - T_{ambient}}{P_{transistor}} = 441.176\ \frac{mK}{W}$$ $$R_{combined_cooling} := \frac{\Delta T_{case}}{P_{transistor}} = 0.071\ \frac{K}{W}$$

Appendix F -Key impact pathways from the Grant Agreement

(a) Key Impacts Pathways (KIPs): how RHODaS will contribute to the described outcomes and impacts.

KIP1: Demonstrate a minimum of 20% cost reduction of power electronic modules and inverters for a given power, to increase the overall affordability of EVs in mass production (in comparison to the cost of the best current-generation or close to market components at proposal submission time).

Cost reduction and increased power density combined with longer lifetime are the main challenges for the development of a new generation of inverters. RHODaS will develop novel converter topologies, integrating advanced WBG semiconductors for high-voltage (1000-1200V) traction power trains, demonstrating more efficient, cost-effective, and power dense electronic modules (150-200 kW per axel). In addition to the use of novel semiconductor materials and the integration of optimised thermal management systems within the Integrated Motor Drives (IMD) with advanced control strategies based on AI will contribute to achieve a 20% cost reduction of powertrains, increasing the affordability and promoting a full-market penetration of heavy-duty EVs (Economic Outcomes&Impacts). Addressed in TO1 and TO3.

KIP2: Significant advancements in efficiency (reduction of losses by 25%) and thermal performance (increased maximum operational temperature), both parameters versus the state of the art of the targeted application.

This allows further driving range extension, faster charging, and easier thermal management of the whole powertrain, as well as possible improvement in cabin-heating and defrosting in winter. Exploiting the wide frequency range of the WBG materials integrated in the powertrains, RHODaS will develop novel control approaches improving the reliability while reducing the losses by 40%, apart from reducing noise and interferences, based on adaptive switching frequency control depending on the driving mode. The capabilities hybrid SiC/GaN switches reduce the complexity of the control, allowing new adaptive switching frequency strategies, and increase the temperature of operation up to 175ºC. In addition, RHODaS will implement a more effective hybrid thermal management system combining micro liquid- cooling and air-cooling systems to mitigate negative effects of high current on health and ageing of the materials and components. This will significantly improve the thermal performance of the powertrains, which allows to extend the truck driving range in a 10% (Technological Outcomes&Impacts). Addressed in TO1.

KIP3: Development of power electronics enabling drastic size and weight reductions for the electric drive, with significant advances beyond 5 kW/kg or 20kW/litre for a BEV.

One of the biggest challenges of power electronics in electric vehicles is increasing the power density, developing smaller components, handling more power while fitting in smaller packages: in other words, to achieve a significant reduction in terms of both size and weight. RHODaS will achieve more than 50% reduction of size and a 30% reduction of weight, taking advantage of the application of GaN and hybrid configurations of SiC-GaN to boost performance using the minimum amount of

material, according to ecodesign principles. Significant power converter's volumetric and gravimetric power densities of 100kW/l and 50kW/kg are expected, which together with the integration of the motor within the IMD will help to achieve the ambitious targets for 2025 of 33kW/l and 5 kW/kg. At system-level, the benefits of using the new semiconductors materials include the possibility of further reducing the size, weight and cost of the power conditioning and thermal systems, resulting in a system volume reduction up to 40% (Technological Outcomes&Impacts). Addressed in TO2.

KIP4: Facilitating the integration of power electronics in batteries/fuel cells and electric motors/axles (including modular approaches).

RHODaS will adopt a modular and eco-design approach to unify 3D design and manufacture, performance, and safety requirements, in order to create cost-efficient integrated IMD approaches. RHODaS will also implement the integration of the DC/DC into the DC/AC converters with a phase-based modular strategy, achieving a greater efficiency level (+5%) in the IMD due to less energetic losses at the power conversion (-40%), and easier installation compared to present technologies. RHODaS circular design strategies will allow to develop circular product concepts: it will develop and fabricate highly integrated base modules for modular power electronics using 3D design and simulation for making easier further dismantling and reusing of components and materials. (Technological Outcomes&Impacts). Addressed in TO2 and TO5.

KIP5: Increased reliability and availability of powertrain by intelligent control and diagnostics techniques, predictive maintenance of machine and inverter.

RHODaS will implement the most advanced digital and simulation tools and AI technologies tools to improve the robustness, reliability, and lifetime of power converters. First, RHODaS will achieve the effective integration of embedded sensors within the materials and components of the IMD for an advanced monitoring of the system in real time. Second, cloud-based intelligent control, simulation and diagnostics techniques will be implemented to improve the powertrain design, performance and lifetime using cloud computing, big data, AI, ML algorithms and IoT platforms. This will allow to detect changes in relevant operation parameters at material, component, and system level in real time to develop physic and data-driven models which are integrated in a complete Digital Twin to further implement health management strategies for optimising design, operation, reduce failures and extend lifecycle of the materials. components and systems in a holistic approach. Ultimately, by applying its intelligent control and predictive maintenance technologies, RHODaS will achieve a 30% reduction of critical failures, 20% reduction of costs, 25% extension of lifetime and 30% improvement in LCA. (Technological Outcomes&Impacts). Addressed in TO3 and TO5.

KIP6: Achieve automotive quality levels in the whole system with new, robust, and reliable functionalities and materials.

Appendix G – Low/high-power Inverter Specifications

Appendix G discloses precise technical details, including dimensions and power board mounting, for AIT's high-power and UPC's low-power inverters.

High-power inverter geometry

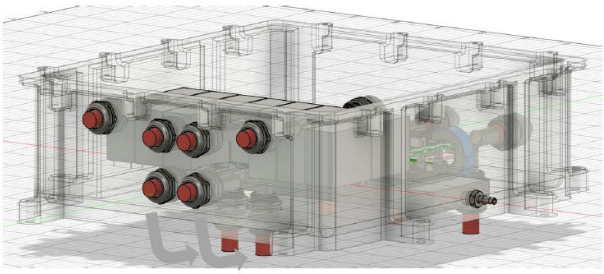

Flexible Positioning!

- Flexible arrangement of the cable gland
- Short Version & Long Version possible

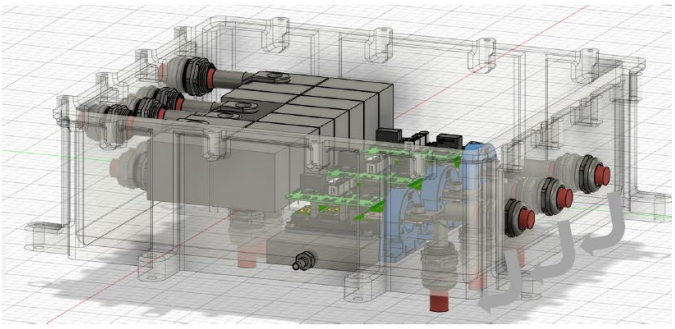

Flexible Positioning!

High-power inverter geometry

Long Version

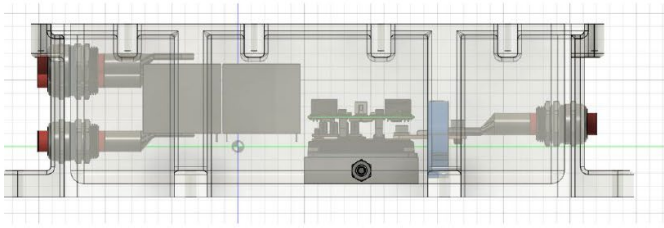

382mm

Short Version

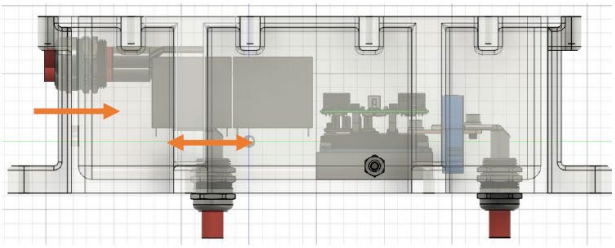

352mm

- Further length reduction possible → dependent on the Fiberglass cables / connectors

High-power inverter Mounting Points

Long Version

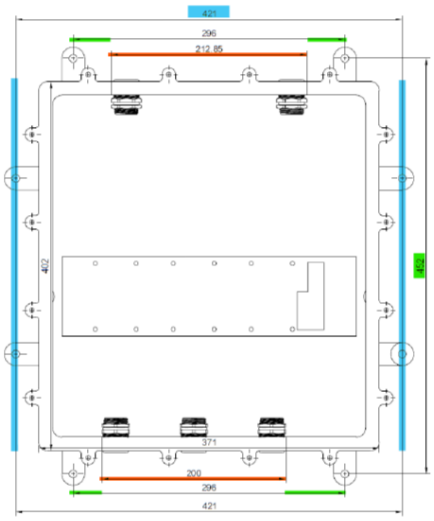

- Possible mounting points (green & blue)
- Not possible mounting points (red)
- Arrangement of the mounting points is flexible → changes possible

Short Version

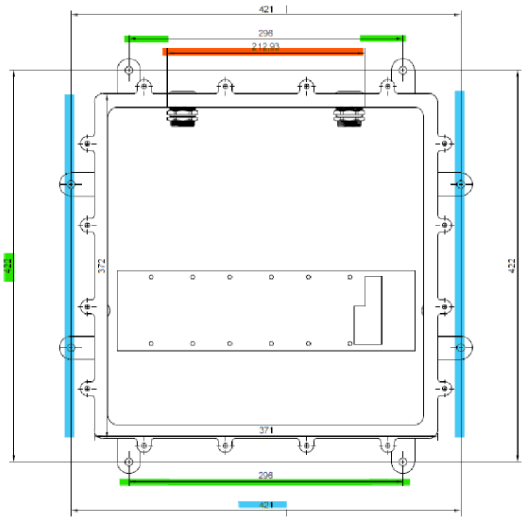

Status. Low-power converter.

- Modular design
- Three PCBs: motherboard, control board (x3) & power board (x3)

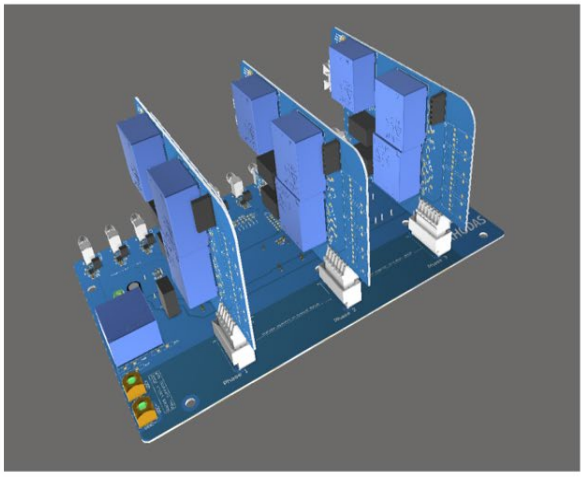

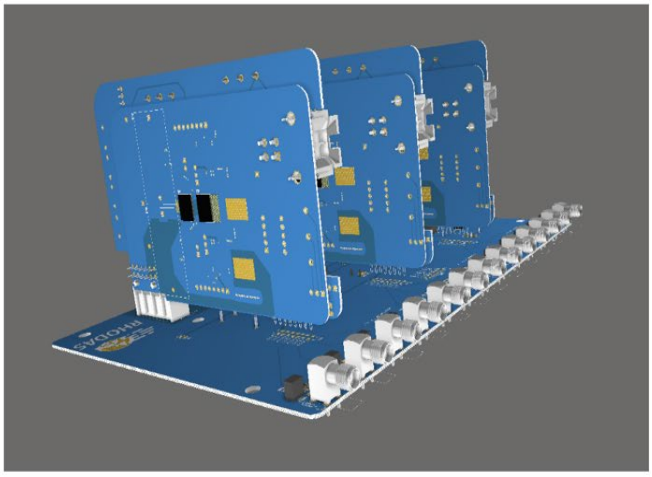

Status. Low-power converter.

- Adaptable distance to accommodate heatsinks

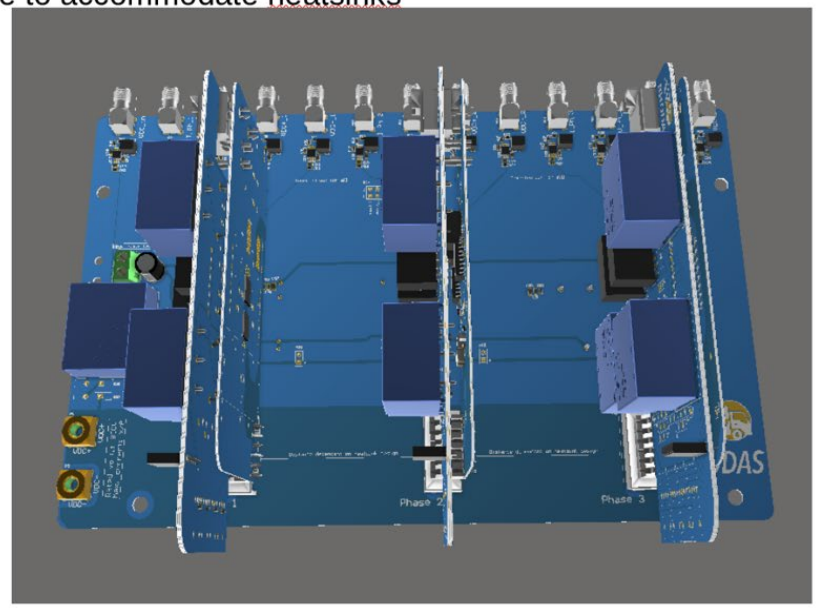

Status. Low-power converter. Power board.

- Heatsink dimensions

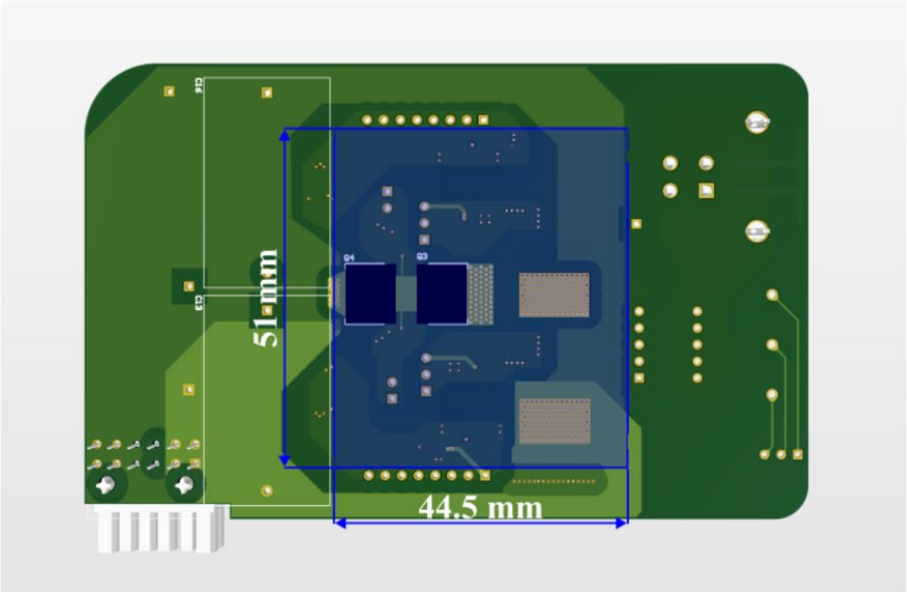

Appendix H – SiC-CAB450M12XM3 from Wolfspeed Cree

V_{DS}	1200 V
I_{DS}	450 A

CAB450M12XM3

1200V, 450A All-Silicon Carbide
Conduction Optimized, Half-Bridge Module

Technical Features

- High Power Density Footprint
- High Junction Temperature (175 °C) Operation
- Low Inductance (6.7 nH) Design
- Implements Conduction Optimized Third Generation SiC MOSFET Technology
- Silicon Nitride Insulator and Copper Baseplate

Applications

- Motor & Traction Drives
- Vehicle Fast Chargers
- Uninterruptable Power Supplies
- Smart-Grid / Grid-Tied Distributed Generation

Package 80 x 53 x 19 mm

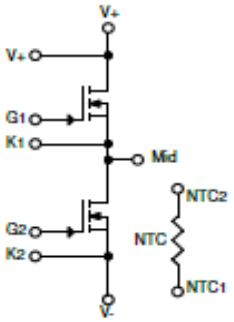

System Benefits

- Terminal layout allows for direct bus bar connection without bends or bushings enabling a simple, low inductance design.
- Isolated integrated temperature sensing enables high-level temperature protection.
- Dedicated drain Kelvin pin enables direct voltage sensing for gate driver overcurrent protection.

Key Parameters (T_C = 25 °C unless otherwise specified)

Symbol	Parameter	Min.	Typ.	Max.	Unit	Test Conditions	Note
$V_{DS\,max}$	Drain-Source Voltage			1200	V		
$V_{GS\,max}$	Gate-Source Voltage, Maximum Value	-4		+19	V	AC frequency ≥ 1Hz.	Note 1
$V_{GS\,op}$	Gate-Source Voltage, Recommended Op. Value	-4		+15	V	Static	
I_{DS}	DC Continuous Drain Current			450	A	V_{GS} = 15 V, T_C = 25 °C, T_{VJ} ≤ 175 °C	Fig. 20
			409		A	V_{GS} = 15 V, T_C = 90 °C, T_{VJ} ≤ 175 °C	Note 2
I_{SD}	DC Source-Drain Current			450	A	V_{GS} = 15 V, T_C = 25 °C, T_{VJ} ≤ 175 °C	
$I_{SD\,BD}$	DC Source-Drain Current (Body Diode)		225		A	V_{GS} = - 4 V, T_C = 25 °C, T_{VJ} ≤ 175 °C	
$I_{DS\,(pulsed)}$	Maximum Pulsed Drain-Source Current			900	A	t_{Pmax} limited by T_{Jmax} V_{GS} = 15 V, T_C = 25 °C	
$I_{SD\,(pulsed)}$	Maximum Pulsed Source-Drain Current			900	A		
$T_{VJ\,op}$	Maximum Virtual Junction Temperature under Switching Conditions	-40		175	°C		

Note 1 If MOSFET body diode is not used, $V_{GS\,max}$ = -8/+19 V
Note 2 Assumes $R_{TH\,JC}$ = 0.11°C/W and $R_{DS(on)}$ = 4.6 mΩ. Calculate $P_D = (T_{VJ} - T_C) / R_{TH\,JC}$. Calculate $I_{D_MAX} = \sqrt{(P_D / R_{DS(on)})}$

MOSFET Characteristics (Per Position) (T_C = 25 °C unless otherwise specified)

Symbol	Parameter	Min.	Typ.	Max.	Unit	Test Conditions	Note
$V_{BR(DSS)}$	Drain-Source Breakdown Voltage	1200			V	V_{GS} = 0 V, I_D = 200 µA	
$V_{GS(th)}$	Gate Threshold Voltage	1.8	2.5	3.6		V_{DS} = V_{GS}, I_D = 132 mA	
			2.0			V_{DS} = V_{GS}, I_D = 132 mA, T_J = 175 °C	
I_{DSS}	Zero Gate Voltage Drain Current		5	200	µA	V_{GS} = 0 V, V_{DS} = 1200 V	
I_{GSS}	Gate-Source Leakage Current		0.05	1.3		V_{GS} = 15 V, V_{DS} = 0 V	
$R_{DS(on)}$	Drain-Source On-State Resistance (Devices Only)		2.6	3.7	mΩ	V_{GS} = 15 V, I_D = 450 A	Fig. 2 Fig. 3
			4.6			V_{GS} = 15 V, I_D = 450 A, T_J = 175 °C	
g_{fs}	Transconductance		355		S	V_{DS}= 20 V, I_{DS}= 450 A	Fig. 4
			360			V_{DS}= 20 V, I_{DS}= 450 A, T_J = 175 °C	
E_{On}	Turn-On Switching Energy, T_J = 25 °C T_J = 125 °C T_J = 175 °C		11.0 11.7 13.0		mJ	V_{DS} = 600 V, I_D = 450A, V_{GS} = -4 V/15 V, $R_{G(ext)}$ = 0.0 Ω, L= 13.6 µH	Fig. 11 Fig. 13
E_{Off}	Turn-Off Switching Energy, T_J = 25 °C T_J = 125 °C T_J = 175 °C		10.1 11.3 12.1				
$R_{G(int)}$	Internal Gate Resistance		2.5		Ω		
C_{iss}	Input Capacitance		38.0		nF	V_{GS} = 0 V, V_{DS} = 800 V, V_{AC} = 25 mV, f = 100 kHz	Fig. 9
C_{oss}	Output Capacitance		1.5				
C_{rss}	Reverse Transfer Capacitance		90		pF		
Q_{GS}	Gate to Source Charge		355		nC	V_{DS} = 800 V, V_{GS} = -4 V/15 V I_D = 450 A Per IEC60747-8-4 pg 21	
Q_{GD}	Gate to Drain Charge		500				
Q_G	Total Gate Charge		1330				
$R_{th\,JC}$	FET Thermal Resistance, Junction to Case		0.11	0.13	°C/W		Fig. 17

Body Diode Characteristics (Per Position) (T_C = 25 °C unless otherwise specified)

Symbol	Parameter	Min.	Typ.	Max.	Unit	Test Conditions	Note
V_{SD}	Body Diode Forward Voltage		4.7		V	V_{GS} = -4 V, I_{SD} = 450 A	Fig. 7
			4.2			V_{GS} = -4 V, I_{SD} = 450 A, T_J = 175 °C	
t_{rr}	Reverse Recovery Time		52		ns	V_{GS} = -4 V, I_{SD} = 450 A, V_R = 600 V di/dt = 8 A/ns, T_J = 175 °C	
Q_{rr}	Reverse Recovery Charge		6.6		µC		
I_{rr}	Peak Reverse Recovery Current		195		A		
E_{rr}	Reverse Recovery Energy T_J = 25 °C T_J = 125 °C T_J = 175 °C		0.2 1.1 1.9		mJ	V_{DS} = 600 V, I_D = 450A, V_{GS} = -4 V/15 V, $R_{G(ext)}$ = 0.0 Ω, L= 13.6 µH	Fig. 14

Temperature Sensor (NTC) Characteristics

Symbol	Parameter	Min.	Typ.	Max.	Unit	Test Conditions
R_{25}	Rated Resistance		4.7		kΩ	T_{NTC} = 25 °C
ΔR/R	Tolerance of R_{25}			±1	%	
P_{25}	Maximum Power Dissipation			50	mW	

Steinhart-Hart Modified Coefficients for R/T Computation: $\frac{1}{T} = A + B \times \ln\left(\frac{R}{R_{25}}\right) + C \times \ln^2\left(\frac{R}{R_{25}}\right) + D \times \ln^3\left(\frac{R}{R_{25}}\right)$

	A	B	C	D
T_{NTC} < 25 °C	3.3540E-03	3.0013E-04	5.0852E-06	2.1877E-07
T_{NTC} ≥ 25 °C	3.3540E-03	3.0013E-04	5.0852E-06	2.1877E-07

Module Physical Characteristics

Symbol	Parameter	Min.	Typ.	Max.	Unit	Test Conditions
R_{3-1}	Package Resistance, M1		0.72		mΩ	T_c = 125 °C, Note 3
R_{1-2}	Package Resistance, M2		0.63			T_c = 125 °C, Note 3
L_{Stray}	Stray Inductance		6.7		nH	Between Terminals 2 and 3
T_C	Case Temperature	-40		125	°C	
W	Weight		175		g	
M_s	Mounting Torque	2.0	3.0	4.0	N-m	Baseplate, M4 bolts
		2.0	4.0	5.0		Power Terminals, M5 bolts
V_{isol}	Case Isolation Voltage	4.0			kV	AC, 50 Hz, 1 min
CTI	Comparative Tracking Index	600				
	Clearance Distance	12.5			mm	From 2 to 3, Note 4
		11.5				From 1 to Baseplate, Note 4
		5.7				From 2 to 5, Note 4
		13.7				From 5 to Baseplate, Note 4
	Creepage Distance	14.7				From 2 to 3, Note 4
		14.0				From 1 to Baseplate, Note 4
		14.7				From 2 to 5, Note 4
		14.3				From 5 to Baseplate, Note 4

Note 3 Total Effective Resistance (Per Switch Position) = MOSFET $R_{DS(on)}$ + Switch Position Package Resistance.

Note 4 Numbers reference the connections from the Schematic and Package Dimensions sections of this document.

Typical Performance

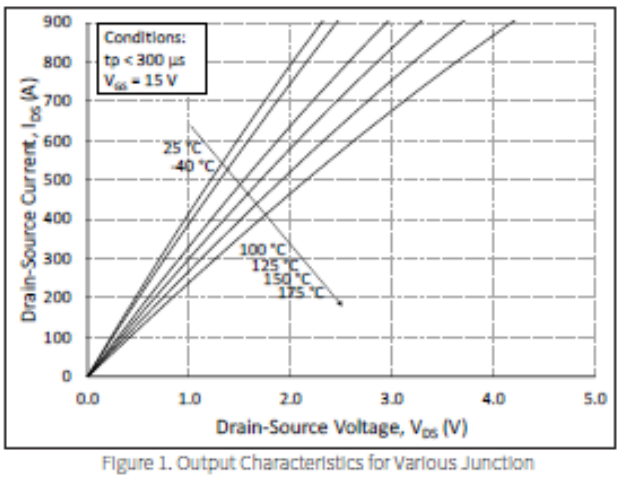

Figure 1. Output Characteristics for Various Junction Temperatures

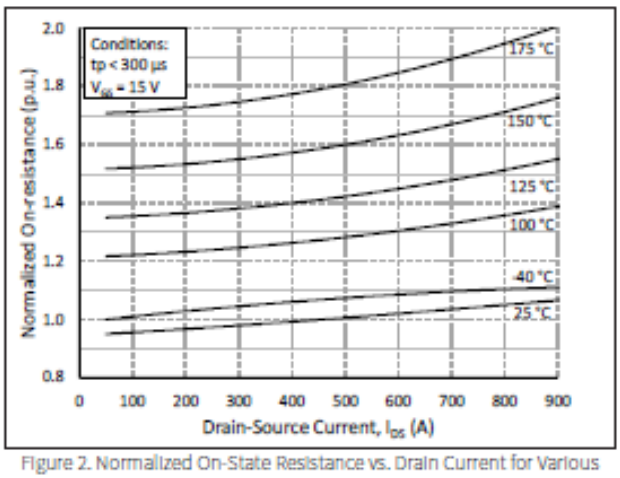

Figure 2. Normalized On-State Resistance vs. Drain Current for Various Juction Temperatures

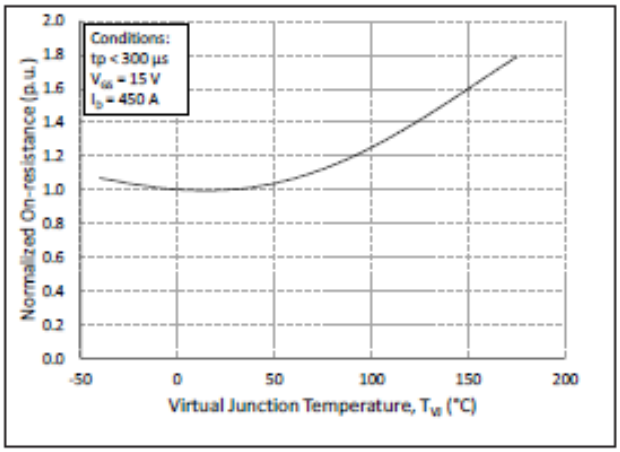

Figure 3. Normalized On-State Resistance vs. Juction Temperature

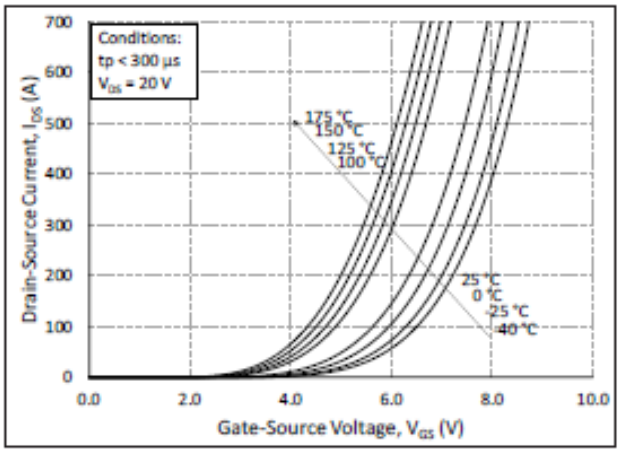

Figure 4. Transfer Characteristic for Various Junction Temperatures

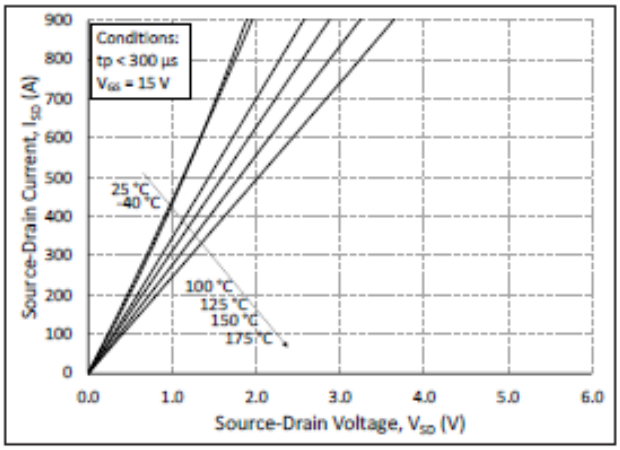

Figure 5. 3rd Quadrant Characteristic vs. Junction Temperatures at V_{GS} = 15 V

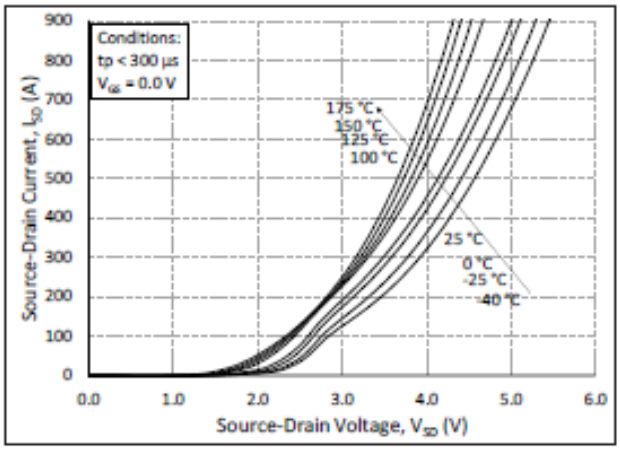

Figure 6. 3rd Quadrant Characteristic vs. Junction Temperatures at V_{GS} = 0 V (Body Diode)

Typical Performance

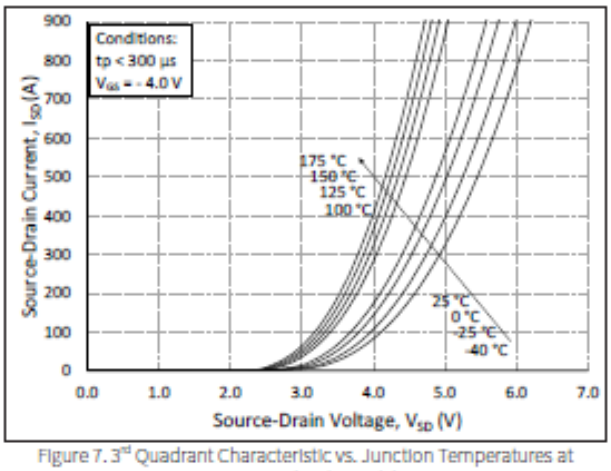

Figure 7. 3rd Quadrant Characteristic vs. Junction Temperatures at V_{GS} = - 4 V (Body Diode)

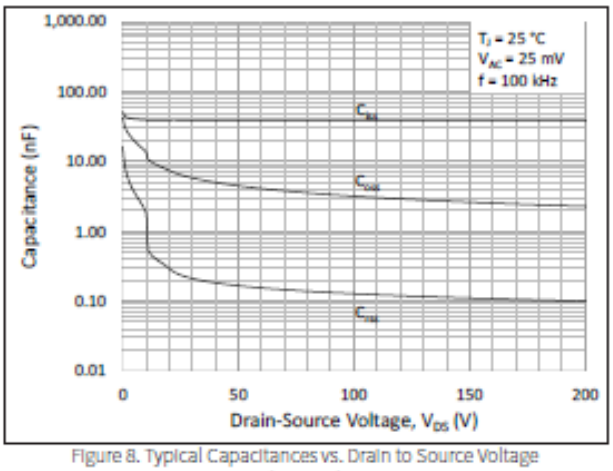

Figure 8. Typical Capacitances vs. Drain to Source Voltage (0 - 200V)

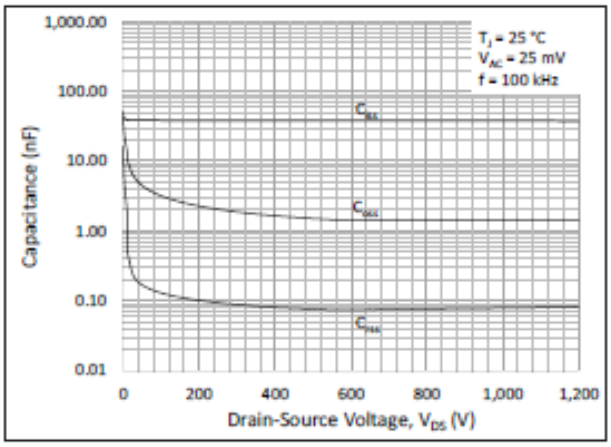

Figure 9. Typical Capacitances vs. Drain to Source Voltage (0 - 1200V)

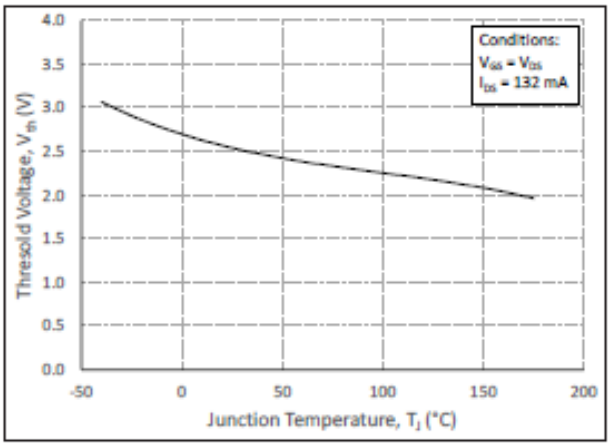

Figure 10. Threshold Voltage vs. Junction Temperature

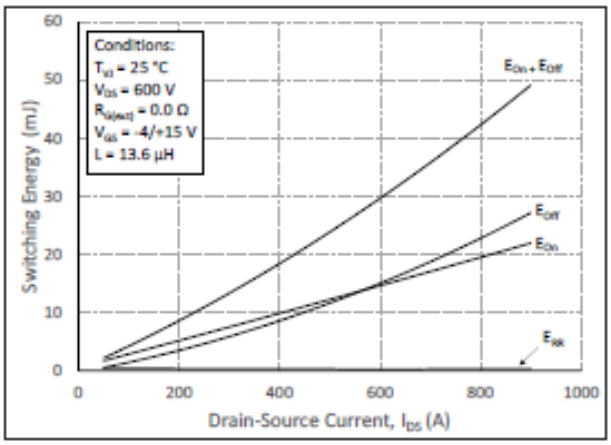

Figure 11. Switching Energy vs. Drain Current (V_{DS} = 600 V)

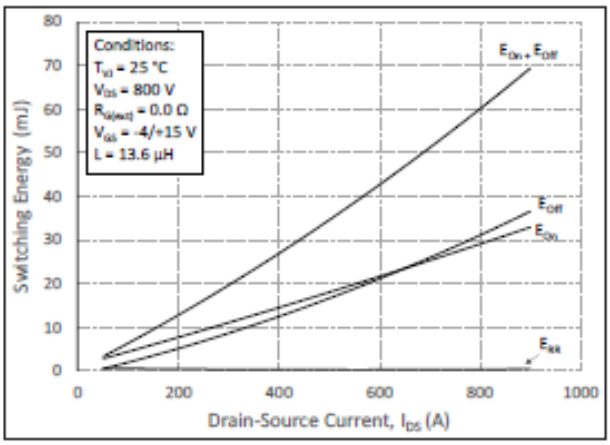

Figure 12. Switching Energy vs. Drain Current (V_{DS} = 800 V)

Typical Performance

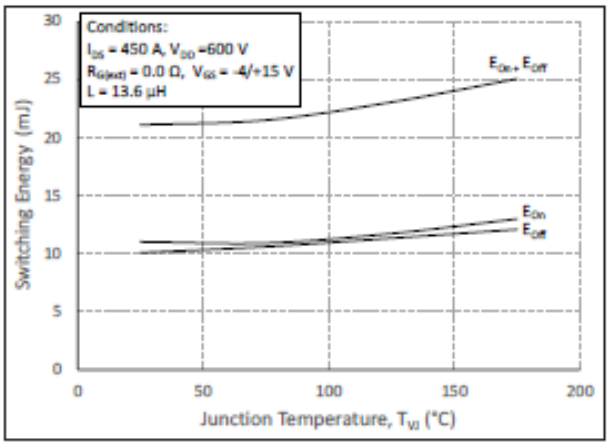

Figure 13. MOSFET Switching Energy vs. Junction Temperature

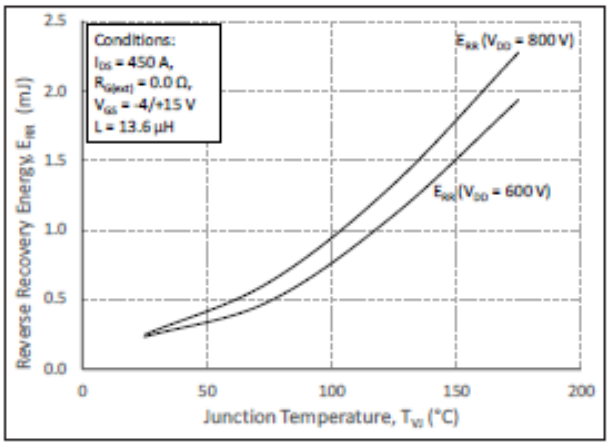

Figure 14. Reverse Recovery Energy vs. Junction Temperature

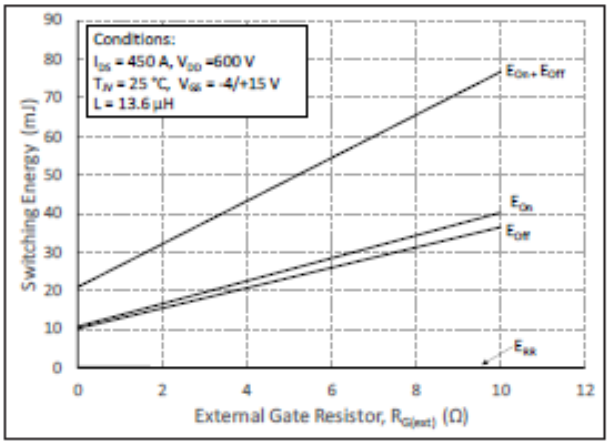

Figure 15. MOSFET Switching Energy vs. External Gate Resistance

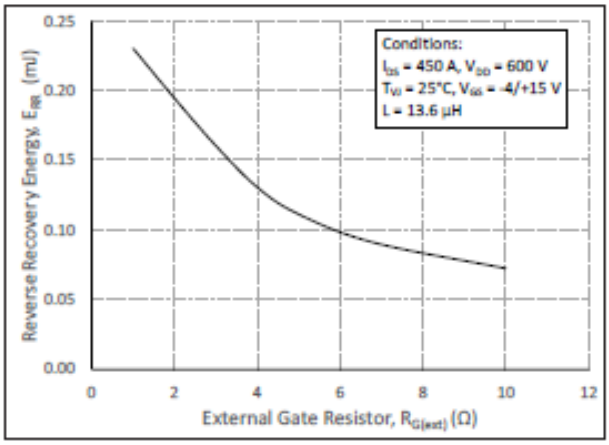

Figure 16. Reserve Recovery Energy vs. External Gate Resistance

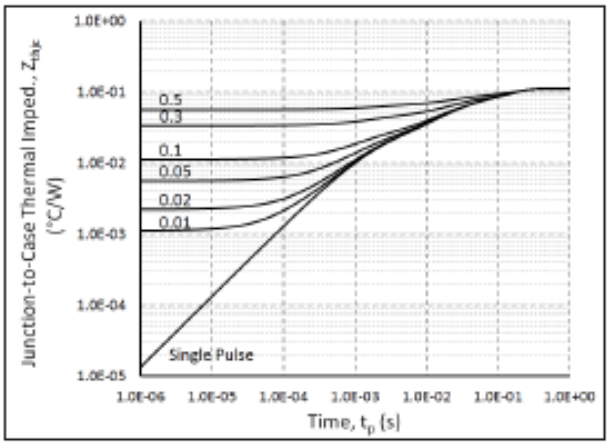

Figure 17. MOSFET Juction to Case Transient Thermal Impedance, $Z_{th\,JC}$ (°C/W)

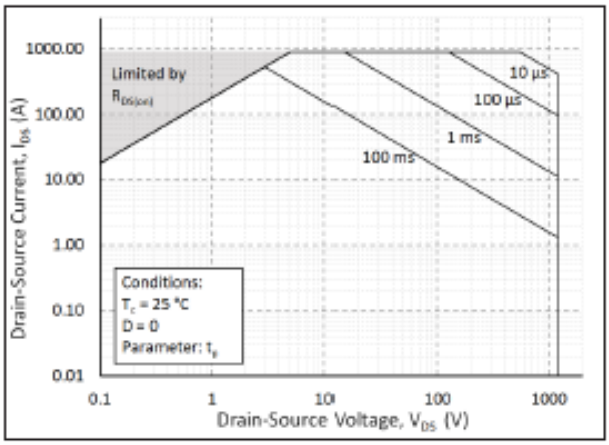

Figure 18. Forward Bias Safe Operating Area (FBSOA)

Typical Performance

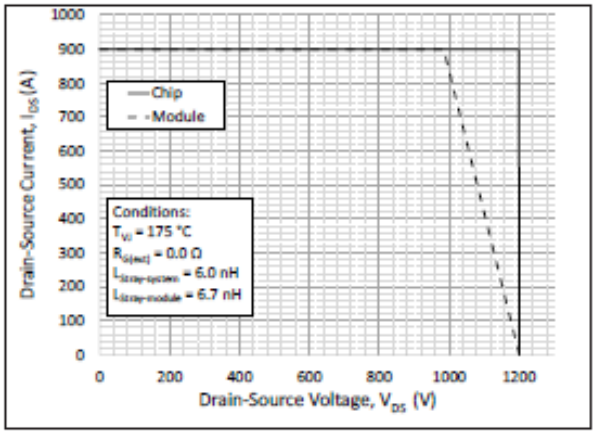

Figure 19. Reverse Bias Safe Operating Area (RBSOA)

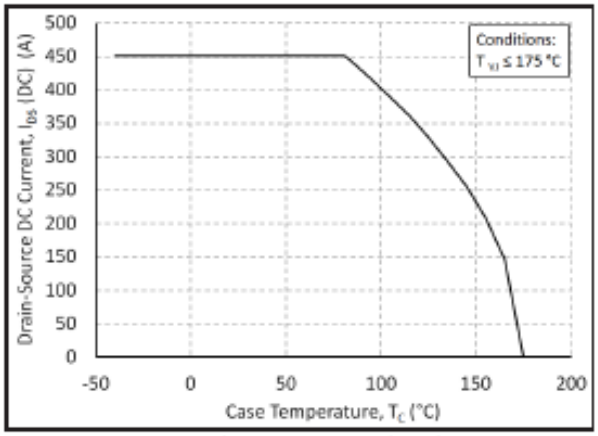

Figure 20. Continuous Drain Current Derating vs. Case Temperature

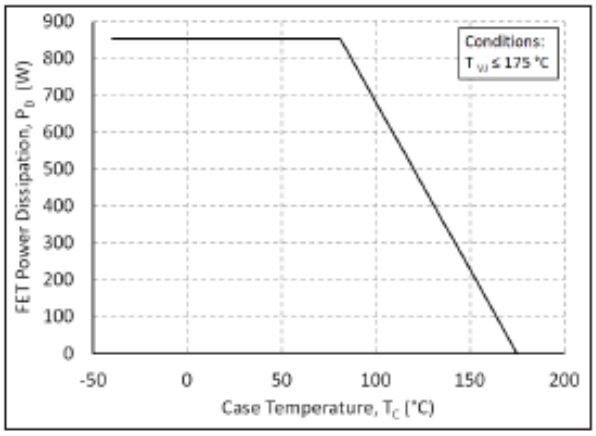

Figure 21. Maximum Power Dissipation Derating vs. Case Temperature

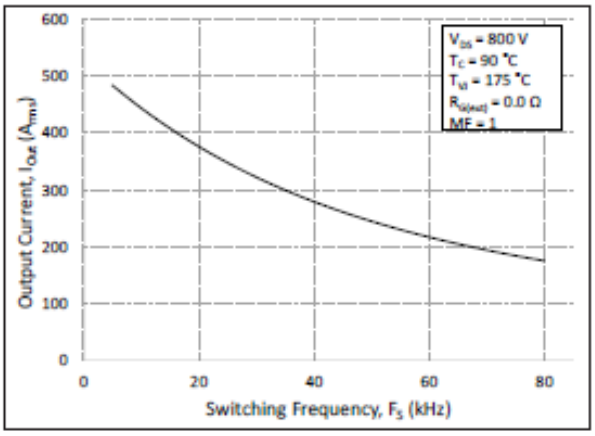

Figure 22. Typical Ouput Current Capability vs. Switching Frequency (Inverter Application)

Schematic and Pin Out

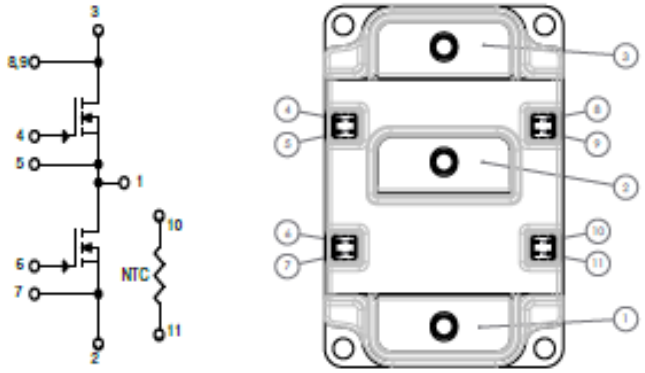

Package Dimmension (mm)

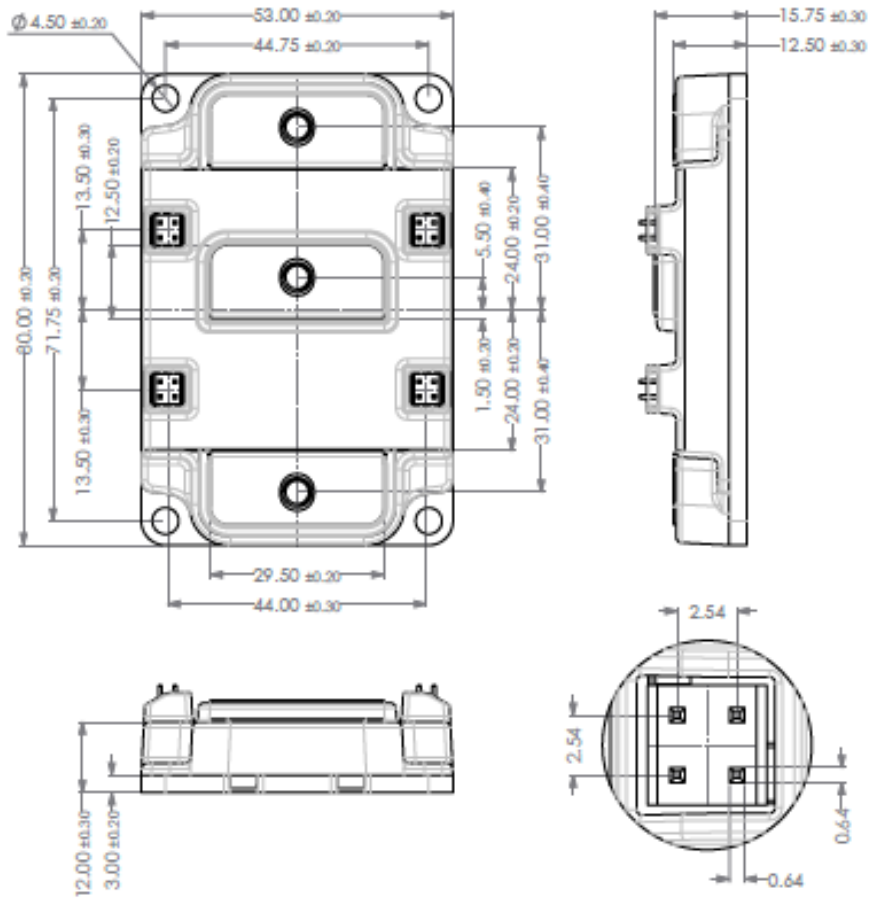

CREE Wolfspeed.

Package Dimmension (mm)

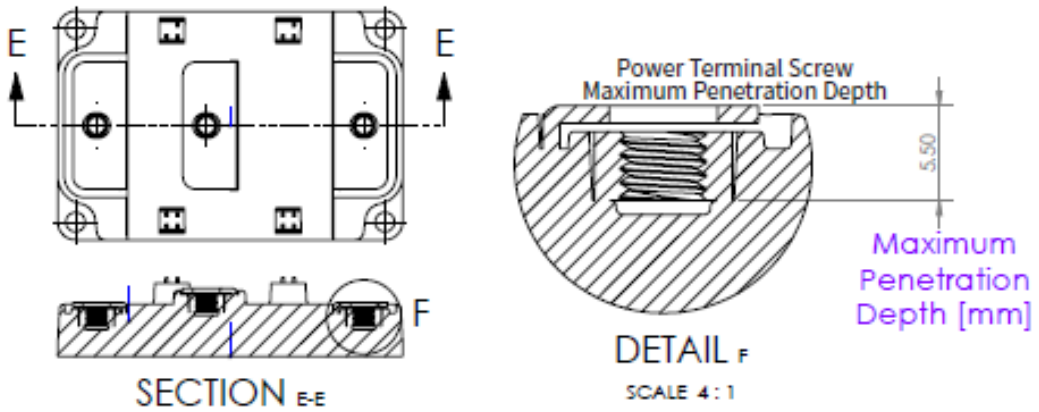

Supporting Links & Tools

- CGD12HBXMP: XM3 Evaluation Gate Driver
- CGD12HB00D: Differential Transceiver Board for CGD12HBXMP
- CRD300DA12E-XM3: 300 kW Inverter Kit for Conduction-Optimized XM3 (CPWR-AN30)
- KIT-CRD-CIL12N-XM3: Dynamic Performance Evaluation Board for the XM3 Module (CPWR-AN31)
- CPWR-AN28: Module Mounting Application Note
- CPWR-AN29: Thermal Interface Material Application Note

Notes

- This product has not been designed or tested for use in, and is not intended for use in, applications implanted into the human body nor in applications in which failure of the product could lead to death, personal injury or property damage, including but not limited to equipment used in the operation of nuclear facilities, life-support machines, cardiac defibrillators or similar emergency medical equipment, aircraft navigation or communication or control systems, or air traffic control systems.

- The SiC MOSFET module switches at speeds beyond what is customarily associated with IGBT-based modules. Therefore, special precautions are required to realize optimal performance. The interconnection between the gate driver and module housing needs to be as short as possible. This will afford optimal switching time and avoid the potential for device oscillation. Also, great care is required to insure minimum inductance between the module and DC link capacitors to avoid excessive VDS overshoot.

Rev. A, 2019-06-01 CAB450M12XM3 4600 Silicon Dr., Durham, NC 27703

Copyright ©2019 Cree, Inc. All rights reserved. The information in this document is subject to change without notice. Cree®, the Cree logo, Wolfspeed®, and the Wolfspeed logo are registered trademarks of Cree, Inc.

Appendix I – GaN-GS66516T from GAN systems

GaN Systems

GS66516T
Top-side cooled 650 V E-mode GaN transistor
Datasheet

Features

- 650 V enhancement mode power transistor
- Top-side cooled configuration
- $R_{DS(on)}$ = 25 mΩ
- $I_{DS(max)}$ = 60 A
- Ultra-low FOM die
- Low inductance GaNPX® package
- Simple drive requirements (0 V to 6 V)
- Transient tolerant gate drive (-20 / +10 V)
- Very high switching frequency (> 10 MHz)
- Fast and controllable fall and rise times
- Reverse current capability
- Zero reverse recovery loss
- Small 9.0 x 7.6 mm^2 PCB footprint
- Dual gate pads for optimal board layout
- RoHS 3 (6+4) compliant

Package Outline

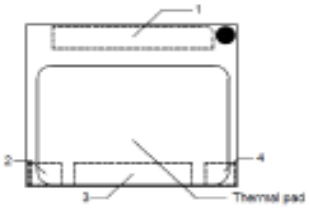

Circuit Symbol

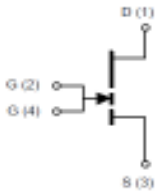

The thermal pad is internally connected to Source (S pin 3) and substrate

Applications

- AC-DC Converters
- DC-DC Converters
- Bridgeless Totem Pole PFC
- Inverters
- Energy Storage Systems
- On Board Battery Chargers
- Uninterruptable Power Supplies
- Solar Energy
- Industrial Motor Drives
- Laser Drivers
- Traction Drive
- Wireless Power Transfer

Description

The GS66516T is an enhancement mode GaN-on-silicon power transistor. The properties of GaN allow for high current, high voltage breakdown and high switching frequency. GaN Systems innovates with industry leading advancements such as patented **Island Technology®** and **GaNPX®** packaging. **Island Technology®** cell layout realizes high-current die and high yield. **GaNPX®** packaging enables low inductance & low thermal resistance in a small package. The GS66516T is a top-side cooled transistor that offers very low junction-to-case thermal resistance for demanding high power applications. These features combine to provide very high efficiency power switching.

GaN Systems

GS66516T
Top-side cooled 650 V E-mode GaN transistor
Datasheet

Absolute Maximum Ratings (T_{case} = 25 °C except as noted)

Parameter	Symbol	Value	Unit
Operating Junction Temperature	T_J	-55 to +150	°C
Storage Temperature Range	T_S	-55 to +150	°C
Drain-to-Source Voltage	V_{DS}	650	V
Transient Drain-to-Source Voltage (Note 1)	$V_{DS(transient)}$	750	V
Gate-to-Source Voltage	V_{GS}	-10 to +7	V
Gate-to-Source Voltage - transient (Note 1)	$V_{GS(transient)}$	-20 to +10	V
Continuous Drain Current (T_{case}=25 °C)	I_{DS}	60	A
Continuous Drain Current (T_{case}=100 °C)	I_{DS}	47	A
Pulse Drain Current (Pulse width 50 µs, V_{GS} = 6 V) (Note 2)	$I_{DS\ Pulse}$	120	A

(1) For ≤ 1 µs

(2) Defined by product design and characterization. Value is not tested to full current in production.

Thermal Characteristics (Typical values unless otherwise noted)

Parameter	Symbol	Value	Units
Thermal Resistance (junction-to-case) – top side	$R_{\theta JC}$	0.27	°C /W
Maximum Soldering Temperature (MSL3 rated)	T_{SOLD}	260	°C

Ordering Information

Ordering code	Package type	Packing method	Qty	Reel Diameter	Reel Width
GS66516T-TR	GaNPX® Top-Side Cooled	Tape-and-Reel	3000	13" (330mm)	16mm
GS66516T-MR	GaNPX® Top-Side Cooled	Mini-Reel	250	7" (180 mm)	16mm

GaN Systems

GS66516T
Top-side cooled 650 V E-mode GaN transistor
Datasheet

Electrical Characteristics (Typical values at T_J = 25 °C, V_{GS} = 6 V unless otherwise noted)

Parameters	Sym.	Min.	Typ.	Max.	Units	Conditions
Drain-to-Source Blocking Voltage	$V_{(BL)DSS}$	650			V	V_{GS} = 0 V, I_{DSS} = 100 µA
Drain-to-Source On Resistance	$R_{DS(on)}$		25	32	mΩ	V_{GS} = 6 V, T_J = 25 °C I_{DS} = 18 A
Drain-to-Source On Resistance	$R_{DS(on)}$		65		mΩ	V_{GS} = 6 V, T_J = 150 °C I_{DS} = 18 A
Gate-to-Source Threshold	$V_{GS(th)}$	1.1	1.7	2.6	V	V_{DS} = V_{GS} I_{DS} = 14 mA
Gate-to-Source Current	I_{GS}		320		µA	V_{GS} = 6 V, V_{DS} = 0 V
Gate Plateau Voltage	V_{plat}		3.0		V	V_{DS} = 400 V, I_{DS} = 60 A
Drain-to-Source Leakage Current	I_{DSS}		4	100	µA	V_{DS} = 650 V V_{GS} = 0 V, T_J = 25 °C
Drain-to-Source Leakage Current	I_{DSS}		800		µA	V_{DS} = 650 V V_{GS} = 0 V, T_J = 150 °C
Internal Gate Resistance	R_G		0.3		Ω	f = 5 MHz, open drain
Input Capacitance	C_{ISS}		518		pF	V_{DS} = 400 V V_{GS} = 0 V f = 100 kHz
Output Capacitance	C_{OSS}		126		pF	
Reverse Transfer Capacitance	C_{RSS}		5.9		pF	
Effective Output Capacitance Energy Related (Note 3)	$C_{O(ER)}$		207		pF	V_{GS} = 0 V V_{DS} = 0 to 400 V
Effective Output Capacitance Time Related (Note 4)	$C_{O(TR)}$		335		pF	
Total Gate Charge	Q_G		14.2		nC	V_{GS} = 0 to 6 V V_{DS} = 400 V
Gate-to-Source Charge	Q_{GS}		3.8		nC	
Gate-to-Drain Charge	Q_{GD}		5.4		nC	
Output Charge	Q_{OSS}		134		nC	V_{GS} = 0 V, V_{DS} = 400 V
Reverse Recovery Charge	Q_{RR}		0		nC	

(3) $C_{O(ER)}$ is the fixed capacitance that would give the same stored energy as C_{OSS} while V_{DS} is rising from 0 V to the stated V_{DS}

(4) $C_{O(TR)}$ is the fixed capacitance that would give the same charging time as C_{OSS} while V_{DS} is rising from 0 V to the stated V_{DS}.

GaN Systems

GS66516T
Top-side cooled 650 V E-mode GaN transistor
Datasheet

Electrical Characteristics continued (Typical values at T_J = 25 °C, V_{GS} = 6 V unless otherwise noted)

Parameters	Sym.	Min.	Typ.	Max.	Units	Conditions
Turn-On Delay	$t_{D(on)}$		4.6		ns	V_{DD} = 400 V V_{GS} = 0 - 6 V I_D = 16 A, $R_{G(ext)}$ = 5 Ω T_J = 25 °C (Note 5)
Rise Time	t_R		12.4		ns	
Turn-Off Delay	$t_{D(off)}$		14.9		ns	
Fall Time	t_F		22		ns	
Output Capacitance Stored Energy	E_{OSS}		17		µJ	V_{DS} = 400 V V_{GS} = 0 V f = 100 kHz
Switching Energy during turn-on	E_{on}		134.1		µJ	V_{DS} = 400 V, I_{DS} = 20 A V_{GS} = 0 - 6 V $R_{G(on)}$ = 10 Ω, $R_{G(off)}$ = 1 Ω L = 120 µH L_P = 2 nH (Notes 6, 7)
Switching Energy during turn-off	E_{off}		17		µJ	

(5) See Figure 16 for timing test circuit diagram and definition waveforms

(6) L_P = parasitic inductance

(7) See Figure 17 for switching loss test circuit

GaN Systems

GS66516T
Top-side cooled 650 V E-mode GaN transistor
Datasheet

Electrical Performance Graphs

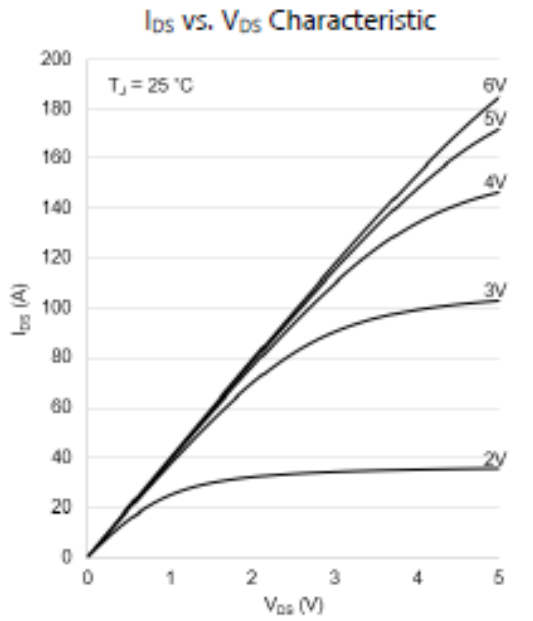

Figure 1: Typical I_{DS} vs. V_{DS} @ T_J = 25 °C

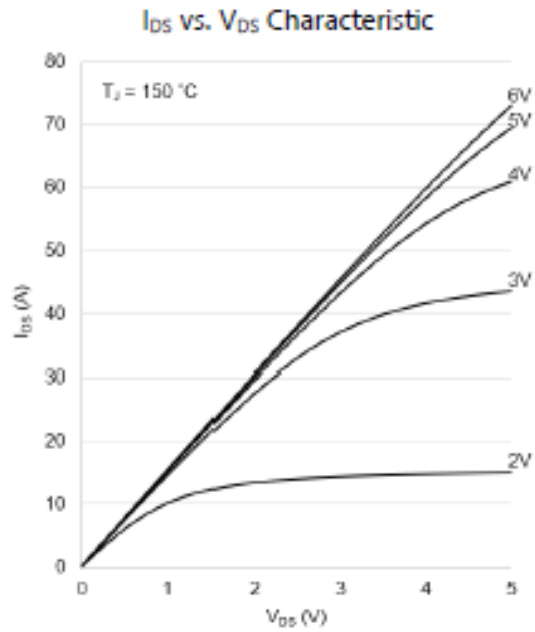

Figure 2: Typical I_{DS} vs. V_{DS} @ T_J = 150 °C

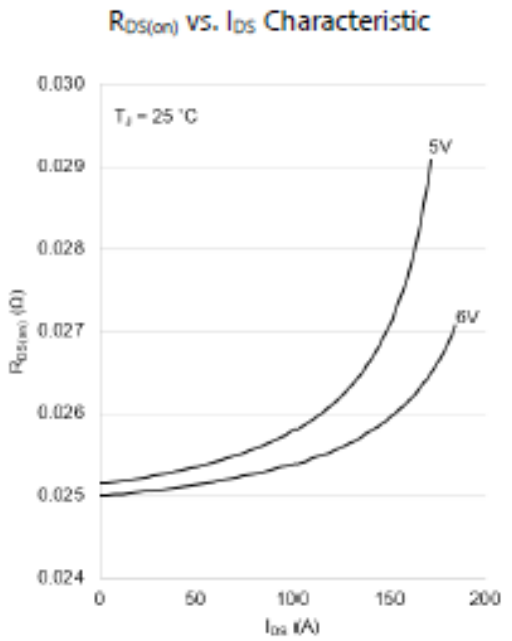

Figure 3: $R_{DS(on)}$ vs. I_{DS} at T_J = 25 °C

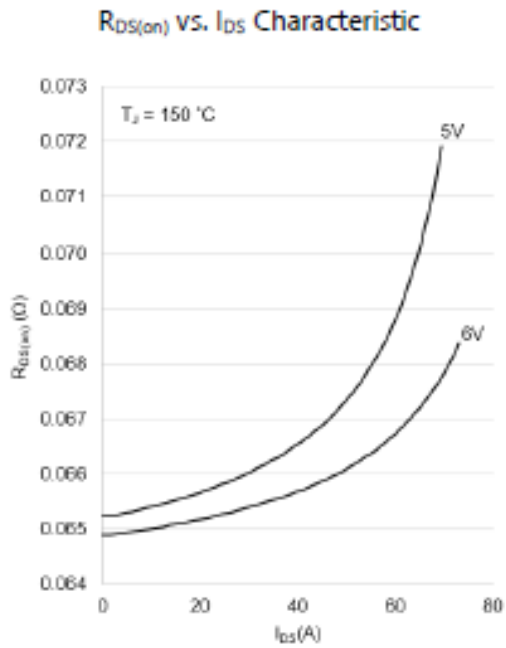

Figure 4: $R_{DS(on)}$ vs. I_{DS} at T_J = 150°C

GS66516T
Top-side cooled 650 V E-mode GaN transistor
Datasheet

Electrical Performance Graphs

I_{DS} vs. V_{DS}, T_J dependence

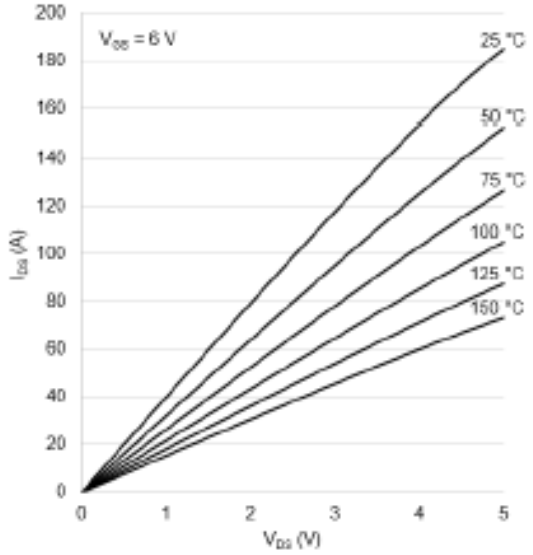

Figure 5: Typical I_{DS} vs. V_{DS} @ V_{GS} = 6 V

Gate Charge, Q_G Characteristic

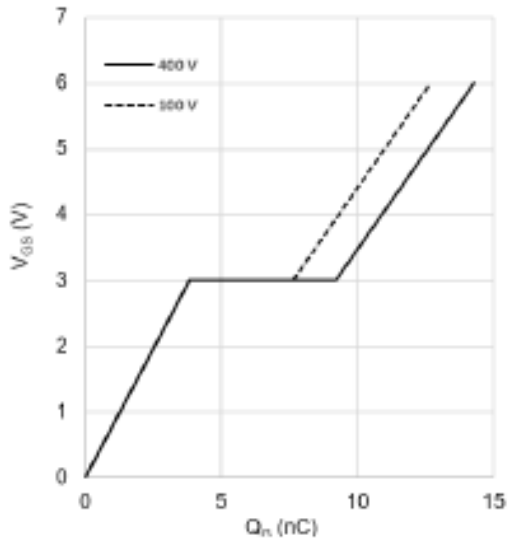

Figure 6: Typical V_{GS} vs. Q_G @ V_{DS} =100, 400 V

Capacitance Characteristics

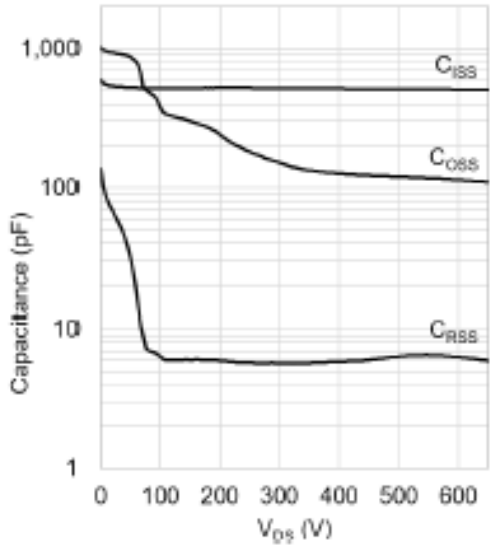

Figure 7: Typical C_{ISS}, C_{OSS}, C_{RSS} vs. V_{DS}

Stored Energy Characteristic

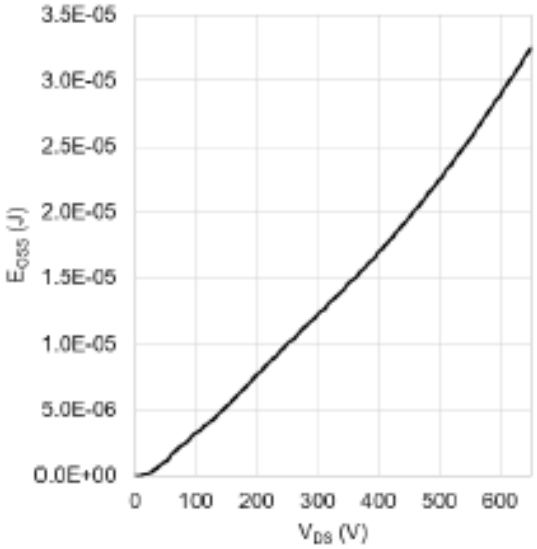

Figure 8: Typical C_{OSS} Stored Energy

GaN Systems

GS66516T
Top-side cooled 650 V E-mode GaN transistor
Datasheet

Electrical Performance Graphs

Reverse Conduction Characteristics

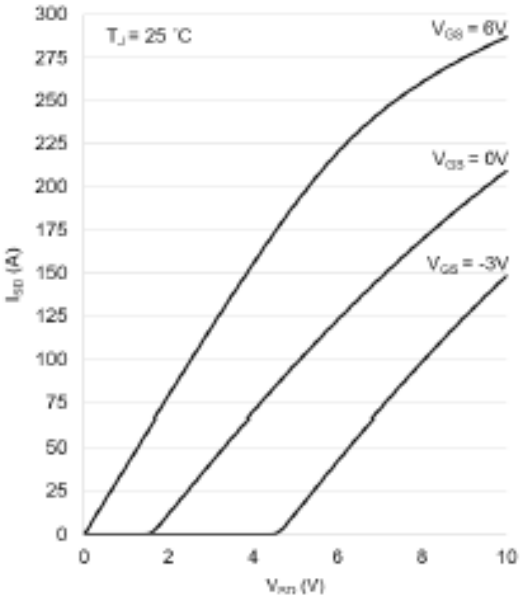

Figure 9: Typical I_{SD} vs. V_{SD} (T_J= 25 °C)

Reverse Conduction Characteristics

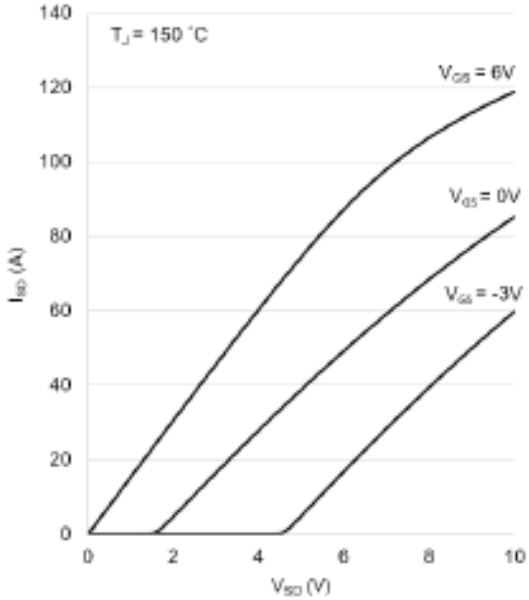

Figure 10: Typical I_{SD} vs. V_{SD} (T_J= 150 °C)

I_{DS} vs. V_{GS} Characteristic

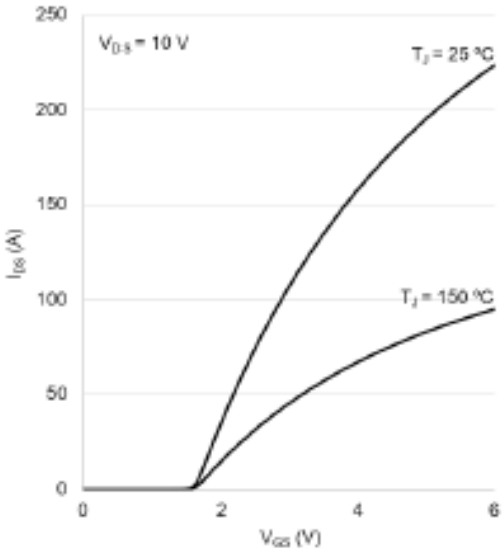

Figure 11: Typical I_{DS} vs. V_{GS}

Normalized $R_{DS(on)}$ vs T_J

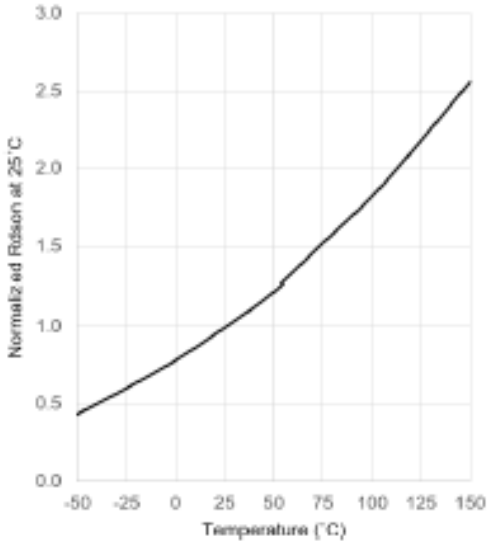

Figure 12: Normalized $R_{DS(on)}$ as a function of T_J

GaN Systems

GS66516T
Top-side cooled 650 V E-mode GaN transistor
Datasheet

Thermal Performance Graphs

I_{DS} vs V_{DS} SOA

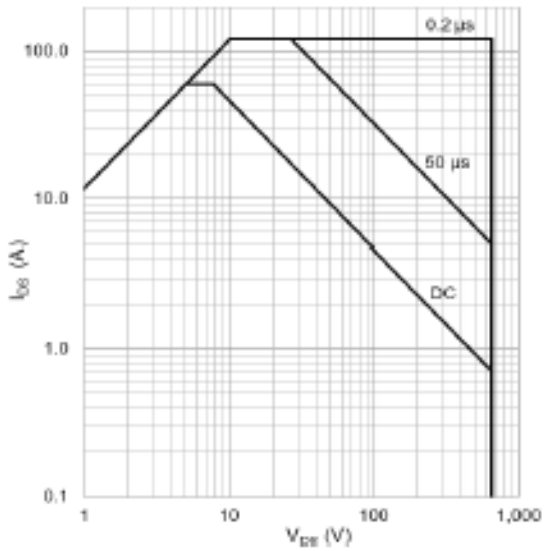

Figure 13: Safe Operating Area @ T_{case} = 25 °C

Power Dissipation Temperature Derating

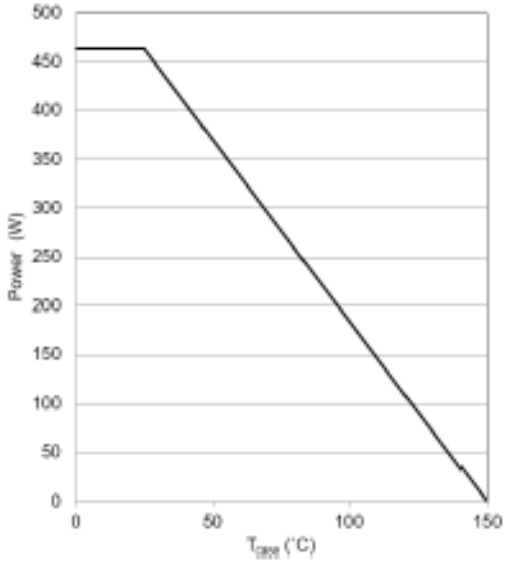

Figure 14: Derating vs. Case Temperature

Transient $R_{\theta JC}$

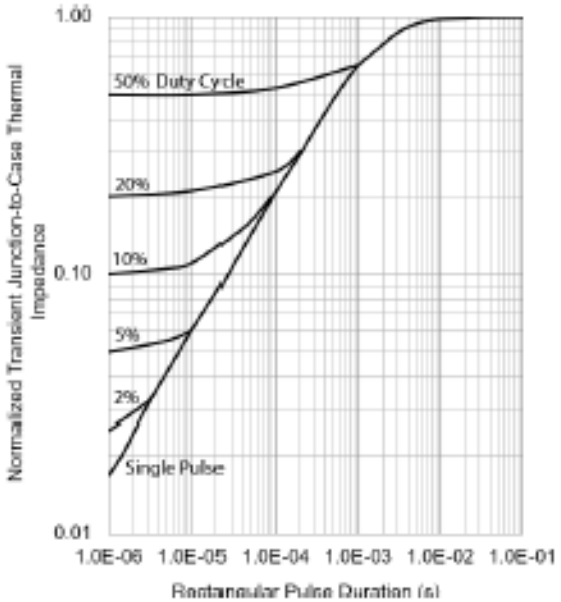

Figure 15: Transient Thermal Impedance
(1.00 = Nominal DC thermal impedance)

GaN Systems

GS66516T
Top-side cooled 650 V E-mode GaN transistor
Datasheet

Test Circuits

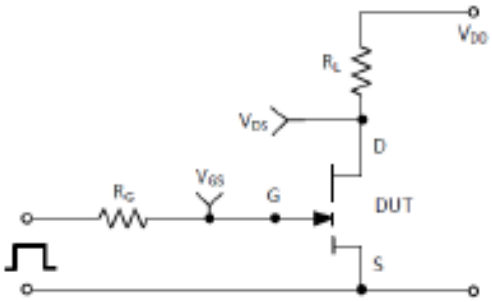

Figure 16: switching time test circuit

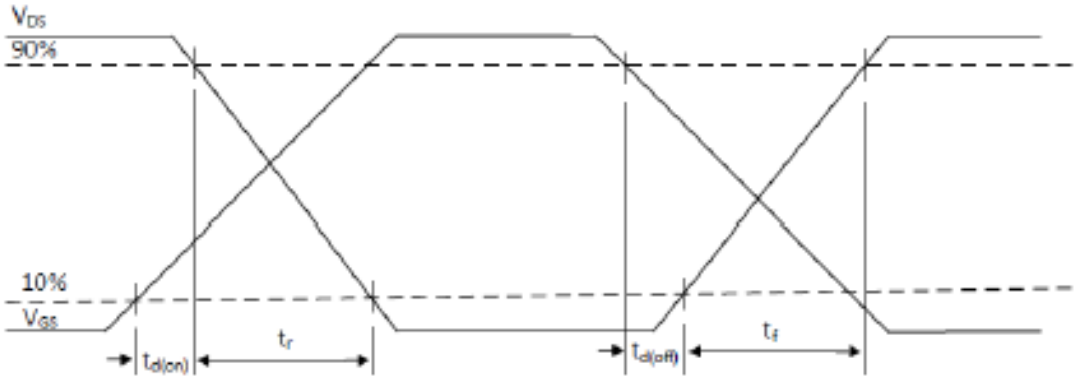

Figure 17: switching time waveforms

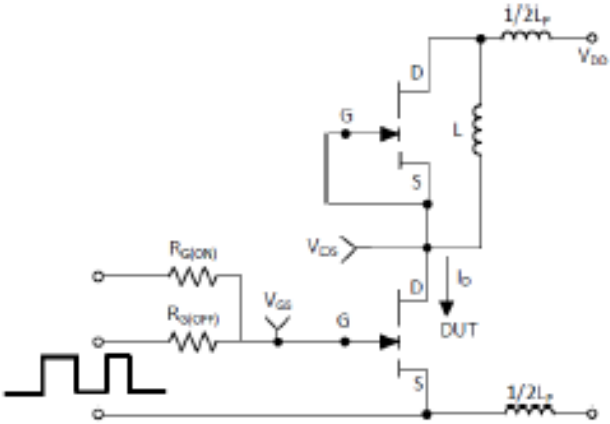

Figure 18: Switching Loss Test Circuit

Appendix J – Thermal interface material

GAP PAD HC 5.0

Highly Conformable, Thermally Conductive, Low Modulus Material

Features and Benefits

- Thermal conductivity: 5.0 W/m-K
- High-compliance, low compression stress
- Fiberglass reinforced for shear and tear resistance

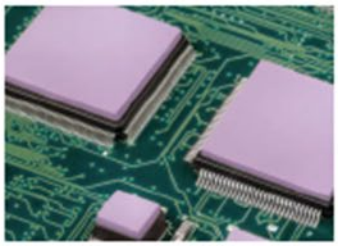

GAP PAD HC 5.0 is a soft and compliant gap filling material with a thermal conductivity of 5.0 W/m-K. The material offers exceptional thermal performance at low pressures due to a unique filler package and low-modulus resin formulation. The enhanced material is ideal for applications requiring low stress on components and boards during assembly. GAP PAD HC 5.0 maintains a conformable nature that allows for excellent interfacing and wet-out characteristics, even to surfaces with high roughness and/or topography.

GAP PAD HC 5.0 is offered with natural inherent tack on both sides of the material, eliminating the need for thermally-impeding adhesive layers. The top side has minimal tack for ease of handling. GAP PAD HC 5.0 is supplied with protective liners on both sides.

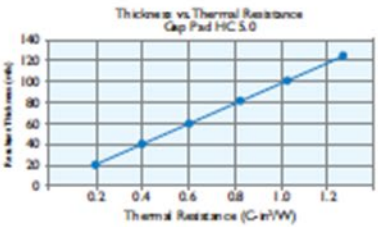

TYPICAL PROPERTIES OF GAP PAD HC 5.0

PROPERTY	IMPERIAL VALUE	METRIC VALUE	TEST METHOD
Color	Violet	Violet	Visual
Reinforcement Carrier	Fiberglass	Fiberglass	—
Thickness (in.) / (mm)*	0.020, 0.040, 0.060 0.080, 0.100, 0.125	0.508, 1.016, 1.524, 2.032, 2.540, 3.175	ASTM D374
Inherent Surface Tack	2	2	—
Density (Bulk Rubber) (g/cc)	3.2	3.2	ASTM D792
Heat Capacity (J/g-K)	1.0	1.0	ASTM E1269
Hardness (Bulk Rubber) (Shore 00)(4)	35	35	ASTM D2240
Young's Modulus (psi) / (kPa)(1)	17.5	121	ASTM D575
Typical Use Temp. (°F) / (°C)	-76 to 392	-60 to 200	—
ELECTRICAL			
Dielectric Breakdown Voltage (Vac.)(3)	5000	5000	ASTM D149
Dielectric Constant (1,000 Hz)	8.0	8.0	ASTM D150
Volume Resistivity (Ohmmeter)	10^{13}	10^{10}	ASTM D257
Flame Rating	V-0	V-0	UL 94
THERMAL			
Thermal Conductivity (W/m-K)(2)	5.0	5.0	ASTM D5470

THERMAL PERFORMANCE VS. STRAIN			
Deflection (% strain)	10	20	30
Thermal Impedance (°C-in.²/W) 0.040 in.(2)	0.35	0.30	0.26

* Custom thicknesses available. Please contact your Henkel Sales Representative for more information.
(1) Young's Modulus, calculated using 0.01 in/min. step rate of strain with a sample size of 0.70 inch² after 5 minutes of compression at 10% strain on a 1mm thickness material.
(2) The ASTM D5470 test fixture was used. The recorded value includes interfacial thermal resistance. These values are provided for reference only. Actual application performance is directly related to the surface roughness, flatness and pressure applied.
(3) Minimum value at 20 mil.
(4) Thirty second delay value on Shore 00 hardness scale.

Typical Applications Include:

- Telecommunications
- ASICs and DSPs
- Consumer electronics
- Thermal modules to heat sinks

Configurations Available:

- Sheet form and die-cut parts

Building a Part Number

GPHCS.0 – 0.020 – 02 – 0816 – NA

- Section A: GPHCS.0 = Gap Pad HC 5.0 Material with fiberglass
- Section B: Standard thicknesses available: 0.020", 0.040", 0.060", 0.080", 0.100", 0.125"
- Section C: 02 = Natural tack, both sides (With Fiberglass)
- Section D: 0816 = Standard sheet size 8" x 16", or 00 = custom configuration
- Section E: NA = Selected standard option. If not selecting a standard option, insert company name, drawing number, and revision level.

Standard Options

◄ example

Note: To build a part number, go to www.bergquistcompany.com/Part_Number_Builder.php.

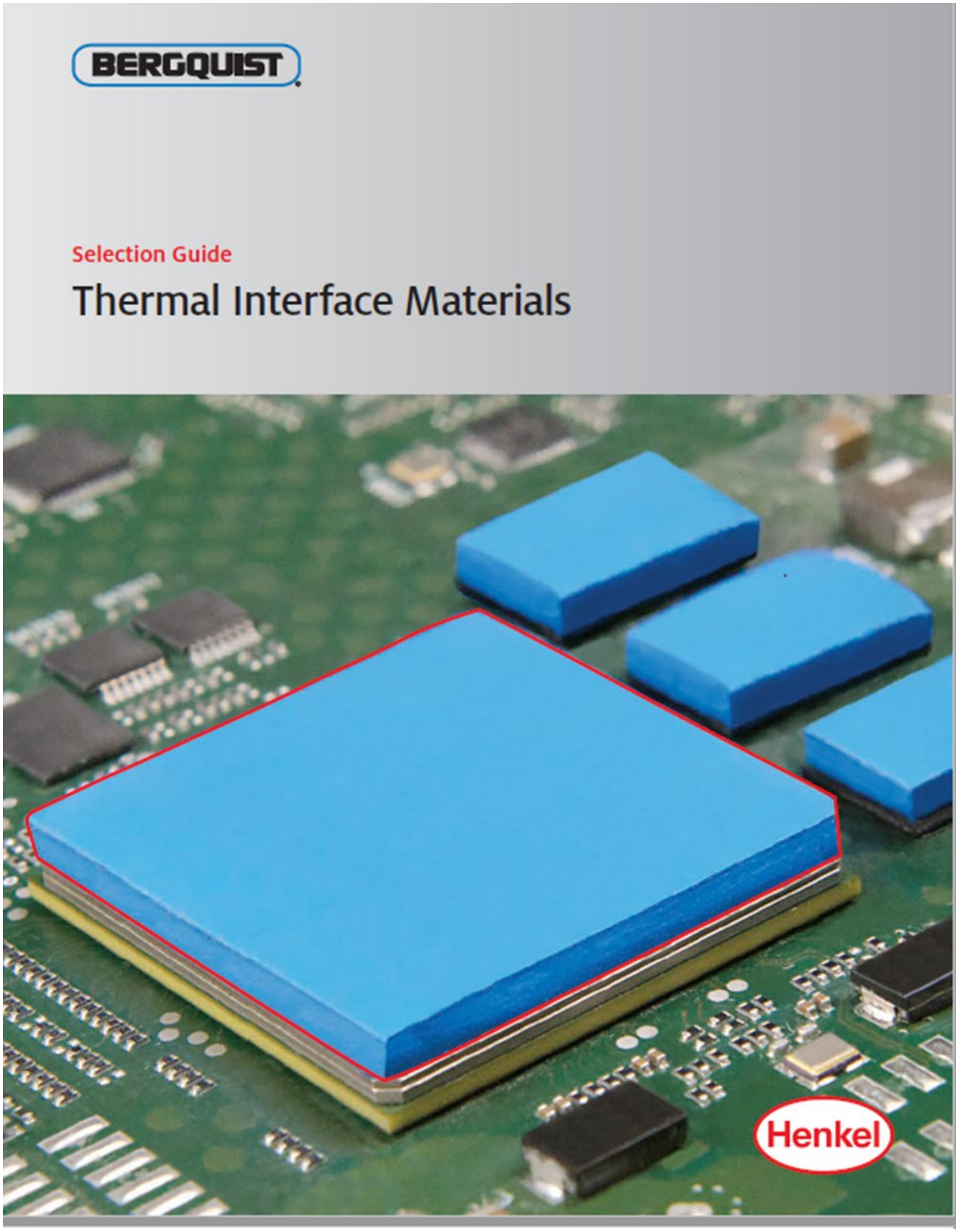
BERGQUIST
Selection Guide
Thermal Interface Materials
Henkel